EXPERIMENTAL MODAL ANALYSIS OF THE LOUDSPEAKER SYSTEM

E. B. SKRODZKA and A. P. SĘK

Institute of Acoustics
A. Mickiewicz University
(60-679 Poznań, Matejki 48/49)

This paper is concerned with an experimental modal analysis of a loudspeaker system. Based on Frequency Response Functions (FRFs) measured in about 500 points uniformly spaced on the front panel of the loudspeaker system several vibrations modes, mainly of the loudspeaker membranes, have been found. Then, the vibrations of the loudspeaker membranes were compared with vibrations of the cabinet of the loudspeaker system. It has been shown that the vibrations of the loudspeaker system cabinet were very small relative to the vibration of the loudspeaker membranes. Thus, the loudspeaker system enclosure, which may be considered as a set of vibrating plates is a source of rather week sound and may be neglected.

1. Introduction

1.1. What is modal analysis?

A term *modal analysis* refers to a process of characterising dynamic response of a structure by describing its vibrational motion by means of a set of mathematical relationships, generally referred to as modal properties [1, 2, 13, 5]. Vibrational modes of a structure can be obtained by means of one of two different approaches: mathematical models or experimental analysis [4].

Mathematical models generally discretize a structure by dividing it into a number of masses and springs, either by assuming a lumped mass and spring approach or by using the Finite Element Method (FEM) where each element is considered as a mass-spring system. A computer program, then, solves the eigenvalue extraction problem to obtain the mass, frequency, damping and mode shapes of each eigenmode of the system. Once the modal properties are determined the system is entirely described.

Experimental modal analysis on the other hand starts from a set of measured Frequency Response Functions (FRFs) of a structure. The FRF is defined as a ratio of a response signal spectrum and an excitation signal spectrum. Based on these functions the modal properties (i.e. modal frequencies, modal damping and mode shapes) are calculated without any specific assumptions concerned with the distribution of mass and stiffness of the structure. The modal model, that consists of the modal properties, is obtained by analytical curve fitting of one or more FRFs. The experimental modal analysis,

based on FRFs measurements, may be used to describe a dynamic behaviour of any vibrating object including a loudspeaker system.

In terms of modal analysis, the FRF for the response X_i, at a point i, due to an excitation force F_k applied at a point k [4, 13, 10, 11], has a form:

$$\frac{X_i}{F_k} = H_{ik}(s) = \sum_{r=1}^{n} \left(\frac{r_{ikr}}{s - p_r} + \frac{r_{ikr}^*}{s - p_r^*} \right), \tag{1}$$

where r_{ikr} – residue for r-th mode, s – Laplace variable, $p_r = \sigma_r + j\omega_r$, for $k = 1, ..., r$ – eigenvalue or the pole of the FRF, σ_r – modal damping of the r-th mode, ω_r – modal frequency of the r-th mode.

If all points i and k are taken into consideration, then Eq. (1) takes form:

$$H(\omega) = \sum_{r=1}^{n} \left(\frac{\{u_r\}\{u_r\}^t}{j\omega - p_r} + \frac{\{u_r^*\}\{u_r^*\}^t}{j\omega - p_r^*} \right). \tag{2}$$

The Laplace variable s in Eq. (1) has been replaced by the frequency ω along the frequency axis; p_r and $\{u_r\}$ are complex quantities. Thus, each mode of vibration is defined by a pair of complex conjugate poles (p_r, p_r^*) and a pair of complex conjugate mode shapes $(\{u_r^*\}, \{u_r^*\})$; $\{u_r\}^t$ and $\{u_r^*\}^t$ are transpositions of $\{u_r\}$ and $\{u_r^*\}$ respectively. A set of FRFs with indices i and k is usually arranged in a matrix called a modal matrix.

1.2. Assumptions

Modal analysis imposes following assumptions on the investigated object:

⇒ The system is linear. It means that a response of the system is proportional to an excitation. This assumptions has three following implications for FRFs measurements:

• Superposition. A measured FRF is not dependent on the type of excitation waveform used.

• Homogeneity. A measured FRF is independent of the excitation level.

• Reciprocity. The FRF measured between any two points of the structure is independent of which of them is used for excitation or response. Therefore, only one row or column of the modal matrix needs to be measured in order to identify the modal parameters of the structure. The only exceptions to the above statement are rows and columns corresponding to components of the modal vector which are zero. These are known as the nodal points of the mode shape.

⇒ The structure is causal. It does not start to vibrate before it is excited.

⇒ The structure is stable. The vibrations dies out when the excitation is removed.

⇒ The structure is time-invariant. The dynamic characteristics do not change during the measurements.

⇒ Modes are defined in a global sense. Mode shapes are defined for all degrees of freedom of the model. Frequency and damping of the mode do not vary significantly from one part of the structure to another.

⇒ Only one mode exists at each modal frequency.

These assumptions can be satisfied in a large number of test situations. However, accuracy of the resulting modal parameters depends largely on how closely the analysed system follows them.

In many cases, to simplify calculations, it is necessary to assume that a loudspeaker and a loudspeaker system are approximately linear systems. However, this assumption is only reasonable true for small displacements of the structure. In this case loudspeaker systems can be treated as linear systems in the whole explored frequency range. The other conditions which modal analysis imposes on the investigated system, as causality, stability and time-invariantness, are undoubtedly met by the loudspeaker system.

1.3. The role of modal analysis with respect to acoustics. Aim of the experiment

In classic experimental modal testing a structure is excited at one or more points and the response is determined at one or more points. It was the reason that at the beginning the modal analysis was used for dynamic investigation of large objects [3], like cars, ships, aircrafts, buildings, mill elements, vibrating machines, etc. It was relatively easy to excite the structure by a shaker or by an impact hammer with a force transducer and to measure the response signal by means of an accelerometer attached at some key points [7]. In this classic form experimental modal analysis is successfully used in acoustics in the investigations of the dynamic behaviour of music instruments like violins, pianos, guitars, handbells, etc. [3].

However, application of modal analysis to investigation of objects whose mass was comparable to mass of accelerometer, like commonly encountered in electroacoustics loudspeaker membranes, was almost impossible. It is possible to attach the accelerometer to the loudspeaker membrane, but the response signal determined by the accelerometer will not be the response of the membrane itself, but the response of the membrane loaded by the accelerometer. Such a signal is rather useless in modal investigations. This serious drawback has disappeared when a non-contact method of detection and measuring the structure response signal has appeared. A laser velocimeter enables successful measurements of the loudspeaker membrane response. It is not necessary to cover the membrane by a reflective material, so the problem of unwanted mass attached to the membrane does not exist.

Then, the use of the laser velocimeter is the only chance of successful modal analysis of loudspeaker membranes and complete loudspeaker systems. However, some more modifications of the classic experimental modal analysis technique have to be made too (see next paragraph for details).

In this paper the modal analysis was used to analyse vibrations of a complete loudspeaker system. The main purpose was to find, visualise and compare all vibrating areas of the loudspeaker system including both the speakers and the cabinet of the system. It is well known that the loudspeaker system cabinet vibration can influence the reproduced sound by a loudspeaker system giving so-called "colouration" effect. The effect may be simply due to the interference of reproduced sound from loudspeakers with unwanted sound produced by thrilling surfaces or due to resonances of the cabinet. If areas with unwanted significant vibrations are well known, it will be possible to eliminate them or,

at least, to change their resonant frequency by attaching an additional mass, a damping element or a stiffening element.

2. Measuring setup and measuring conditions

A block diagram of a measuring system used in the investigation is presented in Fig. 1. The object under investigations was a typical ZgP-40-8-85 "Tonsil" loudspeaker system taken by chance from the manufacture. The system consisted of one woofer (GDN 20/40/12) and two tweeters (GDW 9/15/6 and GDW 5/40/9). The dimensions of the system were: $256 \times 456 \times 210$ mm. The loudspeaker system was mounted on a motor-step table controlled by a computer, enabling its positioning.
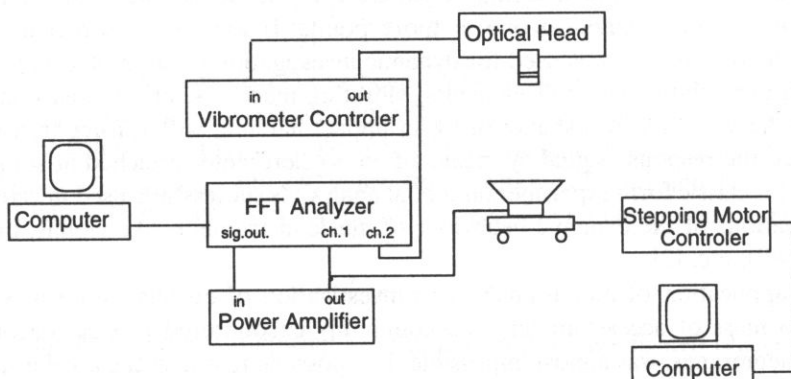
Fig. 1. Measuring setup for modal analysis used in the investigations.

The system was excited by a constant voltage (RMS), flat spectrum, pseudo-random noise. The frequency range of the signal was $0 - 4$ kHz. An example of the exciting signal spectrum is shown in Fig. 2. To preserve natural working condition of the system the signal was delivered to the loudspeaker's voice-coils. The signal was also delivered to one channel of the dual channel spectrum analyser (ONO SOKKI CF 6400) which was the main part of the measuring equipment.

The response signal from the vibrating body, i.e. the changes of the velocity of a vibrating point of the system, was measured in a non-contact way by means of a laser velocimeter based on the Doppler effect. Velocity was measured in the parallel direction to the main axes of symmetry of the loudspeakers. The velocimeter was fixed on a frame and its position did not change during experiment. The signal from the velocimeter was fed to the second channel of the analyser.

The spectrum of the excitation evoked by the stimulating pseudo-random noise was broadband and contained discrete components whose frequencies corresponded to the frequencies of analysis. A repeatable nature of the stimulating waveform enabled successful application of time averaging procedure for FRFs. So the signal-to-noise ratio was significantly improved.
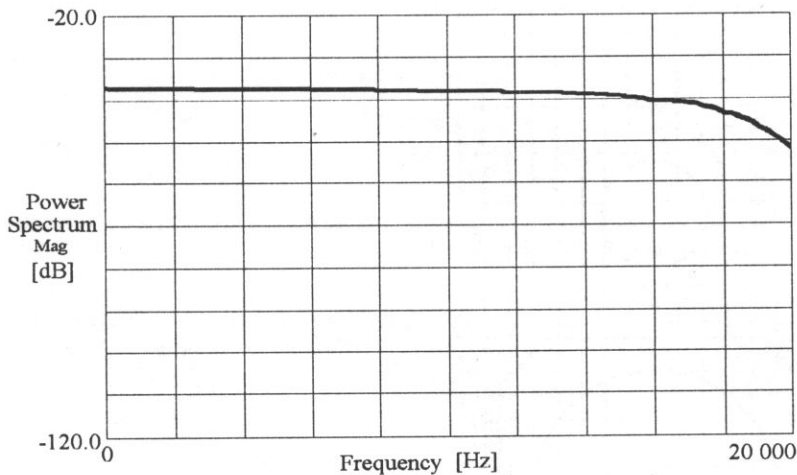
Fig. 2. The spectrum of the excitation signal used in the investigation.

The rectangular window, as the most appropriate for pseudorandom noise and transient signals, was used in both measuring channels. The analyser calculated FRFs based on the Eq. (1). Then, FRFs were transferred via GPIB card to a computer and stored for further analyse by means of the SMS STAR*Modal*® software.

Experimental modal analysis is based on a set of measured Frequency Response Functions (FRFs). A distribution and a number of the measuring points applied to the object are very important for the accuracy and the resolution of the analyse. They must reflect the geometry of the investigated object in an optimal and the best possible way. The maximum number of the data points that the STAR*Modal*® software could cope with was 500. A measuring "net" consisting of 17 points placed along x-axis and 29 points placed along y-axis was constructed. Thus, the loudspeaker system was characterised by means of 493 points uniformly spaced on the front panel of the system. The distance between two adjacent measuring points was approximately equal 1.5 cm. The distribution of the measuring points, plotted in Cartesian coordinates is given in Fig. 3.

It would be the best if the majority of measuring points were placed in areas of the most significant possible vibrations. However, as before the experiment positions of nodal points were unknown we decided to distribute all available measuring points uniformly. If some modes of a single loudspeaker were of the main interest then all points should cover it.

In the carried out experiments it was necessary to adopt the classic modal analysis to measurements performed directly on a loudspeaker [8, 9]. The classic modal analysis assumes that the excitation signal is a force signal. However, in the presented experiments the membrane was driven by the voice-coil. Thus, it was impossible to fulfil this requirement because the value of exciting force was unknown. The voice-coil voltage was taken as the input variable instead of the force.

For the carried out analysis a point excitation was assumed. The central point of the woofer's membrane was chosen as the stimulation point in all calculation. The only way
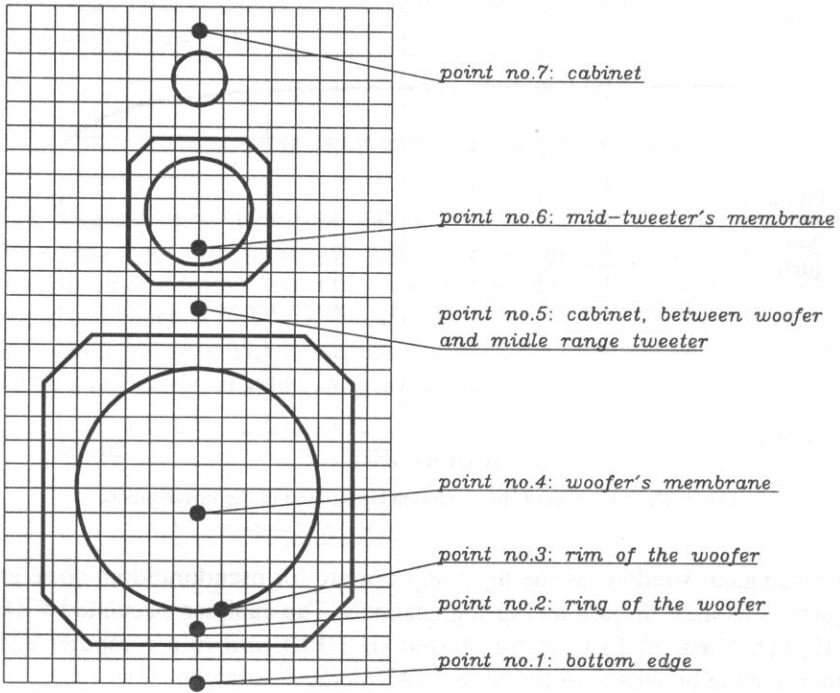
Fig. 3. Measurement geometry of the front panel of the "Tonsil" loudspeaker system.

of measuring vibrations of the loudspeaker, that reflects a normal condition of its action, is to excite the loudspeaker by means of its voice-coil. This necessity results from the nature and the structure of the loudspeaker. On the other hand this assumption might be a source of a certain error. This error can be estimated by means of the multi-point excitation version of the modal analysis and is under investigation.

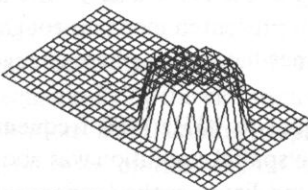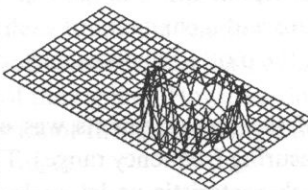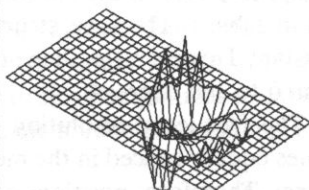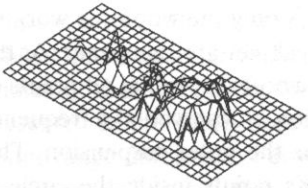## 3. Results of modal analysis of the loudspeaker system
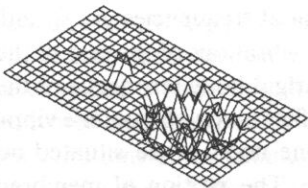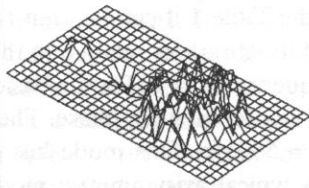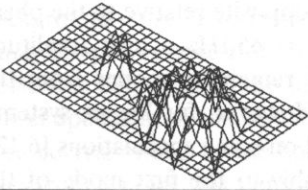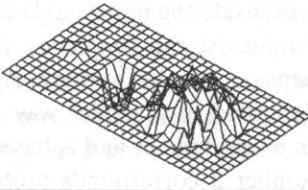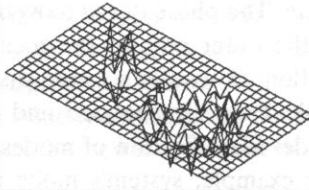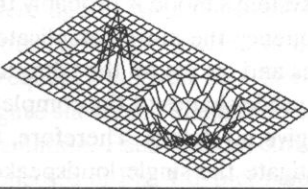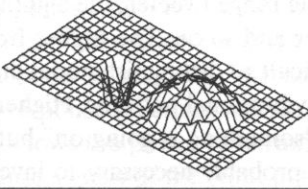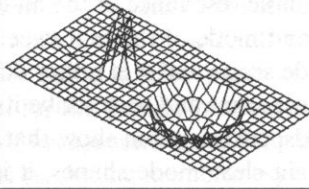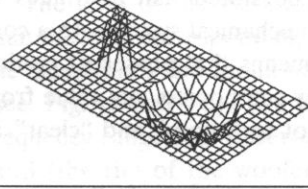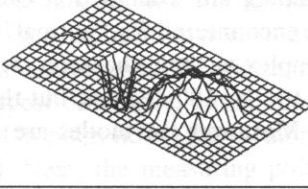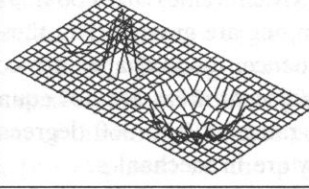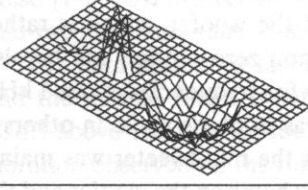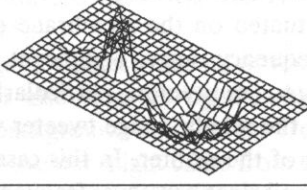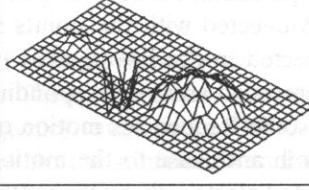
Based on the frequency response functions measured in all 493 points the modal parameters (i.e. modal frequencies, modal damping and mode shapes) were calculated. The results of modal analysis are listed in Table 1. Each cell of the table shows modal frequency, the mode shape and the percentage of critical damping. The percentage of critical damping is defined as [10]:

$$\xi_r = \frac{\sigma_r}{\sqrt{(\sigma_r^2 + \omega_r^2)}} \cdot 100\%, \tag{3}$$

where σ_r – damping value in s^{-1} for r-th mode, ω_r – damped natural angular frequency in s^{-1} for r-th mode.

The shape of the mode is simply a plot of motion in z direction expressed in a linear scale, determined in each measuring point of the loudspeaker system for one

Table 1. Results of modal analysis for the complete loudspeaker system.

$f_0 = 90$ Hz $\xi_0 = 39.0\%$	$f_1 = 580$ Hz $\xi_1 = 6.0\%$	$f_2 = 650$ Hz $\xi_2 = 5.4\%$
$f_3 = 1.16$ kHz $\xi_3 = 7.0\%$	$f_4 = 1.44$ kHz $\xi_4 = 4.9\%$	$f_5 = 1.64$ kHz $\xi_5 = 4.3\%$
$f_6 = 1.80$ kHz $\xi_6 = 3.7\%$	$f_7 = 1.99$ kHz $\xi_7 = 3.8\%$	$f_8 = 2.30$ kHz $\xi_8 = 1.9\%$
$f_9 = 2.55$ kHz $\xi_9 = 3.3\%$	$f_{10} = 2.68$ kHz $\xi_{10} = 2.7\%$	$f_{11} = 2.85$ kHz $\xi_{11} = 3.6\%$
$f_{12} = 2.97$ kHz $\xi_{12} = 4.7\%$	$f_{13} = 3.20$ kHz $\xi_{13} = 5.0\%$	$f_{14} = 3.43$ kHz $\xi_{14} = 4.6\%$
$f_{15} = 3.55$ kHz $\xi_{15} = 5.3\%$	$f_{16} = 3.74$ kHz $\xi_{16} = 1.4\%$	$f_{17} = 3.92$ kHz $\xi_{17} = 3.8\%$

particular phase of the vibrating movement. The units along z-axis are the same in each cell in Table 1. The basic structure and a character of each of presented modes is roughly constant. However, the shape of the plotted surfaces may somewhat vary as phase changes from 0 to 360 degrees.

The frequency resolution of the measurements was equal to 10 Hz (400 frequency values equally spaced in the measuring frequency range). The spatial resolution was about 1.5 cm. Therefore, positions of characteristic nodal circles and lines on the loudspeaker membranes are difficult to identify. However, from the sequence of mode shapes shown in the Table 1 it can be seen that at frequencies f_0, f_1 and f_2 only the woofer is working and its vibrations relative to the vibrations of the rest of the cabinet are significant. At the frequency $f_0 = 90$ Hz the basic rigid-body resonance of the woofer is visible; all points of the woofer move in phase. The first mode of woofer's vibration is observed at a frequency $f_1 = 580$ Hz. This mode has one nodal circle situated near the outer suspension. This is a typical axisymmetric mode. The motion of membrane's points inside the circle is characterised by a smaller amplitude than the motion of the points outside of the nodal circle. The phase of the movement inside the nodal circle is opposite relative to the phase of the outer part of the membrane. At the frequency $f_2 = 650$ Hz a high-amplitude motion of woofer's outer suspension can be noticed. All remaining modes from the Table 1 can by analysed and described in a similar way. However, for higher system's modes identification of modes is more difficult and is based on some speculations [6,12]. For example, system's mode number 3 corresponds probably to the first mode of the mid-tweeter; the fifth system's mode probably fits in the second mode of the woofer and the basic resonance of the middle range tweeter; the eighth system's mode is probably the second mode of the mid-tweeter and so on. The higher frequency the more complicated mode shape and it is rather difficult to distinguish nodal lines and circles on the vibrating loudspeaker and to describe its vibrational patterns. Higher mode shapes of the complete loudspeaker system show that "something is going on" but give no details. Therefore, to obtain clear mode shapes, it is probably necessary to investigate the single loudspeaker placed in the system.

When values of modal damping are examined it can be stated that all values of damping are greater than these encountered for "normal" mechanical systems. In a consequence, mode shapes are complex in their character. It means that phases of motion of adjacent areas are not equal to 0 or 180 degrees, but they can possess any value from the range of 0 to 360 degrees. Moreover the modes are not so "sharp" and "clear" as they are in mechanics.

The shapes of the modes presented in the Table 1 express motion of all points in the parallel direction to the main axes of loudspeakers. Generally, the greatest motion is connected with the points situated on the membrane of the woofer, which is rather expected in the investigated frequency range. Significant, non zero motion can be also observed at areas corresponding to the tweeters, particularly for frequencies above 1 kHz. At some frequencies motion of the middle range tweeter was in phase while in others it was in antiphase to the motion of the woofer. In this cases the mid-tweeter was mainly excited electrically by the voice-coil since crossover frequency between the woofer and the middle range tweeter was equal 3.5 kHz and the slope of the crossover filter characteristic

was about 6 dB/octave. The crossover frequency between the mid-tweeter and the tweeter was 10.5 kHz and the slope of the filter was 6 dB/octave. The amplitude of the tweeter's movement was only slightly higher than the motion of the cabinet. Due to frequency range of measurement this result was not unexpected. Both tweeters were also excited mechanically by the vibrations of the cabinet. However, due to small amplitudes of cabinet vibrations and damping properties of the suspension of the membrane their influence on membranes motion was rather small.

All active points situated on the front panel of the system correspond to the vibration of the speakers. The points beyond the membranes (excluding some points in the adjacent area to the woofer) may be characterised by a near zero velocity. It means that cabinet must be relatively rigid. It may transmit some vibrations (to excite the membranes of the tweeters in some way) but it behaves quite calm. However, mode shapes presented in the Table 1 are expressed in a linear scale. So it is difficult to asses the dynamic range differences between vibrations of the cabinet relative to the vibrations of the membranes. To asses this differences some additional measurements were carried out. These measurement were concerned with determination of the power spectrum of the background noise, and the power spectrum of the response signal in all measuring points. First, the power spectrum of the velocity was determined while exciting pseudo-random noise was delivered to the loudspeaker system. Then, the signal was turned off and the power spectrum of the velocity was determined again. The velocity measured in the later case corresponded to the background noise vibrations, thus the power spectrum of the background noise was determined.

Examples of the power spectra are presented in Figs. 4 a – g (the data presented in these figures were collected in points which are shown in Fig. 3 by means of black dots). Both curves are plotted in a logarithmic scale (in dB) and are scaled on a 20 dB units. Frequency is given in a linear scale on abscissa. The upper curve in each panel of the figure shows the magnitude of response spectrum measured for the pseudo-random noise excitation. Each bottom curve shows the power spectrum of background noise. The data collected in Fig. 4 depict response signals of the front panel (including membranes) only, since significant vibrations were observed on this plate only.

The level of the vibration connected with the stimulating signal is generally higher than the level corresponding to the background noise particularly for the points placed on the membranes and for all points situated no further than 3 cm from vibrating membrane (see. Fig. 4 c and 4 d). The largest difference, equal approximately 60 – 75 dB in whole frequency range, was observed in point no. 4 (the membrane of the woofer) and in point no. 3 (the rim of the woofer). Next, the measuring point (no. 2) placed on the plastic ring of the woofer showed also significant vibrations, about 30 dB above the background noise (Fig. 4 b). Significant vibrations were also observed in point no. 6 situated on the mid-tweeter membrane (Fig. 4 f).

The data presented in Fig. 4 e suggest that point no. 5 situated between the woofer and the middle range tweeter also vibrated significantly. These vibrations were about 20 dB above the level of the background noise in the frequency range up to 3 kHz. The vibration observed on the mid-tweeter might came from the electric stimulation and were not caused by vibrating air-volume bounded within the cabinet.

a) p. no. 1
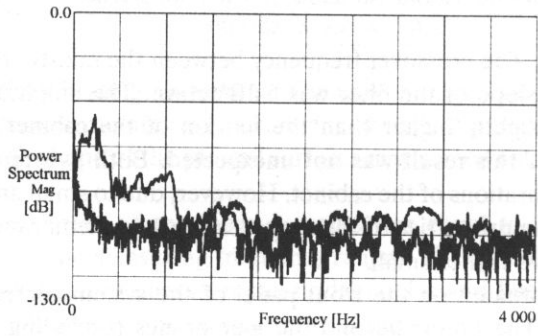
b) p. no. 2
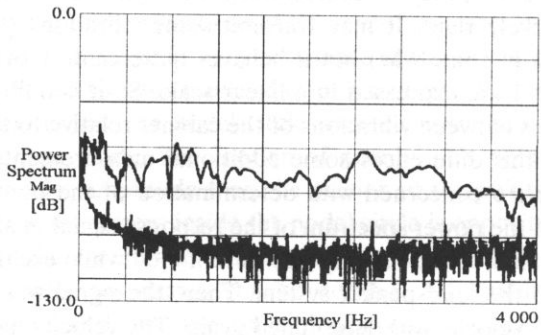
c) p. no. 3
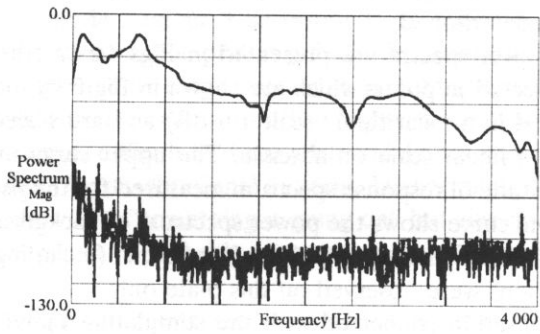
d) p. no. 4
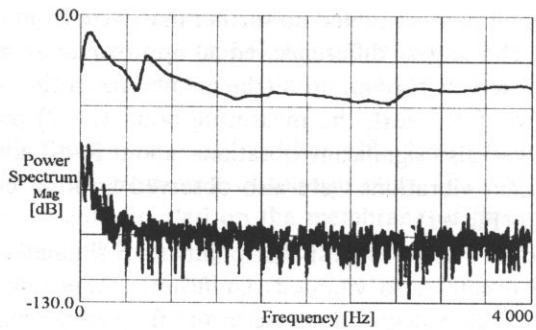
e) p. no. 5
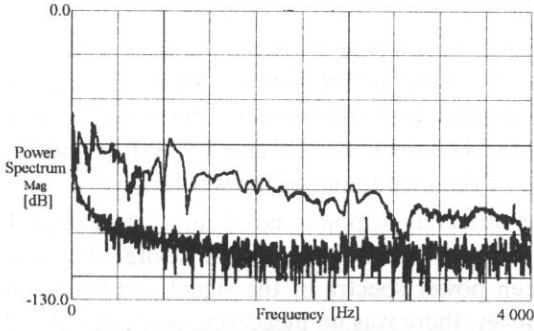
f) p. no. 6
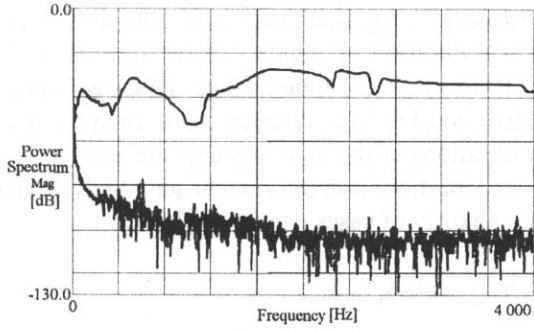
g) p. no. 7
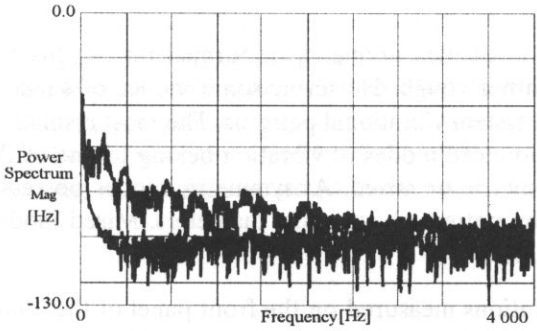
Fig. 4. Response signal – upper curve; noise signal – bottom curve for the loudspeaker system in the different points placed on front panel of the system (see also Fig. 3).

[125]

It is worthwhile to say that this type of results were also gathered for all points placed close (no further than 2 – 3 cm) to the woofer. So the data presented in Fig. 4 e are representative for whole area around the woofer. They suggest that in real conditions this area vibrates significantly. However, the observed vibrations were approximately 40-50 dB below the vibration of the membrane of the woofer.

No vibrations were observed in points no. 1 and 7 (see Figs. 4 a and g) and in all other points situated further than 3 cm from the woofer. For these points there is a small difference between power spectra of the signal and background noise in the low frequency region. However, there was no measuring point that this difference was higher than 5 dB in the whole frequency range. Similar measurements have been carried out on the back and side plates of the cabinet and very similar results have been obtained. On the other hand it is necessary to say that there is a huge difference between vibrations of the membrane and the vibration of points situated outside of the membranes. This difference is at least 60 dB in whole frequency range. Thus, assuming that the front panel of the loudspeaker system is a kind of vibrating plate, then its vibrations are 1 000 000 times smaller than the vibrations of the membrane of the woofer. It means that the front panel is almost calm, its vibrations are very small and their contribution to the total vibration pattern in the majority of cases can be neglected.

4. Conclusions

1) Spatial resolution of measurements performed on the front panel of the loud-speaker system was rather rough. However, some modes of single loudspeakers were found in the set of the system vibrational patterns. The most distinct, the most character-istic and the best pronounced modes of vibration belong to one of the three categories: axisymmetric, antisymmetric or mixed. Axisymmetric modes possess only nodal circles. Antisymmetric vibration patterns have nodal diameters. Mixed modes exhibit nodal cir-cles and nodal diameters.

2) The biggest vibrations measured on the front panel of the loudspeaker system are related mainly to the vibrations of the membranes of the speakers. Vibrations of the woofer and the middle range tweeter are at least 60 dB higher than vibrations observed in the most points of the front panel of the cabinet.

3) Vibrations of the front panel of the loudspeaker (excluding the areas of the mem-branes) are very week relative to the vibrations of the membranes. They are no higher than 5 dB above the background noise. The only exception is the area close to the woofer where the vibrations were about 20 dB above the level of the background noise.

4) The contribution of the vibrations of the front panel of the investigated loudspeaker system (excluding the membranes) to the sound field radiated by this system is rather small and may be neglected.

References

[1] D.J. EWINS, *On predicting point mobility plots from measurements of other mobility parameters*, J. Sound and Vibration, **70**, 69–75 (1980).

[2] D.J. EWINS, *Modal Testing: Theory and Practice*, RSP Ltd John Wiley & Sons Inc., London 1986.

[3] N.H. FLETCHER and T.D. ROSSING, *The Physics of Musical Instruments*, Springer-Verlag, New York 1991.

[4] K.D. MARSHALL, *Modal analysis of a violin*, J. Acoust. Soc. Am., **77**, 695–709 (1985).

[5] H.G. NATKE, *Einfuehrung in Theorie und Praxis der Zeitreihen- und Modalanalyse*, Vieweg, Berlin 1992.

[6] M. SAKAMOTO, K. SATOH, K. SATOH and N. ATOJI, *Loudspeaker with a new disc diaphragm*, 64th Convention of Audio Engng. Soc., New York, 1–31 (1979).

[7] E.B. SKRODZKA and E. HOJAN, *Initial modal testing of a cantilever beam*, Arch. Acoust., **19**, 3, 355–365 (1993).

[8] E.B. SKRODZKA and H. FLEISCHER, *Drgania strukturalne głośników* [in Polish], XLI Open Seminar on Acoustics, Wrocław-Szklarska Poręba, 415–418 (1994).

[9] E.B. SKRODZKA, H. FLEISCHER, T. DILLMANN and H. WINTER, *Vibroacoustic investigation of a loudspeaker*, DAGA, Dresden, 553–556 (1994).

[10] STAR, *The STAR System version 3.02D. Theory and application*, [in:] User's Manual, SMS (1990).

[11] T. UHL, W. LISOWSKI and L. MIĘKINIA, *Wprowadzenie do analizy modalnej. Część I. Podstawy teoretyczne* [in Polish], Energetistic Methods in Vibroacoustics, II School, Krynica, 95–114 (1993).

[12] W. WIENHÖFER and H. SANDER, *Bestimmung der Eigenformen von Wandlermembranen durch berürungslose Messung und Analyse der Impulsantwort*, DAGA, 513–516 (1988).

[13] K. ZAVERI, *Modal Analysis of Large Structures-Multiple Exciter Systems*, Bruel & Kjaer, Naerum 1985.

THE SOUND ABSORPTION PROPERTIES OF A CROSS-SHAPED ISOLATED ACOUSTIC RESONATOR

V. STAUSKIS

Vilnius Gediminas Technical University
(Saulėtekio al. 11, 2040 Vilnius, Lithuania)

The paper examines a new acoustic construction which differs from the classical Helmholtz resonator. The proposed acoustic resonator consists of massive plates with a rectangular-shaped slit of varied width. Sound-absorbing materials are not used in such a resonator, and the effect of absorption is achieved due to the resonance qualities of such a construction.

In a theoretical model of such construction, both the main resonance and the overtones, i.e. the odd harmonics, the impedance of the slit itself, the impedances of added air masses outside and inside the slit, the impedance of the resonator air volume, and the radiation impedance are taken into account.

On the basis of the formulas obtained, the change in the sound absorption depending on the slit width and the distance between the slit and the rigid surface is computed. It has been established that the absorption has a resonant nature and it is enhanced with the increase in the slit width. When the slit width is 65 cm, the absorption area reaches almost $4\,\mathrm{m}^2$ at 60 Hz. The volume of the resonator is significant. When the resonator's height is increased to 150 cm and the slit width is 30 cm, the area of absorption is as large as $3.5\,\mathrm{m}^2$ at 35 Hz.

The dependence of the real and imaginary parts of the slit impedance and the radiation impedance on the slit width is computed, as well as the dependence of the real and imaginary parts of the resonator volume impedance on the slit width under constant distance to the rigid surface of the ceiling.

1. Introduction

Certain quantities of sound-absorbing materials must be placed in music halls for the optimization of their acoustics. These materials must have different acoustic characteristics, i.e. sound must be absorbed differently at various frequencies. This is necessary in order to obtain an optimum frequency characteristics of the hall reverberation time which is one of the most important objective criteria of the hall acoustics. The reverberation time depends on the intended purpose of the hall, its volume, the musical work being performed, the listener's location in relation to the sound source, and the quantity and acoustic properties of the sound-absorbing materials.

The halls' reverberation time usually requires reduction at low and medium frequencies, whereas at high frequencies the reduction is practically unnecessary because high-frequency are well-absorbed by the air itself. There are almost no materials showing both considerable absorption of low frequency energy and poor absorption of high frequency energy. Therefore special perforated acoustic structures are made employing

an air gap which is usually filled with a sound-absorbing material. Such a structure is represented by the classic Helmholtz resonator. A thin plate with varied perforation percentage is used in such a resonator with an air gap left behind it. The air gap is filled with a sound-absorbing material.

The aim of this work is to design a resonant structure that would be characterized by high absorption of low-frequency sound energy and poor absorption of the high-frequency one. The essence of the structure is that, in contrast to the Helmholtz resonator, a thick rigid plate without perforation is used, while the sound absorption effect is obtained by employing variously-shaped slits several tens centimetres wide and made of planes instead of small holes. These planes form the structure of the sound reflections which is very important for obtaining good acoustics. It is impossible to create an adequate sound reflection structure solely by using the classical Helmholtz resonant structure for the ceiling. In order to apply the proposed acoustic structure for practical purposes one must know how it absorbs sound at different frequencies and how does the absorption depend on the geometric parameters of the resonator.

2. Theory

The sound absorption properties of Helmholtz-type resonators have been investigated by many scientists in various countries. U. INGARD [1], F.P. MECHEL [2], P. GUIGNOUARD [3], B. BROUARD [4], J.F. ALLARD [5] and others have examined the changes in the sound absorption properties and impedances of thin, small-diameter, differently-shaped perforated plates made of various materials depending on the plate thickness and other parameters.

In the slit-shaped acoustic resonator, we will determine both the main resonance and the overtones, i.e. the odd harmonics, the added air masses outside and inside the slit, the energy losses in the case of a closed slit, and the effect of the resonator volume on the sound absorption.

The air gaps between the planes may be examined as holes. The calculated diagram for these gaps is shown in Figure 1.

The sound absorption of such a resonator may be calculated by the formula (1).

$$A = 4\varrho_0 c_0 \frac{\text{Re}\, Z}{|Z_r + Z|^2} S_r\,, \tag{1}$$

where ϱ_0 is the air density; c_0 is the speed of sound in the air; S_r is the area of the resonator; Z is the impedance of the hole; Z_r is the radiation impedance.

It is seen from the formula that in order to obtain the resonator's sound absorption, the impedance of the hole itself Z and the radiation impedance Z_r must be found.

The radiation impedance of the resonator can be computed from the formula:

$$Z_r = \varrho_0 c_0 \frac{k_0^2}{4\pi^2} S_r^2 \int\limits_0^{2\pi} d\varphi \int\limits_0^{\pi/2+j\infty} |D(\gamma,\varphi)|^2 \sin\gamma\, d\gamma\,, \tag{2}$$

where k_0 is the wave number; $D(\gamma,\varphi)$ is the radiation directivity pattern.
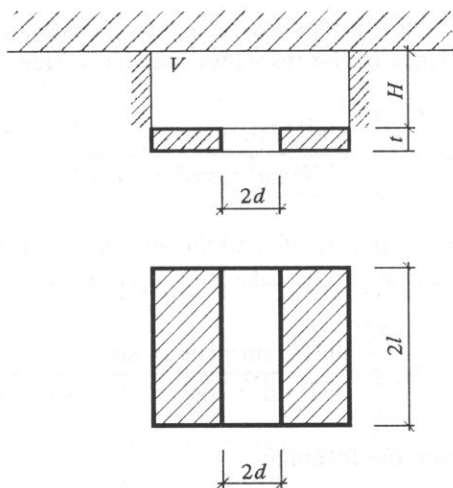
Fig. 1. The calculated diagram for the suspended ceiling with a slit-shaped hole. a) bottom view; b) front view.

The angles of the radiation directivity pattern γ and φ can be determined from the diagram shown in Figure 2.
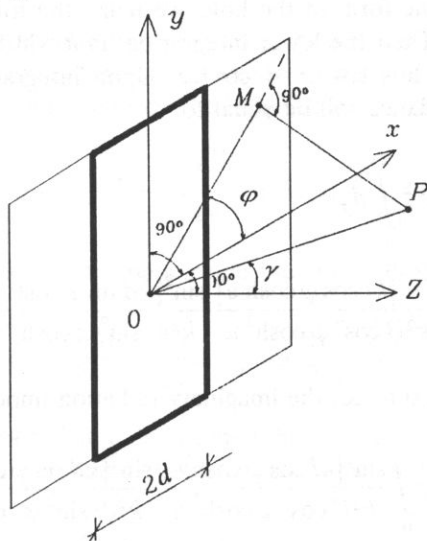
Fig. 2. The diagram for determining the angles γ and φ of the radiation directivity pattern.

In the rectangular hole with the sides a and B, the axis X will be directed along the side a and the axis Y along the side B. Then the radiation directivity pattern will be computed by the formula:

$$D(\gamma, \varphi) = \frac{\sin[kl\cos(r, x)]}{kl\cos(r, x)} \frac{\sin[kd\cos(r, y)]}{kd\cos(r, y)}, \tag{3}$$

where r is the line connecting the origin of the coordinates with the observation point P.

Now we will make the substitutions $\cos(r, x) = \sin \gamma \cos \varphi$ and $\cos(r, y) = \sin \gamma \sin \varphi$. Then the radiation impedance of the resonator may be written as follows:

$$Z_r = \varrho_0 c_0 \frac{k_0^2}{4\pi^2} S_r^2 \int_0^{2\pi} d\varphi \int_0^{\pi/2+j\infty} \frac{\sin^2[kl \sin \gamma \cos \varphi]}{k^2 l^2 \sin^2 \gamma \cos^2 \varphi} \frac{\sin^2[kd \sin \gamma \sin \varphi]}{k^2 d^2 \sin^2 \gamma \sin^2 \varphi} \sin \gamma \, d\gamma . \qquad (4)$$

Let us separate out the real part Re Z_r and the imaginary part Im Z_r of the impedance. The real part of the impedance can be calculated then from the formula:

$$\text{Re } Z_r = \varrho_0 c_0 \frac{k_0^2}{4\pi^2} S_r^2 \int_0^{2\pi} d\varphi \int_0^{\pi/2} \frac{\sin^2[kl \sin \gamma \cos \varphi]}{k^2 l^2 \sin^2 \gamma \cos^2 \varphi} \frac{\sin^2[kd \sin \gamma \sin \varphi]}{k^2 d^2 \sin^2 \gamma \sin^2 \varphi} \sin \gamma \, d\gamma , \qquad (5)$$

and the imaginary part from the formula:

$$\text{Im } Z_r = \frac{\varrho_0 c_0}{j} \frac{k_0^2}{4\pi^2} S_r^2 \int_0^{2\pi} d\varphi \int_{\pi/2+j0}^{\pi/2+j\infty} \frac{\sin^2[kl \sin \gamma \cos \varphi]}{k^2 l^2 \sin^2 \gamma \cos^2 \varphi} \frac{\sin^2[kd \sin \gamma \sin \varphi]}{k^2 d^2 \sin^2 \gamma \sin^2 \varphi} \sin \gamma \, d\gamma . \qquad (6)$$

In order to evaluate the form of the hole, we make the following substitution: $u = \pi/2 - j\gamma$; $du = -j \, d\gamma$. Then the lower integration limit will be equal to zero and the upper one equals $-\infty$. Thus $\cos jx = \cos hx$. Upon integrating from 0 to $-\infty$, the imaginary radiation impedance will be equal to:

$$\text{Im } Z_r = \frac{\varrho_0 c_0}{j} \frac{k_0^2}{4\pi^2} S_r^2 \int_0^{2\pi} d\varphi$$

$$\cdot \int_0^{-\infty} \frac{\sin^2[kl \cos \varphi \cosh u]}{k^2 l^2 \cos^2 \varphi \cosh^2 u} \frac{\sin^2[kd \sin \varphi \cosh u]}{k^2 d^2 \sin^2 \varphi \cosh^2 u} \cosh u (-j \, du). \qquad (7)$$

When integrated from 0 to ∞, the imaginary radiation impedance is:

$$\text{Im } Z_r = \varrho_0 c_0 \frac{k_0^2}{4\pi^2} S_r^2 \int_0^{2\pi} d\varphi \int_0^{\infty} \frac{\sin^2[kl \cos \varphi \cosh u]}{k^2 l^2 \cos^2 \varphi \cosh^2 u} \frac{\sin^2[kd \sin \varphi \cosh u]}{k^2 d^2 \sin^2 \varphi \cosh^2 u} \cosh u \, du. \qquad (8)$$

This is a numerical integration procedure.

In order to calculate the sound absorption area of the resonator, one must find the impedance of the hole itself. It consists of four parts and is expressed as:

$$Z = Z_{m0} + Z_{ma} + Z_{mi} + Z_v , \qquad (9)$$

where Z_{m0} is the impedance of the hole itself; Z_{ma} is the impedance of the added air mass outside the hole; Z_{mi} is the impedance of the added air mass inside the hole; Z_v is the impedance of the resonator volume.
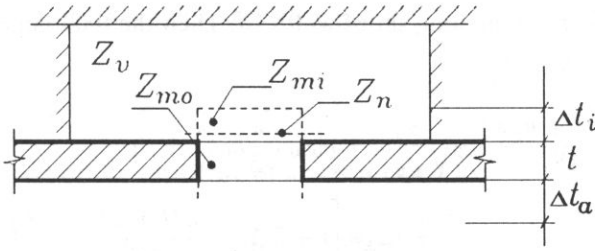
Fig. 3. The lay-out diagram for the hole impedances.

The location of the impedances of the air masses added to the hole are shown in Figure 3.

The fluctuation of the air in the hole may be considered to be of plunger-type provided the velocities of the air particles are uniform over the whole area of the hole. Then the impedance of the hole itself will be equal to:

$$Z_{m0} = \frac{\varrho_0 t}{2r_0}\sqrt{\frac{8\eta}{\varrho_0}}\omega + j\omega\varrho_0 t\left(1 + \frac{1}{2r_0}\right)\sqrt{\frac{8\eta}{\varrho_0\omega}}. \tag{10}$$

The real part of this impedance determines the friction losses that arise when the air moves through the hole. Similar losses must occur on both sides of the hole. Then the impedance of the added air mass outside the hole will be equal to:

$$Z_{ma} = Z_R + \frac{\varrho_0\Delta t_a}{2r_0}\sqrt{\frac{8\eta}{\varrho_0}}\omega + j\omega\varrho_0\frac{\Delta t_a}{2r_0}\sqrt{\frac{8\eta}{\varrho_0\omega}}. \tag{11}$$

The impedance of the added air mass inside the hole will be equal to:

$$Z_{mi} = \frac{\varrho_0\Delta t_i}{2r_0}\sqrt{\frac{8\eta}{\varrho_0}}\omega + j\omega\varrho_0\frac{\Delta t_i}{2r_0}\sqrt{\frac{8\eta}{\varrho_0\omega}}. \tag{12}$$

The added radiation mass that is determined during the calculation of the radiation impedance Z_R must also be included. The radiation impedance Z_R is expressed in the following way:

$$Z_R = R_r + j\omega m_r = R_r + j\omega\varrho_0 r_0, \tag{13}$$

where R_r is the resistivity of the radiation losses.

Upon inserting the formulas (10), (11) and (12) into (9), we obtain the hole impedance:

$$Z_m = \frac{u + (t + u/\pi)}{4S_r}\varrho_0\sqrt{\frac{8\eta}{\varrho_0}}\omega + \varrho_0 c_0(k_0 a_{ef}) + \beta_1 u$$

$$+ j\omega\varrho_0\left[t + 2\Delta t + \frac{u/t + u/\pi}{4S_r}\sqrt{\frac{8\eta}{\varrho_0\omega}}\right] + Z_v, \tag{14}$$

where $k_0 a_{ef} = \dfrac{\pi}{2} k_0 d$ for the long slit of width $2d$. Then the final impedance of the long slit of width a is equal to:

$$Z_m = \frac{u + (t + u/\pi)}{4S_r} \varrho_0 \sqrt{\frac{8\eta}{\varrho_0}} \omega + \varrho_0 c_0 \left(\frac{\pi}{2} k_0 d\right) + \beta_1 u$$

$$+ j\omega\varrho_0 \left[t + 2\Delta t + \frac{u/t + u/\pi}{4S_r} \sqrt{\frac{8\eta}{\varrho_0 \omega}} \right] + Z_v , \qquad (15)$$

where η is the air viscosity; u is the slit perimeter; ω is the angular frequency; β_1 is the coefficient measuring the friction losses and r_0 is radius of the hole.

The impedance of the air volume of the resonator must also be determined. It can be obtained from the formula:

$$Z_v = \varrho_0 c_0 \frac{Z_1 \coth k_0 H + \varrho_0 c_0}{\varrho_0 c_0 \coth k_0 H + Z_1} \frac{S_r H}{V} , \qquad (16)$$

where Z_1 is the impedance of the rigid surface of the ceiling; k_0 is the wave number; H is the height of the resonator; V is the volume of the resonator.

The last factor of this formula represents the relationship between the air column formed along the length of the hole and the volume of the resonator. It arises because the pressure in the air column is a variable and depends on the impedance of the added air mass inside the hole. This member characterizes the transfer of pressure to the whole volume of the resonator since the pressure undergoes changes over the whole resonator.

If the rigid surface of the ceiling is characterized by the absorption factor α, then

$$Z_1 = Z_0 \frac{1 + \sqrt{1 - \alpha}}{1 - \sqrt{1 - \alpha}} . \qquad (17)$$

The final impedance of the rectangular slit is obtained for the case when the angle of the sound wave incidence is normal. If this angle θ is not equal to $0°$, the sound reflection coefficient must be computed from the formula:

$$R_{\text{refl}} = \frac{Z_0 - Z_0 \cos\theta}{Z_0 + Z_0 \cos\theta} \qquad (18)$$

and from the sound absorption factor $\alpha = 1 - |R_{\text{refl}}|^2$ which depends on the angle of the sound wave incidence θ. In the case of a diffusional sound field, this angle must be averaged over all angles of incidence, i.e. integrated for all angles of incidence from $0°$ to $90°$.

The slit may be covered with various materials with different density and air resistance. Then the loss impedance will be expressed by the formula:

$$Z_n = R_n + jY_n , \qquad (19)$$

where R_n is the real part of the loss resistivity; Y_n is the imaginary part of the loss resistivity.

The real part of the resistivity of losses is equal to:

$$R_n = \varrho_0 c_0 \left[1 + \left(\frac{\varrho_0 f}{r_{\text{din}}} \right)^{-0.754} \cdot 0.0571 \right].$$

(20)

The imaginary part of the resistivity of losses is equal to:

$$Y_n = \varrho_0 c_0 \cdot 0.087 \left(\frac{\varrho_0 f}{r_{\text{din}}} \right)^{-0.0732}$$

(21)

where r_{din} is the air resistivity.

The air resistivity is characterized by the lowest frequency starting from which the loss resistivity increases as $\sqrt{f}$.

3. Results of computations

It was established by computation how do the sound absorption area of the resonator, the imaginary parts of the slit impedance and the radiation impedance, and the real and imaginary parts of the resonator volume impedance change with changes in the slit width and the distance to the rigid surface. The thickness of the plate was chosen as 2 cm. The minimal sound absorption factors of the ceiling surface were assumed, i.e. $0.02 - 0.04$ through the whole frequency range. 100 points are taken for the calculation of each curve. It is assumed in all the computations presented that the angle of incidence of the sound wave is normal.
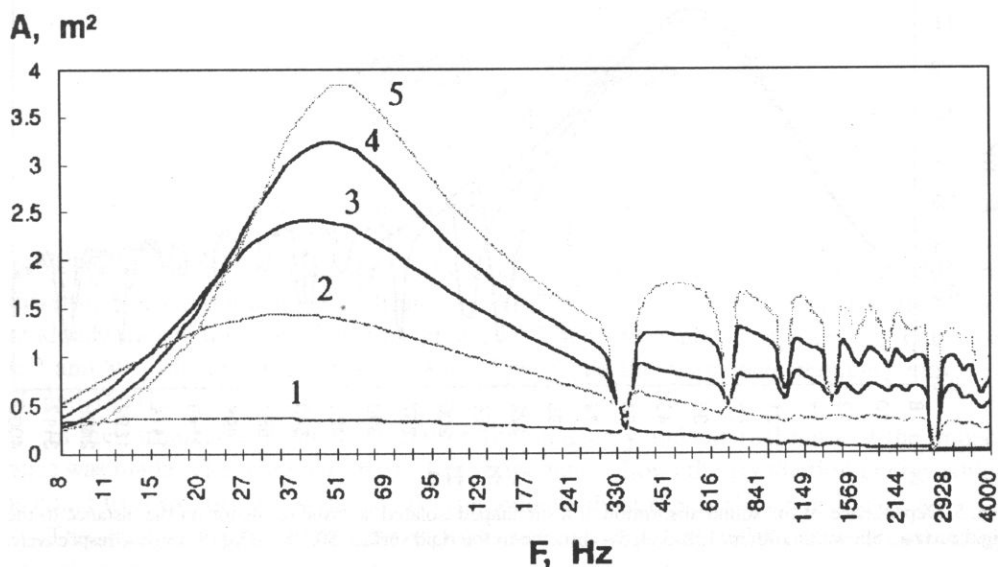

Fig. 4. Dependence of the sound absorption of the slit-shaped isolated acoustic resonator on the width of the slit. The distance to the rigid surface 50 cm. 1, 2, 3, 4, 5 – slit width 5, 20, 35, 50, 65 cm, respectively.

Figure 4 shows the changes taking place in the sound absorption of the resonator with changing slit width. The length and the width of the resonator were assumed to be 200 cm each, while the slit width was increased every 15 cm. The height of the resonator, i.e. the distance to the rigid surface was taken as 50 cm. A computer program has been developed that allows free variation of the geometric parameters of the resonator.

The computations show that the sound absorption is strongly dependent on the width of the slit. When the width is as small as 5 cm, the absorption value is very low too. The absorption increases rapidly with the increase in the slit width and reaches almost $4 \, m^2$ at the slit width of 65 cm. The absorption has a distinct resonant character. It reaches a maximum at $40 - 50 \, Hz$, i.e. at very low frequencies. When the width of the slit increases, the absorption and the width of the resonant curve increases too. At medium and high frequencies – starting from 350 Hz, – the absorption is lowered and repeated resonances are pronounced in this range. They are influenced by the interaction between the impedances of the slit, of the added air masses and of the resonator volume as well as by the overtones determined in the computations.

A quite different character of absorption is obtained when the height of the resonator H is changed, at a remaining constant slit width. When the slit width is only 5 cm and the height changes from 5 cm to 105 cm at 25 cm intervals, the sound absorption area is as small as $0.3 \, m^2$ and does not depend on the slit width. The absorption has a maximum at 30 Hz and decreases uniformly with the increase in frequency.

It is also important to know how the resonator sound absorption changes with changes in the resonator's height and volume if the slit width is kept constant. The results of computations are shown in Figure 5.

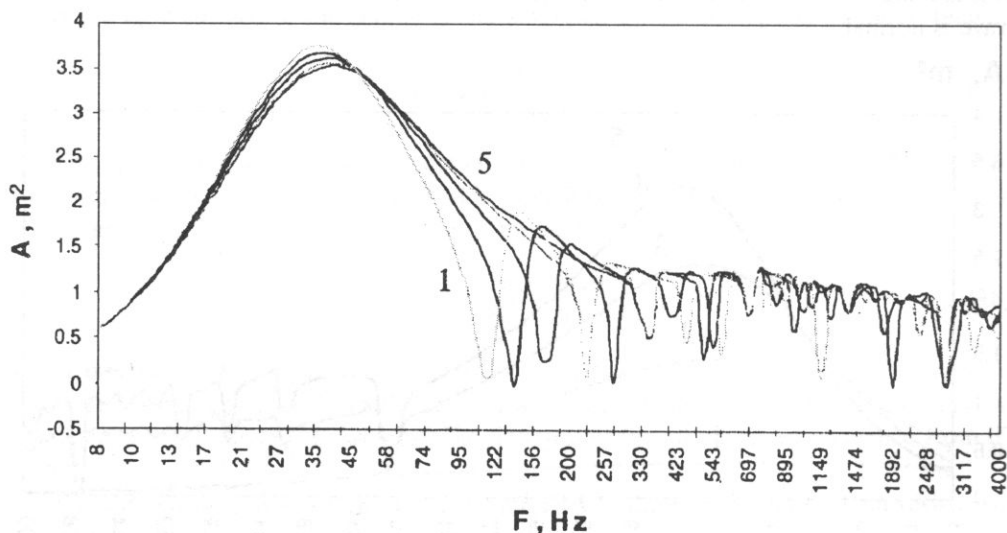Fig. 5. Dependence of the sound absorption of a slit-shaped isolated acoustic resonator on the distance to the rigid surface. Slit width 100 cm. 1, 2, 3, 4, 5 – distance to the rigid surface 50, 75, 100, 125, 150 cm, respectively.

Sound absorption has a quite different character when the volume of the resonator is changed. At low frequencies, the absorption is practically independent of the height

of the resonator. It has a maximum at 37 Hz and achieves as much as 3.5 m². As the frequency increases, the absorption value decreases sharply and in the remaining part of the frequency range it is determined by the repetitive air volume resonances.

The results of the computations show that an isolated acoustic resonator, whose dimensions are 200 × 200 cm and the slit width is only 30 cm, absorbs as much as 3.5 m² of sound energy. The resonator is made of a rigid material whose sound absorption coefficients are very small. Consequently, sound energy is only absorbed by the rectangular-shaped slit which is only 30 cm wide and 0.6 m² in area. Thus, a slit of 0.6 m² in area absorbs as much as 3.5 m² of the sound energy.

The sound absorption coefficient of acoustic materials used in practice is always smaller than one. In our case the coefficient is very large – 5.8. Such coefficient is obtained under resonance only, when, in the frequency range of one to two octaves, the absorbing surface grows in area considerably and the sound absorption is therefore increased. This happens because the air velocity decreases due to friction when the air moves close to the rigid surface. The air flows around the entire plate, but the velocity of fluctuations and sound absorption are the largest in the slit; they are much larger than on the plane. When the wavelength is substantial, then the velocity of fluctuation of air particles is very low far from the slit and no sound absorption takes place on the plane. Sound is only absorbed by the environment close to the slit.

Up to the present, the sound absorption was examined in the case when the angle of incidence of the sound wave is a right one. Figures 6 and 7 show the changes in the sound absorption under other angles of incidence.
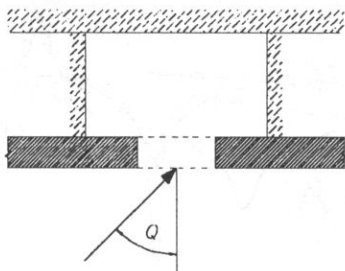
Fig. 6. Diagramm of the angle of incidence of the sound wave to the resonator.

When the angle of incidence of the sound wave is small, i.e. 20°, 23° and 50°, the increase in absorption is insignificant – from 2 m² to 2.5 m². The resonance frequency gradually moves towards higher frequencies. When the angle of incidence is large, i.e. 65° and 80°, the absorption rises to 3 – 3.5 m², while the resonance frequency moves to 70 and 150 Hz.

In the formulas, a distinction between the imaginary and the real parts of the impedance was made. The imaginary part of the impedance shows the reradiation energy which is equal to zero during resonance. The impedance dynamics is shown in Figure 8.

The imaginary parts of the slit increase with growing slit width and decrease along with the increase in frequency. At high frequencies, repetitive resonances are pronounced. The imaginary parts of the radiation impedance decrease as the slit width increases; they also grow along with the increase in frequency, but only at low frequencies.

V. STAUSKIS
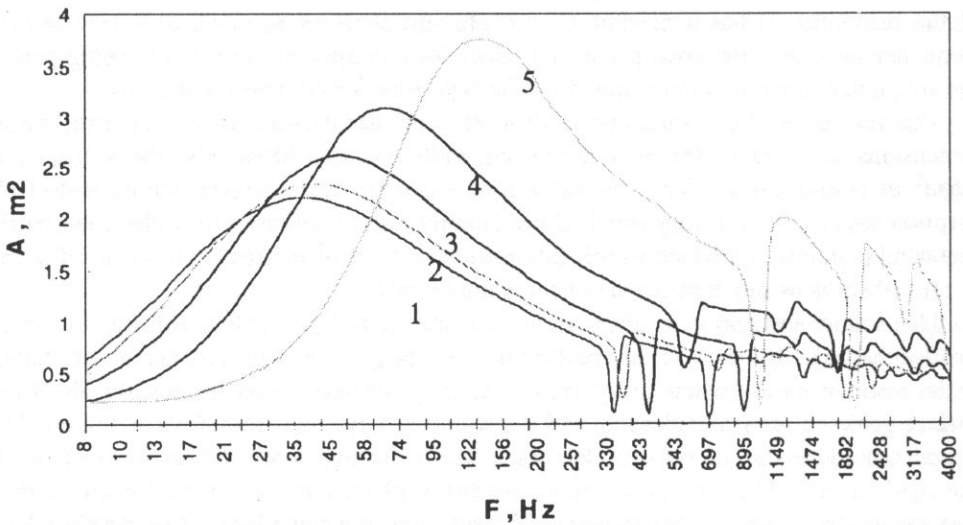
Fig. 7. The relationship between the sound absorption of a slit-shaped resonator and the angle of incidence of the sound wave. Distance to the rigid surface. Slit width 30 cm. 1, 2, 3, 4, 5 – sound wave incidence angles 20°, 35°, 50°, 65°, 80°, respectively.
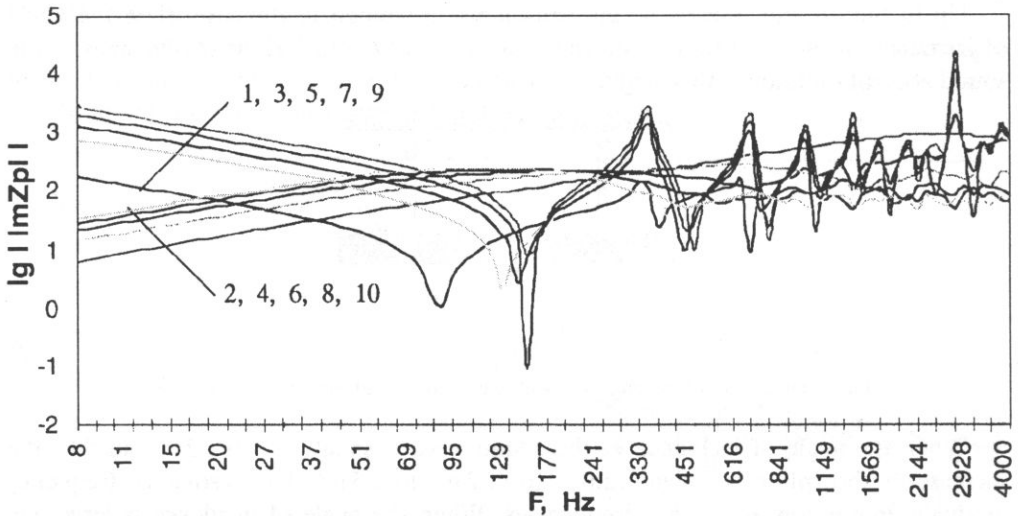
Fig. 8. Dependence of the imaginary part of the slit impedance and the imaginary part of the radiation impedance on the slit width in a slit-shaped isolated acoustic resonator. The distance from the slit to the rigid surface 50 cm. 1, 3, 5, 7, 9 – the imaginary parts of the slit impedance when the slit width is 5, 20, 35, 50, 65 cm, respectively. 2, 4, 6, 8, 10 – the imaginary parts of the radiation impedance when the slit width is 5, 20, 35, 50, 65 cm, respectively.

Figure 9 shows the changes in the real and imaginary parts of the resonator's volume impedances.

Energy losses are shown by the real parts of the impedance. Their dynamics is shown in Fig. 9.
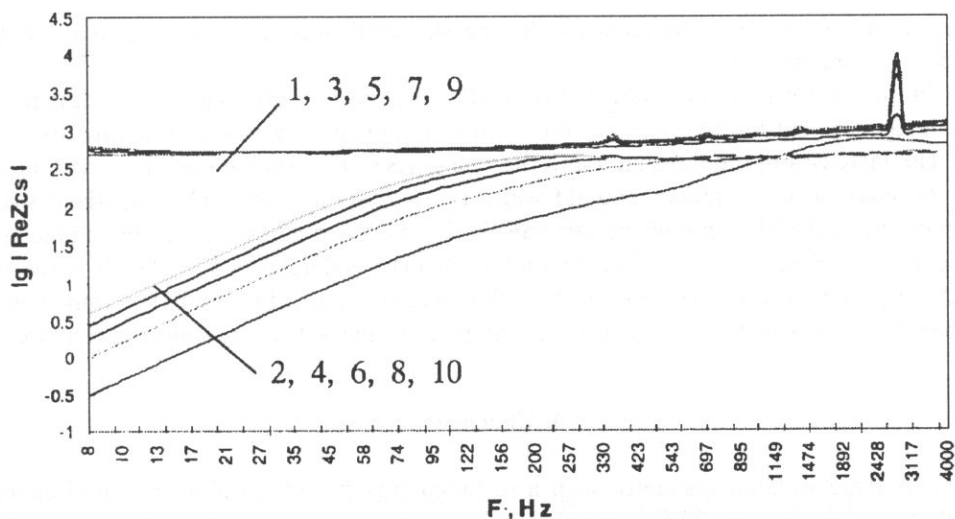
Fig. 9. Dependence of the real part of the slit impedance and the real part of the radiation impedance on the slit width in a slit-shaped isolated acoustic resonator. The distance from the slit to the rigid surface 50 cm. 1, 3, 5, 7, 9 – the real parts of the slit impedance when the slit width is 10, 30, 50, 70, 90 cm, respectively. 2, 4, 6, 8, 10 – the real parts of the radiation impedance when the slit width is 10, 30, 50 70, 90 cm, respectively.

The real part of the slit impedance is independent of the slit width and frequency, while the real part of the radiation impedance increases with the increase in frequency
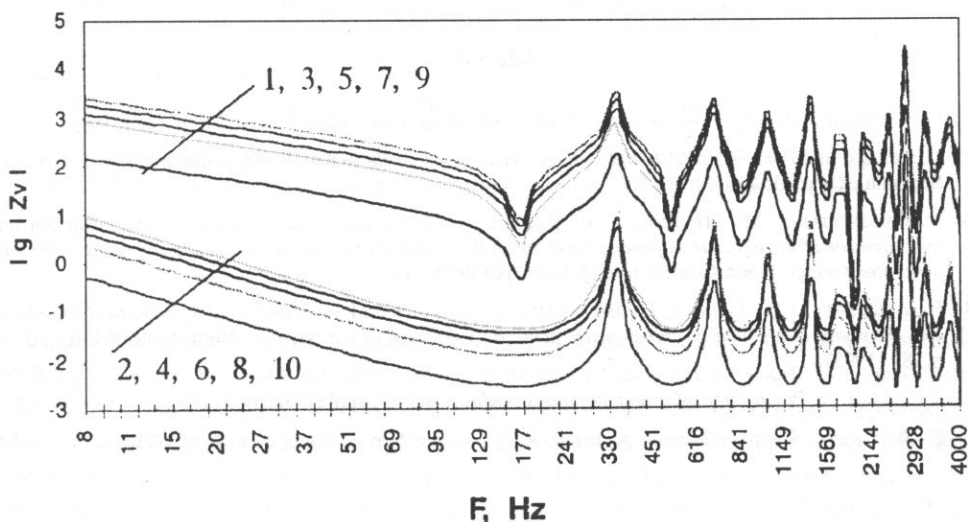
Fig. 10. Dependence of the real and imaginary parts of the volume impedance on the slit width in a slit-shaped isolated acoustic resonator. The distance to the rigid surface 50 cm. 1, 3, 5, 7, 9 – the real parts of the volume impedance when the slit width is 5, 20, 35, 50, 65 cm, respectively. 2, 4, 6, 8, 10 – the imaginary parts of the volume impedance when the slit width is 5, 20, 35, 50, 65 cm, respectively.

but only up to medium frequencies. As the slit width increases, the real part of the impedance increases too.

The resonator's sound absorption is greatly influenced by its volume. The changes in the imaginary and the real parts of the volume impedance are shown in Figure 10.

The increases in the imaginary and the real parts of the volume impedance produced by the increase in frequency and slit width are almost the same. The impedances are influenced by the elasticity of the resonator's air which is determined by the volume and height of the closed air mass. The fluctuating air mass is determined by the air in the slit and the added air mass, which is given by the imaginary part of the radiation impedance. When the air elasticity is equal to the fluctuating air mass, the resonance takes place.

4. Conclusions

1. A large isolated resonator with a rectangularly-shaped slit absorbs sound energy well at low frequencies. The sound absorption increases rapidly with the increase in slit width, while the frequency at which the maximum absorption is reached changes a little. Greater sound absorption is obtained when the height of the resonator, but not the slit width is increased.

2. The real parts of the slit impedance depend on the slit width and frequency, whereas the imaginary parts are little frequency-dependent. The imaginary and the real parts of the resonator's volume impedance depend only on the frequency and the slit width up to medium frequencies. As frequency increases the impedances are determined by repetitive resonances.

References

[1] F.P. MECHEL, *About perforated metal sheets on absorbing layers*, Acta Acustica, 1, p. 175 (1993).

[2] U. INGARD and R.H. BOLT, *Absorbtion characteristics of acoustic materials with perforated facings*, J. Acoust. Soc. Am., 23, p. 533 (1991).

[3] P. GUIGNOUARD, M. MEISSER, J. F. ALLARD, P. REBILLARD and C. DEPOLLIER, *Prediction and measurement of the acoustic impedance and absorption coefficient at oblique incidence of porous layers with perforated facings*, Noise Control Engng. J., 36, p. 129 (1991).

[4] B. BROUARD, J.F. ALLARD, H. BRUNEAU, W. LAURIKS and C. VERHAEGEN, *Acoustical impedance and absorption coefficient of porous layers covered by a facing of parallel slits*, Noise Control Engng. J., 41 p. 289 (1993).

[5] J.F. ALLARD, *Propagation of sound in porous media*, Elsevier Applied Science (1993).

[6] E. SKUDRZYK, *The foundation of acoustics*, V. 2, Springer-Verlag, Wien, New York 1971.

THE INFLUENCE OF A CROSS-SHAPED RESONANCE CEILING ON THE HALL ACOUSTICS

V. STAUSKIS

Vilnius Gedimino Technical University
(Saulétekio al. 11, 2040 Vilnius, Lithuania)

The results of investigations of the influence of a suspended ceiling with cross-shaped slits on the hall reverberation time, sound absorption coefficients, sound absorption of the entire hall, acoustic centre of gravity and musical sound clarity index C 80 are presented.

The investigations were conducted in a scaled physical model of the hall M 1 : 25. The selection of the scale and materials of the model is substantiated. The main characteristics of the spark sound source and the analogue-code transducer are quoted.

The investigations revealed that 100 cm wide slits between the suspended ceiling planes located 100 cm from the rigid surface of the ceiling reduce the reverberation time by 1.14 s at resonant frequencies of 200 Hz and 250 Hz. An increase of the height of the suspended ceiling up to 400 cm is of importance only at low frequencies.

The sound absorption coefficients show a maximum increase at the resonant frequencies of 200 Hz and 250 Hz, the increase being proportional to the decrease in the height of the suspended ceiling. When the height equals 400 cm, the absorption coefficients tend to decrease rather than increase throughout the whole frequency range except for the resonant frequencies.

The overall sound absorption of the hall is increased to 60 m² only at the resonant frequencies and at the ceiling height of 100 cm. At the height of 400 cm, the absorption is reduced by $60 - 100$ m² throughout the frequency range, though the reverberation time is also reduced.

The resonant suspended ceiling affects the acoustic centre of gravity and the music sound clarity index.

The changes in all the above-mentioned acoustic indicators are determined solely by the cross-shaped slits between the ceiling planes. No additional sound-absorbing materials were used.

1. Introduction

For the optimization of the reverberation time in a hall, a certain quantity of sound-absorbing materials with apropriate acoustic characteristics must be used. The reduction of the reverberation time is most often necessary only at low frequencies because at medium and high frequencies the sound is well absorbed by the audience and the air. There exist acoustic materials that are characterized by an easy sound absorption at low frequencies, however, at the same time they absorb sound also at medium and high frequencies which is often undesirable.

A resonant suspended ceiling with cross-shaped slits formed by the space between the ceiling planes may constitute a sound-absorbing structure. The slits may be quite wide, reaching one metre or more, while the suspended ceiling itself may be located at

various distances from the rigid surface. Such a ceiling structure both absorbs the sound energy and reflects sound waves of various length from the planes. This is useful for the formation of the hall reflection structure. Furthermore, slits between planes may be found also in real halls. Therefore the knowledge of how such resonant ceilings absorb sound energy is very important.

The resonant suspended ceiling was examined theoretically earlier [1, 2, 3]. The aim of the present paper is to determine the influence of the resonant suspended ceiling on the acoustic indicators of the hall by means of studies conducted with a physical model of the hall.

2. The peculiarities of modelling of the hall

To the factors influencing the hall acoustics belong the width and form of the slits of the suspended ceiling, the distance between the ceiling and the rigid surface, the absorption of the hall walls and the absorbing material that may be placed above the plane of the suspended ceiling. There are thus many variables. It is absolutely clear that there exists no possibility for determining the acoustic effect of such variables in a real hall. The best results are therefore expected from the investigation of acoustic processes in the physical model of a hall.

If the model is similar to the original by its geometrical parameters and is executed on a linear scale, n_l, then, upon meeting the corresponding initial and boundary conditions, one may expect a similarity of the acoustic processes in the air volume of the model and the original hall. From the condition $n_l = n_L$ it follows that the similarity will occur in the model at frequencies $f_m = f_{or} n^{-1}$.

2.1. Scale and materials of the model

A recording studio hall of a symphony orchestra was chosen for the investigation. Its dimensions are $34 \times 22 \times 12.7$ m. The model scale of 1 : 25 was selected for such big a hall. Consequently, the frequencies of both the model and the original must meet the condition $f_m = f_{or} n^{-1}$, i.e. model frequencies must be 25 times higher than those of the original. When investigating the real hall acoustics, the frequency range of $100 - 4000$ Hz was used. If the scale of 1 : 25 is used, the frequency range must be expanded to $2500 - 100000$ Hz, occupying a large ultrasound area.

There exist difficulties in the area of boundary conditions. In the cases when the planes in the original hall are made of isotrophic materials, in which energy losses are incurred due to internal friction, these materials may be characterized by the Young and shift modules. The boundary conditions mean that the model structures must be executed to the scale and complex modules of both the original and the model and must be equal at certain frequencies. Consequently, at certain frequencies the loss coefficients must be equal for the model and the original. In practice, such requirements may be fulfilled only in a few materials, e.g., in concrete, and solely for the frequency range in that the loss coefficients are not frequency-dependent. It is impossible to make a model of such materials; therefore materials used for the model are different from those of the original.

While the surfaces of the original are characterised by the complex impedance Z_{or}, which does not depend on the sound wave incidence angle, the boundary conditions for the internal planes of the model must satisfy the condition that the impedances of the original and the model are equal at frequencies of f_{or} and f_m respectively, i.e.

$$Z_m(f_{or} \cdot n_L^{-1}) = Z_{or}(f_{or}). \tag{1}$$

In practice, the reverberational sound absorption coefficients are chosen for the model's materials in such a way that they equal approximately the original's absorption coefficients at corresponding frequencies $f_m = f_{or} \cdot n_L^{-1}$. However, these are not exact boundary conditions.

In the model, all wall and floor planes are made of a fabric-based laminate. Its absorption coefficient at 10 Hz is 0.15 [4]. The suspended ceiling is made of plywood 6 mm thick, lacquered three times along the entire contour. Its absorption coefficients were close to those of the fabric-based laminate. The orchestra dais was closed with a 5 mm thick flannel, the absorption coefficient of which being about 0.5–0.6.

2.2. Sound absorption in air

Difficulties arise when, conducting investigations in a model, one must estimate the sound absorption in air because the frequency range embraces an ultrasound area in that the sound absorption is very large. The sound wave that is transmitted in the model over a fixed distance loses part of its intensity. This may be characterized by the multiplier e^{-mx}, where m is the attenuation index. It consists of two components m_1 and m_2. The first one describes the density and the heat conductivity of the air. It is proportional to the frequency square and depends on the temperature of the air. The second component characterizes the molecular absorption in air. It reaches its maximum when $\omega = 1/\tau$, where τ is the process relaxation time, i.e. the time per which the pressure is reduced e times. The relative humidity of the air has a considerable influence on this component; when it increases, the index m is also increased and the sound absorption is determined by the molecular absorption. WINKLER [5] has established that sound absorption increases with the increase in frequency, while the absorption maximum moves towards greater relative humidity. The condition of similarity of absorption in the air of both the model and the original will be satisfied when, under the corresponding frequencies, $m_m = m_{or} \cdot n_L^{-1}$. The sound absorption in air may be reduced by making the model hermetic and filling it with a gas of lower attenuation index, e.g. nitrogen. Then there would be no molecular absorption up to 100 kHz – it is clear that such conditions are hardly feasible.

All the results obtained from the examinations made within this work are relative ones.

3. Methods of investigation

A special flow chart was used for recording the acoustic signals in the model. It consists of a sound source, a microphone, a microphone amplifier, an analogue-code transducer and a computer signal-analyzing program.

A spark impulse was used as sound source. It was formed by a spark generator with preset technical parameters specially produced by us. Its main acoustic characteristics include the impulse duration, power, spectrum and form. The duration of the impulse may be regulated from 0.36 ms to 0.14 ms. The power and the spectrum maximum of the impulse may also be altered. Under the maximum power, the spectrum maximum is at 16 kHz, while at minimum power the maximum is reached at 31 kHz. At the maximum impulse power, the sound energy radiated is eight times greater than that radiated at minimum power. A maximum impulse power was chosen for the investigation because the maximum radiated sound energy is concentrated on lower frequencies. In this case, the radiation of high frequencies is worse; therefore insufficient dynamic range is obtained when determining certain acoustic indices. The spark impulse results in a spheric directivity diagram. The impulses emitted by the generator are stable, the automatic and remote control over them being possible.

A 1/4" microphone was used for the investigations. Its sensitivity up to 100 kHz is sufficient and its frequency characteristics are flat in the frequency range 0.1–70 kHz. In order to improve the directivity diagram at high frequencies, the microphone was erected vertically using a hole in the floor.

The analogue-code transducer was constructed according to preset characteristics. Its purpose is to convert analogue signals for their further processing into a digital form. The nominal level of the incoming signal is ± 1 V. The resolution of the transducer is 12 bits; the time of conversion is 2 μs and the time of quantization is 5 μs. The quantization frequency is 200 kHz.

For the purpose of analysis of the investigation results, the lower frequency limit of 50 Hz was chosen instead of 100 Hz. In the model's scale of 1 : 25 this would be 1250 Hz instead of 2500 Hz. The aim is to determine how resonators absorb sound energy at very low frequencies because the range of low frequencies is very important and the most interesting physical processes usually take place in it. The upper limit of the frequency range was chosen as 2000 Hz, or 50 kHz in the model. This has been done for two reasons: at the quantization frequency of 200 kHz and the upper limit of the frequency range of 50 kHz, the Nyquist frequency ratio is equal to 4.0, and more exact results are obtained when this frequency ratio is higher; too low a dynamic range is obtained when approximating the attenuation of the sound field at frequencies exceeding 2000 Hz. In my opinion, however, such upper range limit is quite acceptable because just at the low and medium frequencies the resonant ceiling will have the greatest impact on the hall acoustics.

The main acoustic indices of the model were analyzed by means of a specialized computer program developed by our own efforts.

The sound-absorbing material flannel was spread in the floor area occupied by the orchestra players. The area is 119 m². It was possible to locate the microphones at three points: close to the sound source, far from it and above the suspended ceiling. The experiment was planned in such a way that it would be possible to determine the dependence of the main acoustic indices on the form and width of the slits of the suspended ceiling, on the distance between the ceiling and the rigid surface, and on the absorption in the hall and by the suspended ceiling.

In this paper we will present the results of the investigation of the effects of the resonant ceiling from the rigid surface on the acoustic indices when the slit width is constant.

4. Results of investigations

A resonant suspended ceiling with the cross-shaped slits between the planes was chosen for the investigation. The section of the hall and its plan are schematically represented in Figs. 1 and 2.
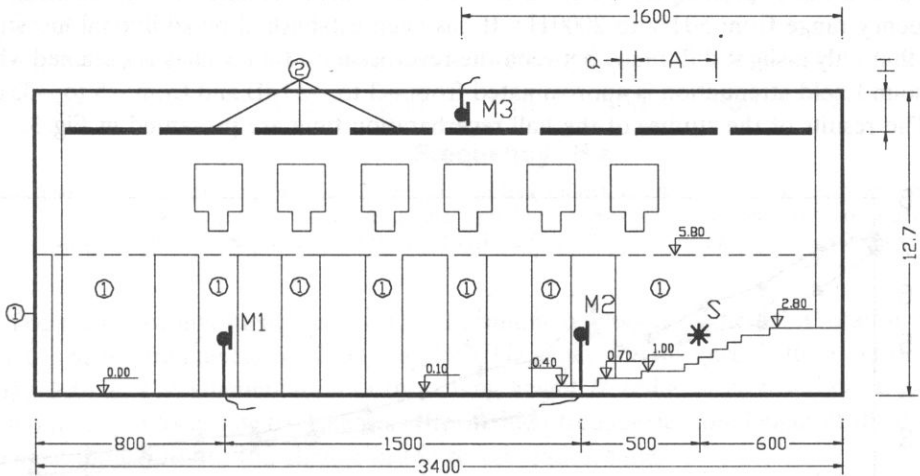
Fig. 1. The longitudinal section of the hall with the resonant suspended ceiling. S – sound source; M1, M2, M3 – positions of the microphones; 1, 2 – possible points of location of the sound-absorbing materials.
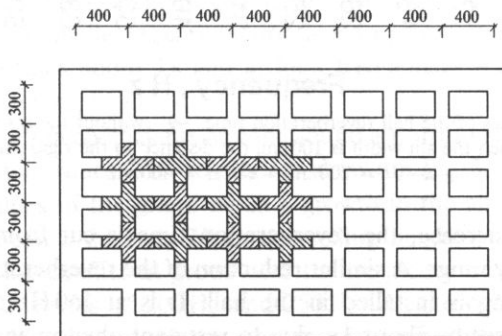
Fig. 2. Plan of the resonant suspended ceiling with cross-shaped slits between the planes.

By examining the influence of such a ceiling on the hall acoustics, we will establish its reverberation time, the index of purity of the music sound, and the acoustic centre of gravity. On the basis of the reverberational sound-field attenuation curves, the sound

absorption coefficients and the overall sound absorption will be computed in the case of a hall with no suspended ceiling and in that with the suspended ceiling.

When computing the values of the reverberation time from the sound-field attenuation curves, there arose the question about the point from which the evaluation of the attenuation should be started. In the computation of the standard reverberation time, the sound-field attenuation is approximated by evaluating the level from -5 dB to -35 dB. In our case, however, a too narrow dynamic range is obtained at high frequencies. It may be expanded by increasing the power of the impulse. It is still not sufficient because the resolution of the 12-bit transducer is too low. For this reason the attenuation of the sound-field was approximated from -3 to -33 dB. Reliable results were obtained in the frequency range from 50 Hz to 2000 Hz. It has been established by additional investigation that only a slight difference between the reverberation time values is obtained when the sound-field attenuation is approximated from -3 to -33 dB and from -5 to -35 dB.

The results of the studies of the hall reverberation time are presented in Fig. 3.
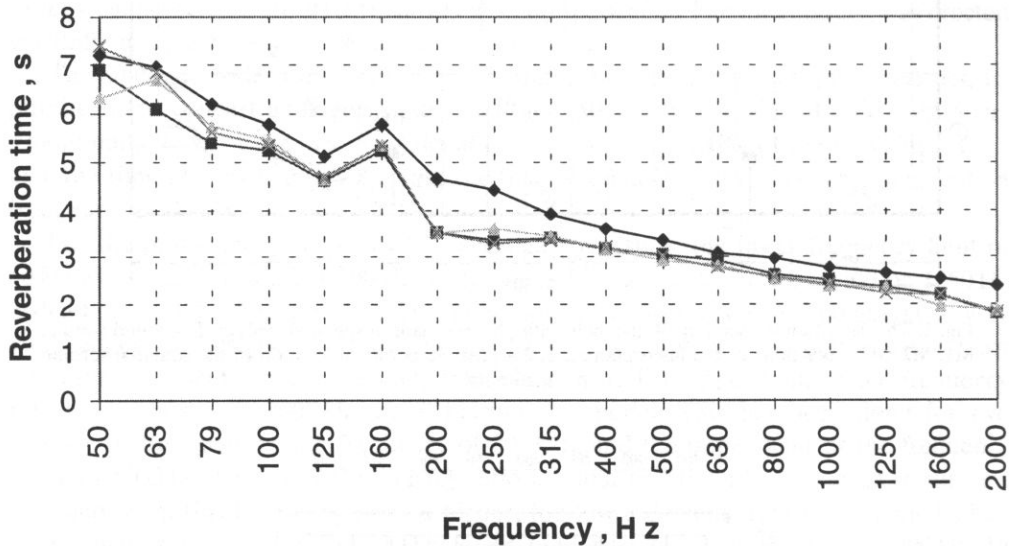
Fig. 3. Frequency characteristics of the hall reverberation time. —♦— without the resonant suspended ceiling; —■— with the ceiling when the slit width is 100 cm, the distance to the rigid surface $H = 100$ cm; —▲— $H = 200$ cm; —×— $H = 400$ cm.

As the frequencies increase, the reverberation time is cut from 7 s to 2.5 s evenly throughout the frequency range. A similar reduction of the reverberation time is observed when the resonant ceiling is installed in the hall. It is at 160 Hz only that this index increases, in all study cases by about 1 s, due to resonant phenomena.

It is very inconvenient to analyze the reverberation time changes in the hall with the resonant ceiling from such a graph. Therefore all investigation results presented below will be relative ones, taking as zero line the results for the hall with no suspended ceiling.

The relative changes in the reverberation time for the hall with a suspended ceiling are shown in Fig. 4.

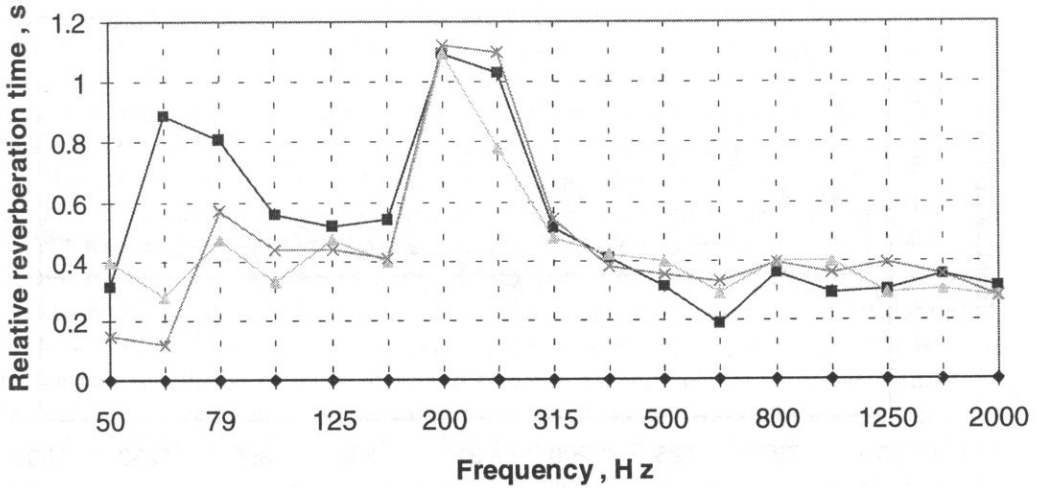Fig. 4. The relative dependence of the hall reverberation time on the distance from the resonant suspended ceiling to the rigid ceiling surface. Slit width 100 cm. Zero line corresponds to the case when no suspended ceiling is installed. —■— distance to the rigid surface $H = 100$ cm; —▲— 200 cm; —×— 400 cm.

The results of investigations reveal a maximum reduction of the reverberation time by 1.14 s at the frequencies of 200 Hz and 250 Hz, when the distance to the rigid surface equals 100 cm. The augmentation of the ceiling height H reduces the reverberation time by about $0.2 - 0.5$ s at low frequencies only. At high frequencies, the height of the ceiling is almost immaterial to the change in the reverberation time.

The early reverberation time is very important for the evaluation of the hall acoustics. It is connected with the early sound reflections and the subjective evaluation of music. The results of the studies are presented in Fig. 5.

In this case, a considerable reduction of the reverberation time of 3 s is obtained when the distance between the suspended ceiling and the rigid surface is 400 cm. When the height of the ceiling is smaller, this reduction has no pronounced resonant character. At low frequencies it equals about 1 s and at high frequencies – about 0.5 s and is almost independent of the ceiling height.

The sound absorption coefficients and the sound absorption area were calculated from the reverberation time values. The results are shown in Fig. 6.

The negative values of the graph mean a growth in the absorption coefficient, while the positive ones mean a decline. When the ceiling height is small and equals 100 cm, the relative absorption coefficient grows over the frequency range reaching its maximum at the resonant frequencies of 200 Hz and 250 Hz. As the ceiling height increases, the character of the change in the relative absorption coefficient remains the same. When the ceiling height is 400 cm, however, the coefficient does not show an increase at low and high frequencies as expected but, on the contrary, is smaller. Thus, the absorption coefficient decreases along with the reduction of the reverberation time.

At the resonant frequencies of 200 Hz and 250 Hz, the reverberation time is shorter by about 1 s. Consequently, the absorption coefficients should be high at these frequencies.

Fig. 5. The relative dependence of the early reverberation time EDT on the distance from the resonant suspended ceiling to the rigid ceiling surface. Slit width 100 cm. The zero line corresponds to the case when no suspended ceiling is installed. —■— distance to the rigid surface $H = 100$ cm; —▲— 200 cm; —×— 400 cm.
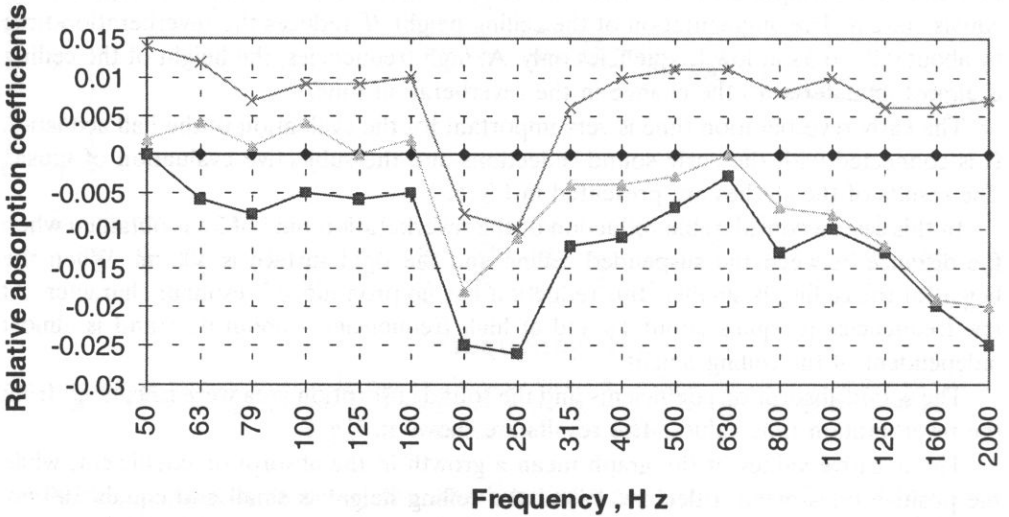
Fig. 6. The relative dependence of the sound absorption coefficients on the distance from the resonant suspended ceiling to the rigid ceiling surface. Slit width 100 cm. The zero line corresponds to the case when no suspended ceiling is installed. —■— distance to the rigid surface $H = 100$ cm; —▲— 200 cm; —×— 400 cm.

The relative values of the coefficient, however, are small. When no suspended ceiling is installed in the hall, its volume is about 9000 m³ and the surface area is 2910 m². The presence of the suspended ceiling reduces the hall volume and the surface area. These

values are again assessed by calculating the above-mentioned indices. Thus, the surface area is assessed twice, whereas the sound energy is only absorbed by the resonant ceiling the area of which is equal to $748\,m^2$ and the area of the slits is $288\,m^2$ only. The overall area of all hall surfaces, i.e. from $2400\,m^2$ to $2790\,m^2$, is assessed in the calculations. For this reason small values of the absorption coefficients are obtained.

The lowering of the sound absorption coefficient along with shortening of the reverberation time may be explained by the fact that when the distance between the suspended ceiling and the rigid surface H increases, the hall volume and the surface area are reduced. However, an interesting change in the reverberation time is of importance too. For example, in the hall without a suspended ceiling it equals 5.77 s at 100 Hz, while at $H = 100$, 200 and 400 cm it equals 5.20, 5.44 and 5.33 s, respectively. The volume of the hall is reduced to 8273, 7500 and $6080\,m^3$, respectively. It is interesting to note that when the ceiling height is increased from 100 cm to 200 cm, the hall volume reduces from $8273\,m^3$ to $7500\,m^3$, i.e. by about 9%. In this case the reverberation time should be shorter but only for the hall volume reduction. However, it is longer by 0.24 s, while the absorption coefficient is reduced from 0.089 to 0.08. Such an interesting change in the reverberation time is most probably determined by the sound energy which reaches the listeners from the volume between the suspended ceiling and the rigid surface.

Such a regularity is also observed at other frequencies.

We will assess the change in the overall sound absorption on the basis of the sound absorption coefficients. The results are presented in Fig. 7.
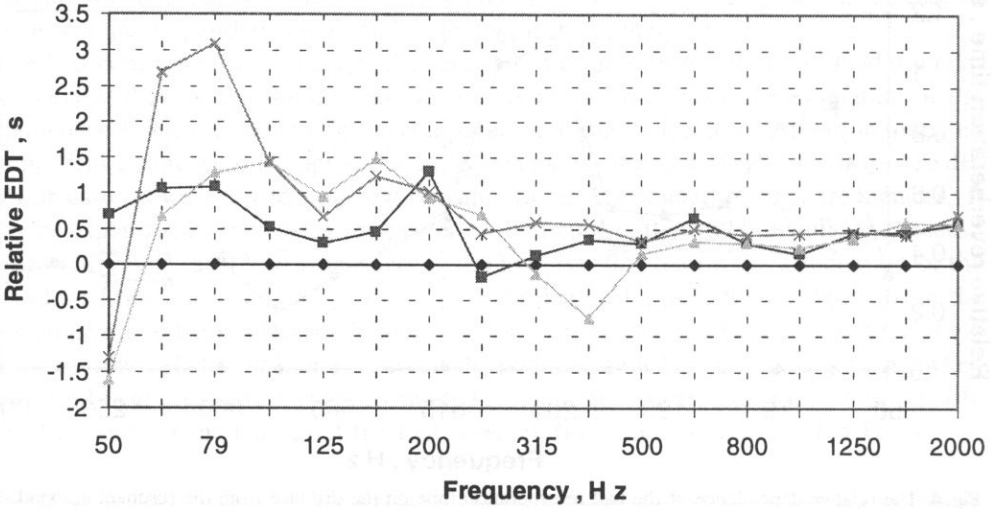

Fig. 7. The relative dependence of the sound absorption on the distance from the resonant suspended ceiling to the rigid ceiling surface. Slit width 100 cm. The zero line corresponds to the case when no suspended ceiling is installed. —■— distance to the rigid surface $H = 100$ cm: —▲— 200 cm; —×— 400 cm.

When the height of the ceiling $H = 100$ cm, the resonant ceiling increases the sound absorption at 200 Hz and 250 Hz up to $60\,m^2$. At low frequencies, the absorption remains almost unchanged, though changes in the reverberation time are marked. As the height

of the ceiling increases, absorption throughout the frequency range becomes smaller in proportion to the increase in H. Here the situation is analogous to the case of the sound absorption coefficients. After the increase in the ceiling height from 200 to 400 cm, the reverberation time is reduced from 5.44 s to 5.33 s, while the absorption area becomes smaller instead becoming larger – from 215 m^2 to 179 m^2. This reduction equals 60 m^2 at low frequencies and as much as 100 m^2 at high frequencies.

The change in the height of the resonant suspended ceiling also influences the change in the acoustic centre of gravity. The results of the investigations are presented in Fig. 8.

Fig. 8. The dependence of the acoustic centre of gravity on the distance from the resonant suspended ceiling to the rigid ceiling surface. Slit width 100 cm; —♦— without resonant ceiling; —■— distance to the rigid surface $H = 100$ cm; —▲— 200 cm; —×— 400 cm.

The change in the acoustic centre of gravity has a similar character both in the hall with the suspended ceiling and in the hall without such a ceiling. At low frequencies up to 160 Hz, the suspended ceiling has almost no influence on the acoustic centre of gravity. This centre is markedly increased, up to 40 ms, at high frequencies due to the influence of the ceiling. A constant growth with the increase in frequency is unexpected in all the studied cases.

The objective acoustic indices of the hall correlate with the subjective ones. The music sound clarity index is one of the most important. The results of the investigations are shown in Fig. 9.

Here the low frequency range may be divided into two parts: up to 160 Hz and above 200 Hz. At the lower frequencies, this index is now increased, now reduced by the suspended ceiling, while its absolute values vary from -7 to -14 dB. This shows that the energy of the late reflections is predominant in this range. Beginning from 200 Hz, the clarity index is increased by the suspended ceiling by $2 - 3$ dB and this increase depends only slightly on the change in the ceiling height.
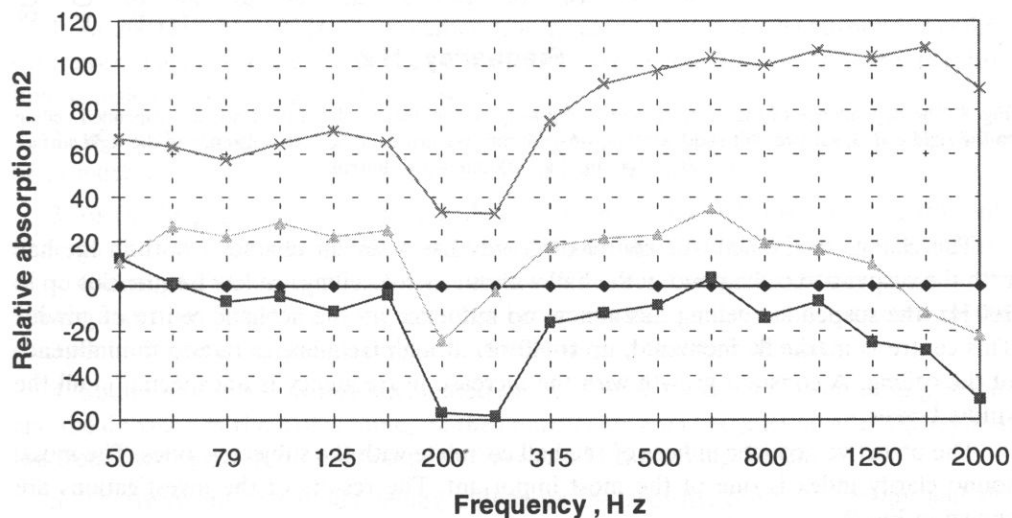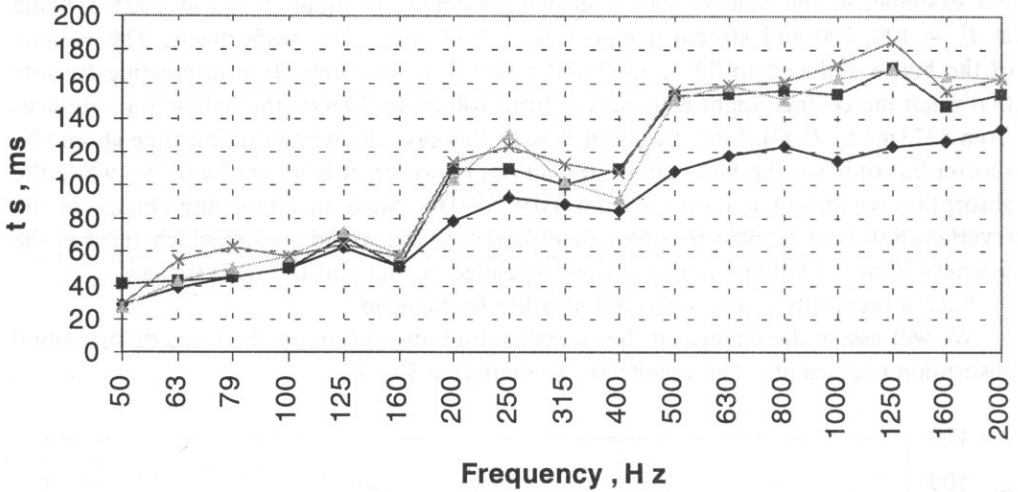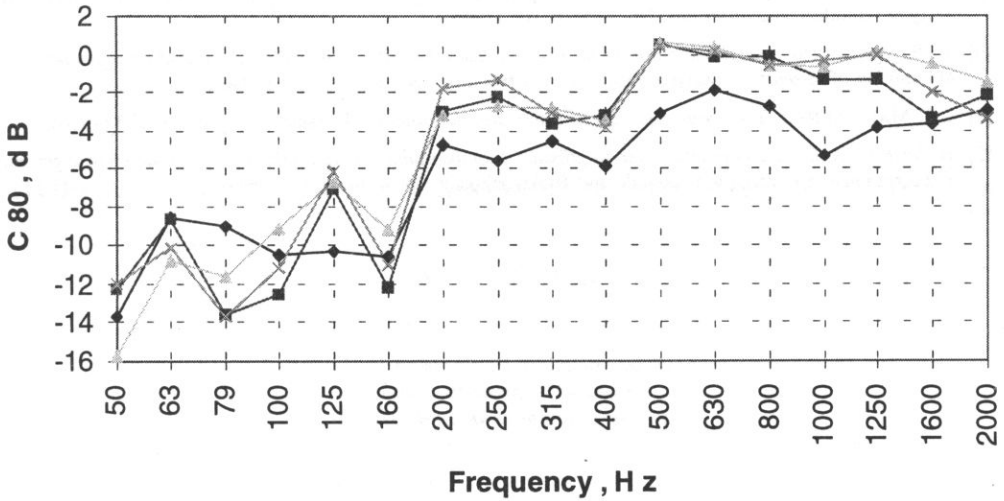
Fig. 9. The dependence of the musical sounds clarity index on the distance from the resonant suspended ceiling to the rigid ceiling surface. Slit width 100 cm. —♦— without resonant ceiling; —■— distance to the rigid surface $H = 100$ cm; —▲— 200 cm; —×— 400 cm.

5. Conclusions

1. At 200 Hz and 250 Hz, the reverberation time is reduced by the suspended ceiling with cross-shaped slits by about 1.14 s. The influence of the slits on the reverberation time is insignificant at high frequencies.

2. When the height of the ceiling equals 400 cm, the early reverberation time is cut by as much as 3 s at 79 Hz and by about 0.5 s at high frequencies.

3. As the height of the suspended ceiling increases, the sound absorption coefficients undergo the greatest rise at the resonance frequencies of 200 Hz and 250 Hz. When $H = 400$ cm, the absorption coefficient does not increase in the frequency range up to 160 Hz and from 315 Hz, as expected, but becomes smaller. This is determined by the changes in the reverberation time, the hall volume and the surface area.

4. Sound absorption is not augmented along with the increase in the ceiling height and the decrease in the hall volume; on the contrary, its area becomes smaller throughout the frequency range in proportion to the increase in the ceiling height.

5. The resonant suspended ceiling influences the acoustic centre of gravity and the music sound clarity index.

References

[1] V. STAUSKIS, *Sound absorption qualities of a cross-shaped isolated acoustic resonator*, Acta Acustica, **82**, Suppl. 1, p. 264 (1996).

[2] V. STAUSKIS, *An impedance method of the suspended ceilings acoustic absorption evluation* [in Lithuanian], Statyba (Building construction), Nr. 1 (5), p. 106 (1996).

[3] V. STAUSKIS, *The sound absorption of an isolated resonator with a cross-shaped slit and its dependence on the number of resonators*, Statyba (Building construction), Nr. 2 (6), p. 105 (1996).

[4] L.I. MAKRINENKO, *The room acoustics of residential buildings* [in Russian], Stroizdat, p. 173 (1986).

[5] H. WINKLER, *Die Kompensation der zu grössten Luftabsorption bei raumakustischen Modellmessungen mit Echogrammen*, Hochfrequenztechnik und Elektroakustik, **73**, 4, 121–131 (1964).

FLOW–EXCITED ACOUSTIC PULSATIONS IN DUCTS WITH CLOSED SIDE BRANCHES

M. MEISSNER

Institute of Fundamental Technological Research
Polish Academy of Sciences
(00-049 Warszawa, Świętokrzyska 21)

In flow ducts with closed side branches strong acoustic pulsations are often induced. This was shown by test results performed for systems with a single side branch and co-axial branches with the same lengths. With growing the flow velocity an excitation of successive resonant modes was observed. Their frequencies were increased together with the flow velocity but at peaks of sound pressure there was an excellent agreement between measurements results and theoretical predictions. A conversion of fluctuating flow energy to energy of resonant acoustic field was included in theoretical consideration by means of negative resistance in impedance model of branches. Hence, it was possible to predict a stronger nonlinearity in the case of a duct with co-axial branches. It was found that a characteristic parameter of the analyzed phenomenon is Strouhal number. Its values for all modes are within the same range approximately and, in addition, it determines a change of acoustic inertance at the branch opening.

1. Introduction

In industrial air transport systems a closed side branch of main duct may be a potential source of strong acoustic pulsations [1, 2]. When dimensions of the branch cross-section are much smaller than a branch length, an excitation of resonant modes corresponding approximately to odd multiples of a quarter wavelength along the branch are observed [6, 18]. A high level of generated sound may induce vibration of the system construction which can cause serious damage.

The mechanism of sound excitation in the system with a single side branch is similar to that causing a generation of self-sustained oscillations in deep cavity [4, 10, 14] or Helmholtz resonator [7, 12, 13] exposed to the grazing flow. An increase of acoustic energy in the system is the result of interaction between unstable shear layer and resonant modes of the branch. First, at the point of flow separation the acoustic field in the branch opening causes a transfer of mean flow energy to shear layer which involves a transformation of continuous shear layer to large scale discrete vortices. These vortices are convected with the flow and interact with the downstream corner of the branch opening. At this point a conversion of fluctuating flow energy to energy of resonant acoustic field takes place [13].

On the other hand, in accord with classical acoustics a presence of the closed side branch in a duct causes substantial reflections of acoustic waves traveling along the duct at frequencies close to resonant modes [8]. This reduces a transmission of acoustic energy past a junction between branch and duct. The filter property of side branch resonators is often used in flow duct systems in order to suppress a narrowband noise produced by machines using atmospheric air as a working medium [15, 17].

From the above it follows that, depending on flow properties such as velocity or turbulence intensity, the side branch in the duct may cause an increase in sound level at resonant frequencies or may reduces transmission of acoustic energy during resonance. In this paper these opposite effects will be analyzed by means of simple models of acoustic waves transmission in two variants of flow systems: a duct with single side branch (Subsec. 2.1) and a duct involving co-axial branches (Subsec. 2.2). The next part of the work presents test results including measurements of frequency and pressure level of pulsations induced in the systems (Sec. 4).

2. Theoretical background

A long circular duct represents an acoustic system which possesses dimensions compared to a wavelength. Therefore, it is not possible to treat the system as one having lumped constants, and it must instead be considered as one having distributed constants. When a diameter of the duct is constant, the acoustic inertance and compliance are distributed uniformly along the duct, and the acoustic motion is wave-like as well as in unbounded space. If walls of the duct are sufficiently smooth to neglect viscous losses, then acoustic waves traveling along the duct may be considered as plane waves. In this case a wave impedance at any cross-section of the duct is

$$R_w = \frac{\varrho c}{\pi r_d^2},$$ (1)

where ϱ denotes the air density, c is the sound speed and r_d is a radius of duct. When there is a motion of air in the duct with mean velocity U, an effect of sound waves convection causes a change of the wave impedance R_w. If the sound waves travel in the direction of the flow then the wave impedance is following

$$R_w^+ = R_w(1 + M),$$ (2)

where $M = U/c$ denotes Mach number. Otherwise

$$R_w^- = R_w(1 - M).$$ (3)

2.1. Transmission of acoustic waves in duct with single side branch

The presence of a single side branch in the duct causes the acoustic impedance at the junction differs from the wave impedance which is the characteristic value for a plane wave, and reflected and transmitted waves are produced consequently. Assume that an incident plane wave is propagated in the direction of the flow (Fig. 1). An acoustic
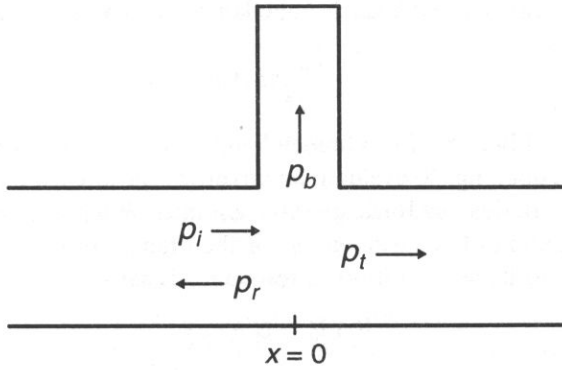
Fig. 1. Transmission of acoustic wave beyond junction of duct and single side branch.

pressure produced by this wave is

$$p_i = A_i e^{j(\omega t - k^+ x)}, \tag{4}$$

where $\omega = 2\pi f$ is an angular frequency, $k^+ = k/(1 + M)$ and $k = \omega/c$ is a wave number. At the junction of the duct and the branch, the reflected wave

$$p_r = B_r e^{j(\omega t + k^- x)}, \tag{5}$$

where $k^- = k/(1 - M)$ and transmitted wave

$$p_t = A_t e^{j(\omega t - k^+ x)}, \tag{6}$$

are created. If cross-sections of the duct and the branch are small in comparison to wavelength, then at the point of junction, chosen in Fig. 1 as the origin of the x coordinate, the following conditions of continuity of pressure and volume velocity are satisfied:

$$p_i + p_r = p_b = p_t, \tag{7}$$

$$U_i + U_r = U_b + U_t, \tag{8}$$

where

$$U_i = \frac{p_i}{R_w^+}, \qquad U_r = -\frac{p_r}{R_w^-}, \qquad U_b = \frac{p_b}{Z_b}, \qquad U_t = \frac{p_t}{R_w^+}, \tag{9}$$

p_b and U_b are a pressure and a volume velocity at a branch opening and Z_b is a branch impedance. An insertion of Eqs. (4)–(6) into Eqs. (7)–(9) leads to an expression for the sound power transmission coefficient α_t

$$\alpha_t = \left| \frac{A_t}{A_i} \right|^2 = \left| \frac{2Z_b}{2Z_b + R_w (1 - M^2)} \right|^2, \tag{10}$$

where operator $|\cdot|$ denotes modulus of complex number. As follows from Eq. (10), an influence of sound wave convection on transmission of acoustic energy beyond the junction is negligible at low Mach number flows ($M^2 \ll 1$). In this case the transmission

coefficient depends only on the branch impedance Z_b. The general expression for this impedance is

$$Z_b = R_s + j\frac{\varrho c}{\pi r_b^2}[k\Delta d - \cot(kd)], \tag{11}$$

where r_b is a radius of branch, d is a branch length and R_s is a resistance due to viscous action in the branch opening. To evaluate an unknown end correction Δd, the theoretical value $\Delta d_0 = 8r_b/3\pi$ derived by Rayleigh [8] is assumed. When viscous losses is negligible, there is not a dissipation of acoustic energy in the branch. In this case the transmission coefficient equals zero if the condition of resonance is satisfied

$$k\Delta d_0 = \cot(kd), \tag{12}$$

which can be approximated to the form

$$f_m \approx \frac{c(2m-1)}{4(d + \Delta d_0)}, \qquad m = 1, 2, 3.... \tag{13}$$

This means that the incident sound wave is totally reflected from the junction and returned towards the source. As may be seen from Eqs. (10) and (11), in frequency ranges between resonant modes f_m the transmission coefficient α_t approaches unity. Therefore the single branch in the duct represents acoustic filter with the highest attenuation at resonant frequencies.

The analysis presented above is valid under the assumption that both the cross-sectional area of the duct and the flow velocity are small enough to maintain laminar motion of air in the duct. When a Reynolds number

$$\mathcal{R}e = \frac{r_d U}{\nu}, \tag{14}$$

where ν is the coefficient of kinematic viscosity, is much greater than 1160 the flow in the duct becomes turbulent [16]. To adopt the outline model of wave transmission to this situation, the incident sound wave will be now interpreted as acoustic perturbation generated by flow disturbances.

As mentioned in Introduction, an existence of unsteady motion in the area close to the branch opening may cause a conversion of fluctuating flow energy to energy of acoustic field inside the branch. Finally the high-level acoustic pulsations may be created in the system. An increase in the system acoustic energy can be incorporated in the theoretical analysis by putting the negative resistance R_n in the impedance model of the branch. Therefore, at low Mach number flows the equation for transmission coefficient may be rewritten in the form

$$\alpha_t = \left| \frac{\dfrac{R_n}{R_w} + jX}{\dfrac{R_n}{R_w} + \dfrac{1}{2} + jX} \right|^2, \tag{15}$$

where $X = (r_d/r_b)^2[k\Delta d_0 - \cot(kd)]$. It results from Eq. (15), that for values of R_n/R_w decreasing from 0 to -0.25 the system behaves like an acoustic filter with attenuation growing at resonant frequencies. When $R_n/R_w = -0.25$ the coefficient α_t is constant and

equals unity for all frequencies. At values of R_n/R_w smaller than -0.25 the coefficient α_t is greater than unity at resonance. This means that initial acoustic perturbations travelling along the duct are amplified in the system.

As can be seen from Eq. (15), for values of R_n/R_w close to -0.5 the coefficient α_t may possess any high value at resonant frequencies. It corresponds to unbounded growth of pulsations amplitude. Theoretically this situation is possible in the undamped oscillator operating as linear system. In real conditions an unbounded increase in amplitude at resonance is limited by nonlinear effects. In the considered system the nonlinearity in the branch opening produces an additional loss resistance which increases with the growth of pulsations amplitude. When a balance between acoustic energy losses and the energy extracted from flow perturbations is reached, the stable acoustic pulsations with frequencies close to resonant modes as well as several harmonics will appear in the system.

2.2. Transmission of acoustic waves in duct with co-axial branches
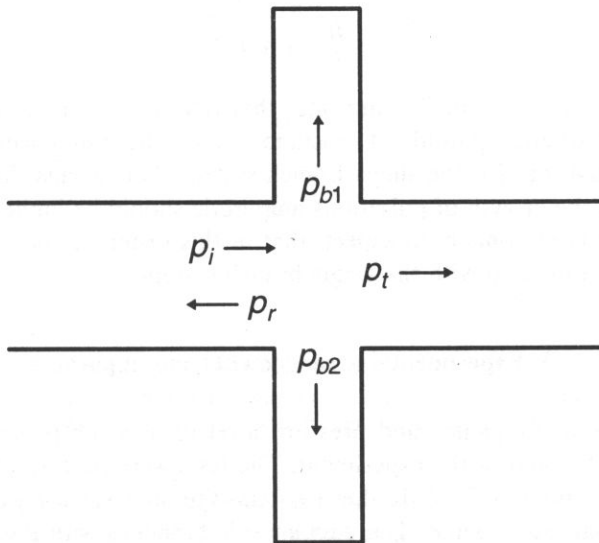
Fig. 2. Transmission of acoustic wave beyond junctions of duct and co-axial branches.

A distribution of pressures of sound waves in the duct, to which are attached co-axial branches, is shown in Fig. 2. At a point of junctions the conditions of continuity of pressure and volume velocity require that

$$p_i + p_r = p_{b1} = p_{b2} = p_t, \tag{16}$$

$$U_i + U_r = U_{b1} + U_{b2} + U_t, \tag{17}$$

where

$$U_i = \frac{p_i}{R_w^+}, \qquad U_r = -\frac{p_r}{R_w^-}, \qquad U_t = \frac{p_t}{R_w^+},$$

$$U_{b1} = \frac{p_{b1}}{Z_{b1}}, \qquad U_{b2} = \frac{p_{b2}}{Z_{b2}} \tag{18}$$

and Z_{b1}, Z_{b2} are impedances of branches. After inserting Eqs. (4)–(6) into Eqs. (16)–(18) the following expression for transsmision coefficient may be obtain

$$\alpha_t = \left| \frac{2Z_{b1}Z_{b2}}{2Z_{b1}Z_{b2} + R_w(1 - M^2)(Z_{b1} + Z_{b2})} \right|^2, \tag{19}$$

Under the assumption that the branches have the same cross-sectional area and length, the expression (19) reduces to the form

$$\alpha_t = \left| \frac{Z_b}{Z_b + R_w(1 - M^2)} \right|^2, \tag{20}$$

where Z_b is the impedance of single branch from Eq. (11). If the transfer of energy from flow disturbances to acoustic field will be included in a impedance model of the branches and, moreover, low Mach number flow will be assumed ($M^2 \ll 1$), then

$$\alpha_t = \left| \frac{\dfrac{R_n}{R_w} + jX}{\dfrac{R_n}{R_w} + 1 + jX} \right|^2. \tag{21}$$

A comparison of Eqs. (15) and (21) indicates that values of α_t calculated from the equations are identical when magnitude of resistance R_n for the system with co-axial branches is twice bigger than that for the single branch system. This means that in the duct with co-axial branches the growth of pulsations amplitude should be limited by stronger non-linearity. Thus, it is reasonably to expect, that in this system a harmonic distortion will be much greater compared with the single branch system.

3. Experimental arrangements and apparatus

Measurements of frequency and pressure level of acoustic pulsations generated in the systems were the aim of the experiment. The tests were performed in the laboratory arrangements presented in Fig. 3. In these systems the duct was composed of the circular pipe with the radius $r_d = 8$ mm. The circular side branches with the radius $r_b = 5$ mm and variable lengths were connected with the ducts under right angle. The lengths used in experiment were from the range $1 - 10$ cm with a step of 1 cm. Since the aim of the tests was to compare the results of measurements obtained in the systems, it was assumed that the lengths of co-axial branches were the same and were denoted as d, likewise as for the single branch system (Fig. 3). The point of junction of the duct and branches was chosen at the distance of 3.2 m from the duct outlet.

The systems were supplied with the compressed air at the maximum pressure 0.5 MPa. The maximum velocity u_{max} of the air stream was measured by using a Pitot tube with diameter of 1.6 mm and a liquid-column manometer in the shape of letter U. The probe was mounted in the center of the duct outlet. The mean flow velocity U of the air in the duct was calculated from formula [11]

$$U = \frac{49}{60} u_{max}. \tag{22}$$
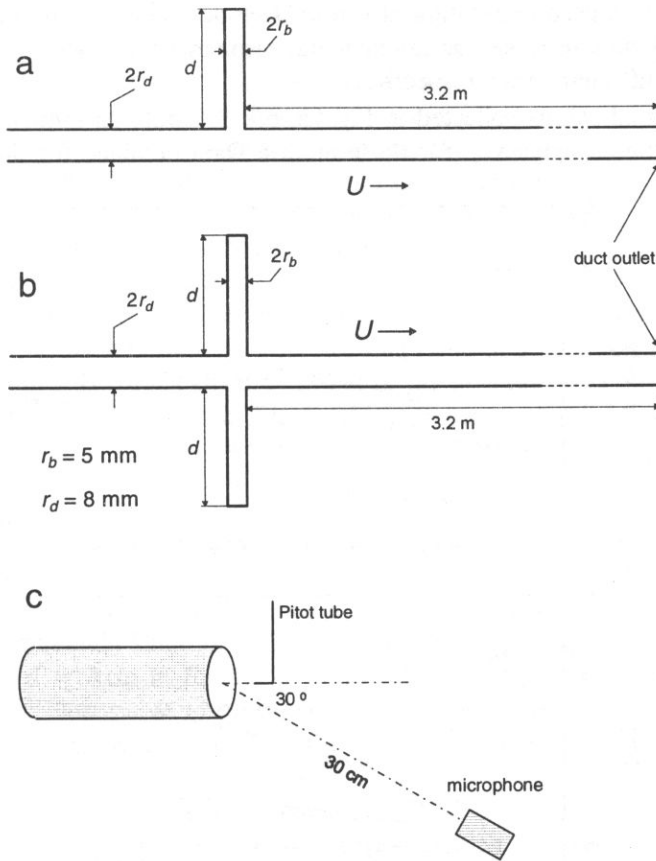
Fig. 3. Experimental setups: a) duct with single side branch, b) duct with co-axial branches, and c) position of Pitot tube and microphone at duct outlet.

The tests were carried out in the range of U from 40 m/s to 128 m/s in which a generation of acoustic pulsations was observed. The maximum value of U corresponds to a maximum efficiency of flow installation. The Reynolds number calculated from Eq. (14) possesses values from the range of $2 \cdot 10^5$ to $7 \cdot 10^5$. Thus, it should be expected that an air flow in the duct was turbulent.

Acoustic measurements were made with the Brüel & Kjær instrument setup consisting a 1" microphone and a high resolution signal analyzer 2033. The microphone was mounted at the distance of 30 cm from the duct outlet. The line joining the centre of the microphone and the centre of the duct outlet made 30° angle with air stream axis.

4. Analysis of test results

At mean flow velocity U from the range $40 - 128$ m/s and lengths of branches $d = 1 - 10$ cm the pulsations corresponding to the resonant modes f_1, f_3 and f_5 were observed

in experiment. A used denotation of resonant modes is given from Eq. (13). Therefore, f_1 mode may be interpreted as fundamental resonant mode, while f_3 and f_5 modes as its third and fifth harmonic, respectively.

Experimental results collected in Fig. 4 a, b, c illustrate an influence of flow velocity U on pulsations frequency f for these modes. Data obtained for the duct with single

Fig. 4. Dependence of frequency of resonant modes on flow velocity U for single side branch system (———) and sytem with co-axial branches (- - - -).

branch and co-axial branches are denoted by solid and dotted lines, respectively. As may be seen, in the both systems the frequency f of acoustic pulsations grows with velocity U. Ho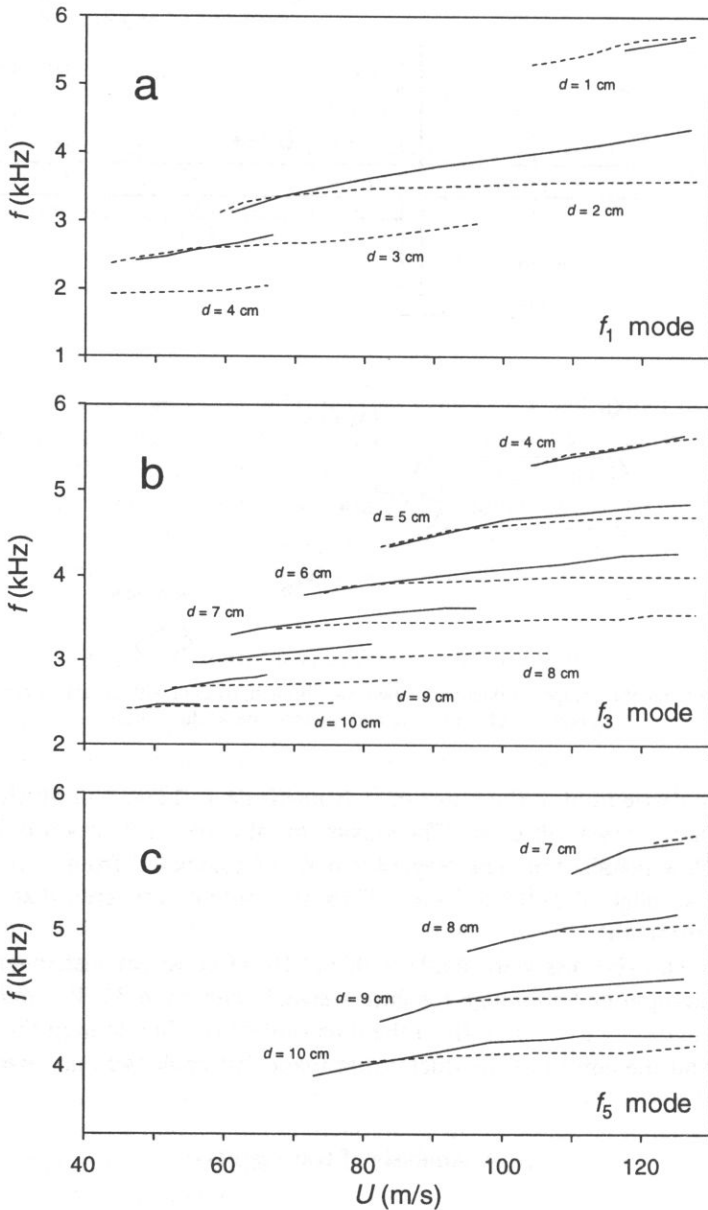wever, the observed increase in f for the duct with co-axial branches is for nearly all lengths of branches smaller distinctly than for the second system. Moreover, pulsations corresponding to particular mode appear for certain values of d at different ranges of velocity U. Additionally, at length $d = 4$ cm a pulsations of fundamental f_1 mode are generated only in the duct with co-axial branches (Fig. 4 a). Note that plots obtained for each mode at the lowest values of d finish at velocity $U = 128$ m/s which corresponds to maximum efficiency of flow installation.

For each resonant mode the different value of branch length d results in a various frequency range of acoustic pulsations. With growing value of d a decrease in pulsations frequency occurs which is accompanied by a shift of the flow velocity U to lower values. This correlation explains the plots in Fig. 5, which present a dependence of Strouhal number S

$$S = \frac{2 f r_b}{U} \tag{23}$$

on the flow velocity U. As may be seen, for all modes generated in the both systems, the maximum values of Strouhal number are close together ($S = 0.45 - 0.54$). The biggest differences are noted in minimum values of S. When U is smaller than the maximum value 128 m/s the minimum value of S is approximately twice smaller in the duct with co-axial branches ($d = 3$ cm in Fig. 5 a, $d = 7 - 10$ cm in Fig. 5 b). For all remaining values of d the flow velocities, at which generation of particular mode would be possible, exceed the velocity $U = 128$ m/s making a precise determination of minimum value of S impossible.

The fact that for certain branch lengths d the values of Strouhal number are very similar has a simple physical meaning. From Eq. (23) and the relation

$$U_c = \mu U , \tag{24}$$

where $\mu = 0.62$ [5] and U_c is the mean convection velocity of flow disturbances, one can obtain

$$\lambda = \frac{2 \mu r_b}{S} . \tag{25}$$

In the above equation $\lambda = U_c / f$ is a distance between two succeeding flow disturbances which cyclically shed from an upstream edge of branch opening. More precisely, λ represents the distance between the two neighbouring points within turbulent shear layer with the highest concentration of fluid vorticity or the distance between centers of two succeeding vortices when the vorticity is accumulated into vortices. In the works [3, 9], where an assumption of wave-like flow disturbances was made, λ is called the hydrodynamic wavelength. The presented experimental results show that λ assumes values from the range $1.1 - 2$ cm and increases with a growth of flow velocity U. The increase in λ with U is evidently larger in the case of the duct with co-axial branches.

The data presented in Fig. 6 a show a change of frequencies f, at which the pressure level L_p reaches the maximum value, with the branches length d. By solid lines are indicated the results of frequency calculations based on Eq. (12). As may be seen, there is an
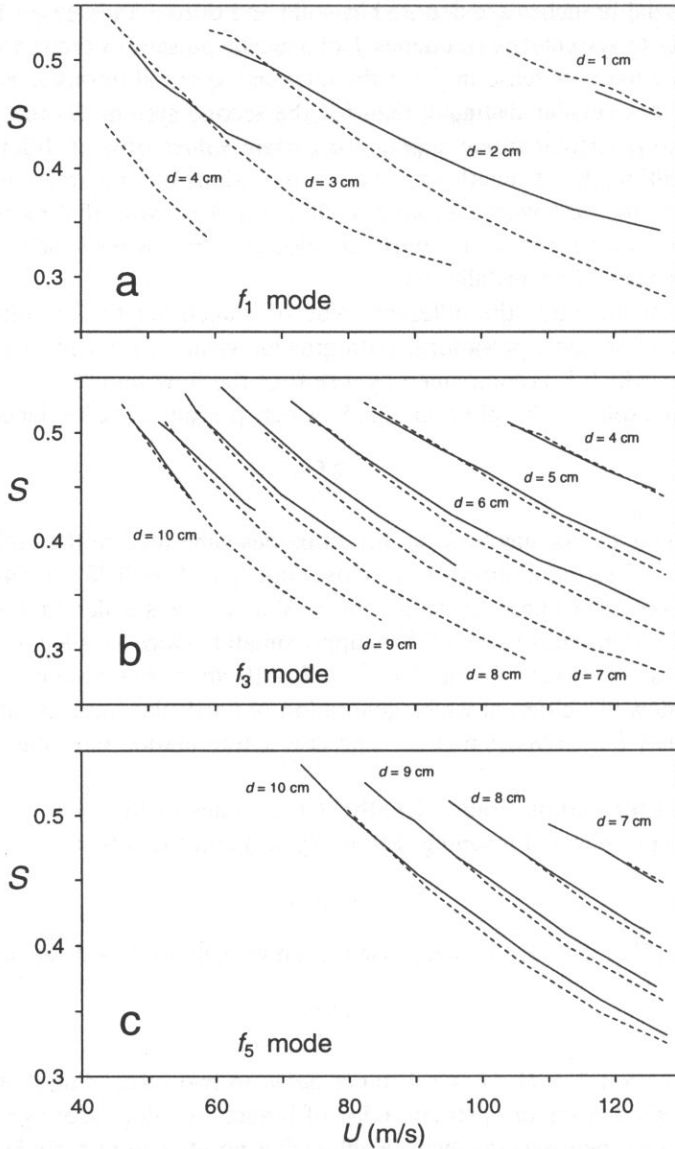
Fig. 5. Dependence of Strouhal number S on flow velocity U for resonant modes;
(———) single side branch system, (- - - -) system with co-axial branches.

excellent agreement between experimental results and theoretical predictions. Therefore, an important conclusion may be drawn that the acoustic condition of resonance (12) is not influenced by air flow in the duct.

In Fig. 6b maximum values of sound pressure level L_p of generated pulsations as a function of d are presented. As it results from experimental data, maximum values of L_p are from the range $70 - 100\,\mathrm{dB}$ and, as a rule, they decrease with increasing d.
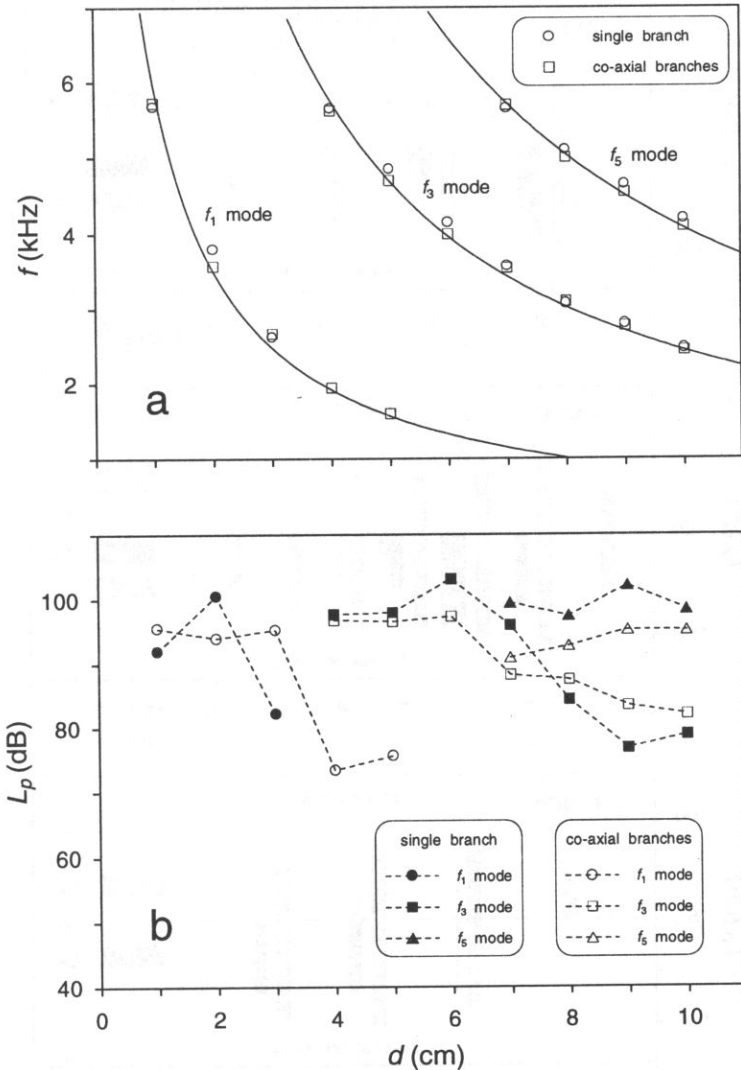
Fig. 6. a) Frequencies of resonant modes at different lengths of branches at maximum
sound pressure level; (———) theoretical results, b) maximum pressure level of resonant modes.

As was well predicted by theoretical analysis (Sec. 2), a process of sound generation
is associated with harmonic distortion. To illustrate this effect in Fig. 7 maximum values
of L_p corresponding to harmonics of resonant modes f_1, f_3 and f_5 are displayed. For the
harmonics a different denotation is used. For example, f_{3h} denotes the third harmonic
of f_1 mode, whereas f_{15h} is the fifth harmonic of f_3 mode or the third harmonic of f_5
mode. From a comparison of data in Fig. 7 it follows, that in the single branch system the
harmonic distortion is much weaker than in the system with co-axial branches. It can be
clearly observed in the experimental data obtained for f_1 and f_3 modes. At some values
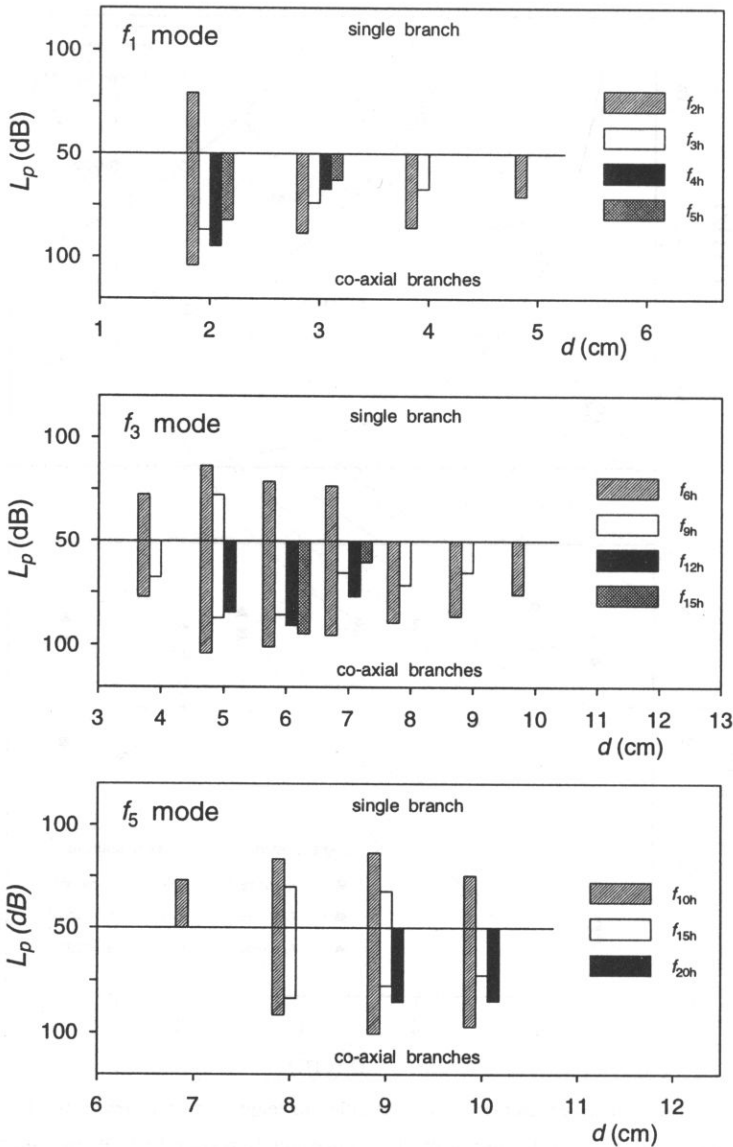
Fig. 7. Maximum pressure level of harmonics of resonant modes.

of d as much as four successive harmonics occur ($d = 2, 3$ cm for mode f_1, $d = 6, 7$ cm for mode f_3). Moreover, in some cases the level of harmonic component is higher than the level of resonant mode ($d = 2$ cm for f_1 mode, $d = 5 - 7$ cm for f_3 mode, $d = 9$ cm for f_5 mode).

As follows from previously presented data, the pulsations frequency f is generally a function of the flow velocity U (Fig. 4) and values of f calculated from the resonance condition (12) agree with measurements only in the case of maximum level of pulsations

(Fig. 6 a). These facts indicate, that in Eq. (11) describing the branch impedance the end correction Δd is the parameter which must vary with flow velocity U. Because Strouhal number seems to be a characteristic quantity of analyzed phenomenon, then it will be reasonable to seek rather a relation between Δd and S.
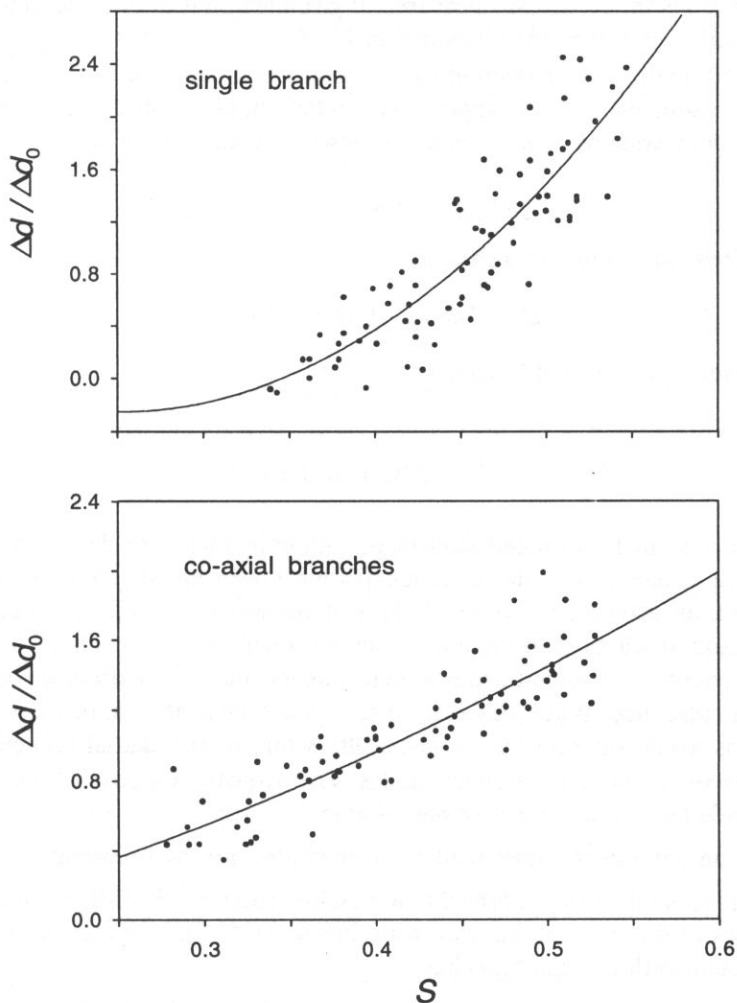
Fig. 8. Dependence of end correction Δd on Strouhal number S for systems with
a) single side branch, b) co-axial branches; (———) best fit lines.

A dependence of nondimensional end correction $\Delta d / \Delta d_0$ on the Strouhal number for both systems is shown in Fig. 8. The values of Δd were calculated from Eq. (12), in which the theoretical value Δd_0 was replaced by unknown Δd

$$\Delta d = \frac{\cot(kd)}{k} . \tag{26}$$

The wave number k was evaluated from experimental results

$$k = \frac{2\pi f(d, U)}{c},$$

(27)

where $f(d, U)$ is the frequency measured at given length d of branches and flow velocity U. All experimental data were included in Fig. 8.

The used method of correlation gave a good result. Since sets of data points in Fig. 8 correlate reasonably well, an approximate relations between $\Delta d/\Delta d_0$ and S may be found for both systems. These relations describe equations of best fit lines drawn in Fig. 8:

$$\Delta d/\Delta d_0 = 1.53 - 14.2S + 28.2S^2$$

(28)

for the system with single branch and

$$\Delta d/\Delta d_0 = -0.32 + 1.9S + 3.2S^2$$

(29)

for the system with co-axial branches.

5. Conclusions

In the paper the flow-excited acoustic pulsations in ducts with closed single side branch and co-axial branches with the same lengths have been investigated. In theoretical part of the work an acoustic response of the systems was examined by means of a simple model of sound waves transmission along the duct. A conversion of fluctuating flow energy to energy of resonant acoustic field was included in theoretical consideration by a negative resistance. When this resistance was not present in impedances of branches, the systems would operate like acoustic filters due to substantial reflections of sound waves at frequencies near resonant modes. The acoustic response of the systems could be unbounded unless nonlinearity was included.

The main findings of experimental investigations are the following:

1. Odd resonant modes of branches are excited successively with growing flow velocity. Frequencies of these modes increase with flow speed but this growth is distinctly smaller for the system with co-axial branches.

2. Pulsations in both systems reach maximum level at frequencies corresponding to classical resonance condition for quarter-wave resonator.

3. The flow-resonant response of branches occurs within the range $0.25 - 0.55$ of Strouhal number.

4. The excitation of resonant modes is accompanied by high nonlinearity. It was especially observed in the case of duct with co-axial branches as was well predicted by theory.

5. Changes of the end correction of side branch resonators depend on Strouhal number.

References

[1] J.C. BRUGGEMAN, A. HIRSCHBERG, M.E. VAN DONGEN, A.P. WIJNANDS and J. GORTER, *Flow induced pulsations in gas transport systems: analysis of the influence of closed side branches*, J. Fluids Engng., **111**, 484–491 (1989).

[2] J.C. BRUGGEMAN, A. HIRSCHBERG, M.E. VAN DONGEN and A.P. WIJANANDS, *Self-sustained aero-acoustic pulsations in gas transport systems: experimental study of the influence of closed side branches*, J. Sound Vib. **150**, 371–393 (1991).

[3] S.A. ELDER, T.M. FARABEE and F.C. DEMETZ, *Mechanisms of flow-excited tones at low Mach number*, J. Acoust. Soc. Amer., **72**, 532–549 (1982).

[4] S.A. ELDER, *The mechanism of sound production in organ pipes and cavity resonators*, J. Acoust. Soc. Jpn., **13**, 11–23 (1992).

[5] M.E. GOLDSTEIN, *Aeroacoustics*, McGraw–Hill, New York 1976, p. 91.

[6] W.M. JUNGOWSKI, K.K. BOTROS and W. STUDZINSKI, *Cylindrical side-branch as tone generator*, J. Sound Vib., **131**, 265–285 (1989).

[7] R. KHOSROPOUR and P. MILLET, *Excitation of Helmholtz resonator by an air jet*, J. Acoust. Soc. Amer., **88**, 1211–1221 (1990).

[8] L.E. KINSLER and A.R. FREY, *Fundamentals of Acoustics*, 2nd ed., Wiley, New York 1962, pp. 181, 205.

[9] M. MEISSNER, *Self-sustained deep cavity oscillations induced by grazing flow*, Acustica, **62**, 220–228 (1987).

[10] M. MEISSNER, *Experimental investigation of discrete sound production in deep cavity exposed to air flow*, Arch. Acoust., **18**, 131–156 (1993).

[11] M. MEISSNER and M. CZECHOWICZ, *Experimental investigation of flow-induced acoustic oscillations in piping system with closed branches*, Appl. Acoustics, **45**, 359–375 (1995).

[12] P.A. NELSON, N.A. HALLIWELL and P.E. DOAK, *Fluid dynamics of a flow excited resonanse. Part I. Experiment*, J. Sound Vib., **78**, 15–38 (1981).

[13] P.A. NELSON, N.A. HALLIWELL and P.E. DOAK, *Fluid dynamics of a flow excited resonanse. Part II. Flow acoustic interaction*, J. Sound Vib., **91**, 375–402 (1983).

[14] S.P. PARTHASARATHY, Y.I. CHO and L.H. BACK, *Sound generation by flow over relatively deep cylindrical cavities*, J. Acoust. Soc. Amer., **78**, 1785–1795 (1985).

[15] M. SALIKUDDIN, *Acoustic characteristics of closed cavity resonators for screech liner design*, Proc. of International Noise and Vibration Control Conference, St. Petersburg, Vol. 3, 199–212 (1993).

[16] B. ŚREDNIAWA, *Hydrodynamics and Theory of Elasticity* [in Polish], PWN, Warszawa 1977, p. 305.

[17] V.I. YAKHONTOV and V.N. MELNIKOV, *Calculation and application of compact broadband mufflers for reducing aerodynamic noise*, Proc. of International Noise and Vibration Control Conference, St. Petersburg, Vol. 3, 223–225 (1993).

[18] S. ZIADA and E.T. BÜHLMANN, *Self-exited resonances of two side-branches in close proximity*, J. Fluids and Structures, **6**, 583–601 (1992).

SINGULARITIES OF THE PLANAR GREEN FUNCTION
IN THE SPECTRAL DOMAIN

W. LAPRUS and E. DANICKI

Institute of Fundamental Technological Research,
Polish Academy of Sciences
(00-049 Warszawa, ul. Świętokrzyska 21)

The surface acoustic wave amplitudes at the boundary of a piezoelectric half-space satisfy a matrix relation which is characteristic of the medium. The elements of the matrix are functions of slowness. In the paper, the singularities of the matrix are investigated at cutoff points of bulk waves. An approximated formula is derived for the matrix in the neighborhood of the greatest cutoff point, which also takes into account the singularity related to the Rayleigh wave. The results of numerical calculations are presented for several piezoelectrics.

1. Introduction

The INGEBRIGTSEN effective permittivity [1, 2] of a piezoelectric half-space, a function of slowness r, is an approximation of the exact effective permittivity $Y(r)$ in the vicinity of the singular point equal to the Rayleigh wave slowness. The counterpart of $Y(r)$ in the space domain, i.e. the Fourier transform of $Y(r)$, is a Green function defined at the boundary of the piezoelectric half-space. The Green integral formula applied to the electric potential at the boundary gives the surface electric charge density.

In the special case of SH waves, the Ingebrigtsen approximation has been improved by including contributions from bulk waves [3]. Since only one component of the particle displacement vector is different from zero, the contributions can be found in an analytic way.

We consider the general case when all the three components of the particle displacement vector may be different from zero, so that numerical calculations are necessary. For this purpose we employ the ADLER form of the field equations [4], which proves to be very useful in the analysis of piezoelectric interfacial waves [5, 6, 7].

We are interested in the approximation of the function $Z(r) = C/Y(r)$ (C is a constant) in the vicinity of the cutoff point of bulk waves; this is a branch point of $Z(r)$ in the complex plane of r. It is shown that the behavior of the function $Z(r)$ near the cutoff point depends on the shape of the corresponding slowness curve at that point.

Starting from the derived approximation of $Z(r)$, we take into account the Rayleigh wave singularity, and find an approximated formula for the function $Z(r)$ that is valid

in the whole range of r. The formula is verified by comparison with the exact function $Z(r)$ calculated numerically.

2. Function $Z(r)$

Let us consider a homogeneous piezoelectric medium and a system of coordinates (x, y, z). The plane $z = 0$ divides the medium into two half-spaces: the upper (for $z > 0$) and the lower (for $z < 0$). We assume that the field is independent of y, and that the time and space dependence is given by the factor $\exp(j\omega t - j\omega r x - j\omega s z)$.

The field equations can be reduced to the system of eight linear algebraic equations, as described in Ref. [7]. Let $i, j = 1, 2, 3$ and $(x_i) = (x, y, z)$. The following field variables will be used: particle displacement u_i, electric potential ϕ, surface force $T_i = T_{3i}$ (where T_{ij} is the stress tensor), and normal component D_3 of the electric displacement D_i. We have

$$H_{KL}(r)F_L = qF_K, \qquad (2.1)$$

where $K, L = 1, \ldots, 8$, $(F_K) = (j\omega r u_i, j\omega r \phi, T_i, D_3)$, and $q = s/r$. For real r, which we assume, the matrix H_{KL} is real and non-symmetric. It depends on material constants (see Ref. [7]).

The summation convention is adopted throughout the paper: summation is performed over repeated indices (within their range) except when they are enclosed in parentheses.

After solving the eigenvalue problem defined by Eq. (2.1) we get eight eigenvectors $\widetilde{F}_K^{(J)}(r)$ corresponding to eight eigenvalues $q^{(J)}(r)$ for $J = 1, \ldots, 8$. The J-th eigenwave has the form

$$F_K^{(J)} = \widetilde{F}_K^{(J)} \exp(j\omega t - j\omega r(x + q^{(J)}z)). \qquad (2.2)$$

The solution of the field equations is a linear combination of the eigenwaves.

The eigenvector $\widetilde{F}_K^{(J)}$ will be called upper (lower) if $\operatorname{Im} q^{(J)} < 0$ ($\operatorname{Im} q^{(J)} > 0$) or, for $\operatorname{Im} q^{(J)} = 0$, if the z component of the real part of the Poynting vector is positive (negative). $\operatorname{Im} q^{(J)} \neq 0$ for $J = 1, \ldots, 8$ if $r > r_c$ where r_c is the cutoff slowness of bulk waves.

Since the surface wave field vanishes at infinity, and there is no energy flux to the boundary (no sources in the space), the solution F_K^+ of the field equations in the upper half-space consists of upper eigenwaves, and the solution F_K^- in the lower half-space consists of lower eigenwaves. At the plane $z = 0$, the complex amplitudes of the two solutions are

$$\widetilde{F}_K^{\pm} = \sum_J^{\pm} C_J \widetilde{F}_K^{(J)}, \qquad (2.3)$$

where the plus (or minus) superscript of the sum symbol means that the summation is performed over J such that $\widetilde{F}_K^{(J)}$ is an upper (or lower) eigenvector. The coefficients C_J are to be determined from boundary conditions.

The field equations can be solved in each half-space separately, provided appropriate boundary conditions are imposed at the plane $z = 0$. In general, all the boundary values $\widetilde{F}_K^+$ (or $\widetilde{F}_K^-$) should be given. However, we consider special solutions (surface waves),

and therefore the field variables satisfy some additional relation at the boundary of each piezoelectric half-space. Below, it will be shown that only four of the eight boundary values may be arbitrary.

Let $R_{KJ} = \widetilde{F}_K^{(J)}$. If we change the order of the columns of the matrix R_{KJ} so that the first four are upper eigenvectors and the last four are lower eigenvectors, then the matrix can be written in the form

$$(R_{KJ}) = \begin{bmatrix} R^+ & R^- \\ S^+ & S^- \end{bmatrix}, \tag{2.4}$$

where R^+, R^-, S^+, and S^- are 4×4 matrices. Denote by $L^\pm$ the inverses of the matrices $S^\pm$.

Using the notation $(\widetilde{F}_K^\pm) = (\widetilde{U}_L^\pm, \widetilde{T}_L^\pm)$ for $L = 1, \ldots, 4$, we rewrite Eq. (2.3) as

$$\widetilde{U}_K^\pm = R_{KJ}^\pm C_J^\pm, \qquad \widetilde{T}_K^\pm = S_{KJ}^\pm C_J^\pm \tag{2.5}$$

for $J, K = 1, \ldots, 4$, where C_J^+ and C_J^- are the coefficients of the upper and the lower eigenvectors in Eq. (2.3). From Eq. (2.5) we find $C_J^\pm = L_{JL}^\pm \widetilde{T}_L^\pm$, and then

$$\widetilde{U}_K^\pm = Z_{KL}^\pm \widetilde{T}_L^\pm, \tag{2.6}$$

where the matrix

$$Z_{KL}^\pm = R_{KJ}^\pm L_{JL}^\pm \tag{2.7}$$

depends on r.

Equation (2.6) is a fundamental relation in the problem of surface wave propagation. It should be satisfied by the field variables at the boundary of each piezoelectric half-space, irrespective of what boundary conditions are imposed there.

If the boundary of the piezoelectric half-space is traction-free then $\widetilde{T}_i^\pm = 0$ for $i = 1, 2, 3$. In this case, from Eq. (2.6) for $K = 4$, we have $\widetilde{U}_4^\pm = Z_{44}^\pm \widetilde{T}_4^\pm$ or

$$j\omega r \widetilde{\phi}^\pm = Z_{44}^\pm \widetilde{D}_3^\pm. \tag{2.8}$$

In the following, we shall be considering the function $Z(r) = -Z_{44}^-(r)$.

3. First order singularities

The function $Z(r)$ is infinite at the singular point $r_i > r_c$ related to the Rayleigh wave. Three other singular points for $r \le r_c$ coincide with the cutoff points of the three slowness curves (in Fig. 1 the slowness curves have appendices for r greater than the corresponding cutoff points). The function $Z(r)$ is finite at these points (see Fig. 2) but its first derivative may be infinite; therefore, the corresponding singularities will be called first-order.

The idea of approximation of $Z(r)$ in the neighborhood of a cutoff point is based on the following observation. Consider the slowness curve with the cutoff point r_c. From Fig. 1 we see that for $r < r_c$ there exist two values of s, $s^\pm = q^{(\pm)}(r)r$ where $q^{(\pm)}(r)$
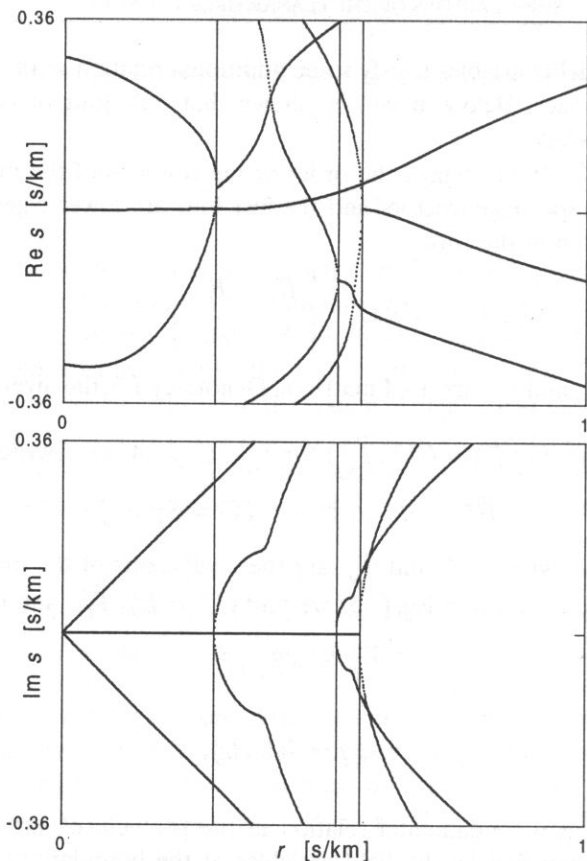
Fig. 1. The real and imaginary part of the slowness s for bismuth germanium oxide (Euler angles: 24°, 70°, 10°). The three vertical lines mark the cutoff points.
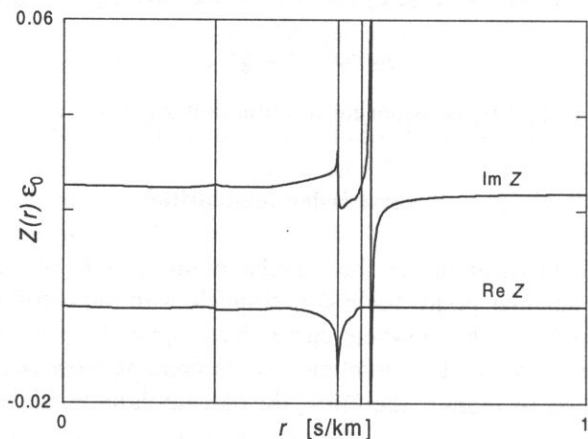

Fig. 2. The function $Z(r)$ for bismuth germanium oxide (Euler angles: 24°, 70°, 10°). The three vertical lines mark the cutoff points.

[172]

are the two real eigenvalues corresponding to the slowness curve. As $r \to r_c$, these two values converge to $s_c = q^{(0)}r_c$ where $q^{(0)} = q^{(\pm)}(r_c)$. The double real eigenvalue $q^{(0)}$ splits into a complex conjugate pair of eigenvalues for $r > r_c$.

It should be noted here that the matrix $H_{KL}(r)$ is defective for $r = r_c$: it has only seven independent eigenvectors. This can be shown by differentiation of the equality

$$\left(H_{KL} - q^{(J)}I_{KL}\right)\widetilde{F}_L^{(J)} = 0 \tag{3.1}$$

(I_{KL} denotes the identity matrix) with respect to s along the slowness curve. In other words, the two eigenvectors $\widetilde{F}_K^{(\pm)}$ corresponding to $q^{(\pm)}(r)$ converge to the eigenvector $\widetilde{F}_K^{(0)}$ corresponding to the double eigenvalue $q^{(0)}$. The eigenvector $\widetilde{F}_K^{(+)}$ is upper, and $\widetilde{F}_K^{(-)}$ is lower in the neighborhood of r_c, because the real part of the Poynting vector is normal to the slowness curve.

The values $s^{\pm}$ are changing fast for $r \to r_c$ (the derivative of $s^{\pm}(r)$ tends to infinity), and so do the two corresponding eigenvalues and eigenvectors, while the other eigenvalues and eigenvectors are relatively constant. Thus, it suffices to take into account only the two eigenvectors $\widetilde{F}_K^{(\pm)}$, to find the approximated formulae for them, and to calculate the function $Z(r)$ with the use of Eq. (2.7).

Suppose we know the function $s^{\pm}(r)$ in the neighborhood of r_c. Regarding the eigenvectors $\widetilde{F}_K^{(\pm)}$ as functions of the variable s, we can write, separately for $s > s_c$ and $s < s_c$, the Taylor expansion

$$\widetilde{F}_K^{(\pm)}(s^{\pm}) = \widetilde{F}_K^{(0)} + \widetilde{F}_K^{\bullet(0)}\Delta s^{\pm}, \tag{3.2}$$

where the higher-order terms are neglected; the dot denotes differentiation with respect to s, $\widetilde{F}_K^{\bullet(0)}$ denotes the common limit of $\widetilde{F}_K^{\bullet(\pm)}(s^{\pm})$ as $s^{\pm} \to s_c$, and $\Delta s^{\pm} = s^{\pm} - s_c$.

The slowness curve in the vicinity of r_c can be approximated by an algebraic curve of second order, such as circle or parabola. We get

$$\Delta s^{\pm} = \pm\alpha\rho(r), \qquad \rho(r) = \text{sign}(r_c^2 - r^2)\sqrt{r_c^2 - r^2} \tag{3.3}$$

with $\alpha = (R_c/r_c)^{1/2}$ where R_c is the radius of curvature $R = (1 + (s')^2)^{3/2}/|s''|$ for $r = r_c$, and the prime denotes differentiation with respect to r. Since $s = qr$, we have

$$s' = q'r + q, \qquad s'' = q''r + 2q'. \tag{3.4}$$

The derivatives q' and q'' can be found by differentiation of Eq. (3.1) as follows.

Let $\widetilde{E}_L^{(I)}$ be the left eigenvector corresponding to the eigenvalue $q^{(I)}$. We assume the normalization

$$\widetilde{F}_L^{(J)}\widetilde{F}_L^{(J)} = 1, \qquad \widetilde{E}_L^{(I)}\widetilde{F}_L^{(J)} = I_{IJ} \tag{3.5}$$

for every r, and introduce the symbols

$$Q_1^{(IJ)} = \widetilde{E}_K^{(I)}H_{KL}'\widetilde{F}_L^{(J)}, \qquad Q_2^{(IJ)} = \widetilde{E}_K^{(I)}H_{KL}''\widetilde{F}_L^{(J)}. \tag{3.6}$$

Differentiating Eq. (3.1) once and twice with respect to r, and multiplying the both sides by $\widetilde{E}_L^{(I)}$ we obtain

$$q'^{(J)} = Q_1^{(JJ)}, \qquad q''^{(J)} = Q_2^{(JJ)} + 2\sum_{I \neq J}C_{IJ}Q_1^{(JI)}, \tag{3.7}$$

where $C_{IJ} = -(q^{(I)} - q^{(J)})^{-1}Q_1^{(IJ)}$ for $I \neq J$, and

$$\tilde{F}_L'^{(J)} = C_{JJ}\tilde{F}_L^{(J)} + \tilde{D}_L^{(J)} \tag{3.8}$$

where $\tilde{D}_L^{(J)} = \sum_{I \neq J} C_{IJ}\tilde{F}_L^{(I)}$, $C_{JJ} = -\tilde{D}_L^{(J)}\tilde{F}_L^{(J)}$. The above formulae are true for all eigenvalues and eigenvectors (for r different from the cutoff values).

Using these formulae we find the radius of curvature $R(r)$ (at two points of the slowness curve), and $\tilde{F}_K^{\bullet(\pm)}(s^\pm) = \tilde{F}_K'^{(\pm)}(r)/s'^\pm(r)$. The next step consists in finding the limits of these quantities, and of $\tilde{F}_K^{(\pm)}(r)$, for $r \to r_c$, i.e. $R_c = R(r_c)$, $\tilde{F}_K^{\bullet(0)}$, and $\tilde{F}_K^{(0)}$. In numerical calculations, this simply means finding the values of the quantities for r reasonably close to r_c.

Inserting the eigenvector given by Eq. (3.2) into Eq. (2.7) we get the approximated matrix

$$Z_{KL}^\pm(r) = Z_{KL}^{\pm(0)} \pm Z_{KL}^{\pm(1)}\alpha\rho(r) \tag{3.9}$$

(the higher-order terms are neglected) where the constant matrices $Z_{KL}^{\pm(0)}$ and $Z_{KL}^{\pm(1)}$ can be easily expressed in terms of $\tilde{F}_K^{(0)}$, $\tilde{F}_K^{\bullet(0)}$, and the remaining six eigenvectors for $r = r_c$ (see Appendix). In particular,

$$Z(r) = Z_0 - Z_1\alpha\rho(r), \tag{3.10}$$

where the coefficients Z_0 and Z_1 are the elements $(4,4)$ of the corresponding matrices in Eq. (3.9).

The above formula is true in a close neighborhood of r_c. To take into account the Rayleigh singularity it should be replaced by

$$Z(r) = Z_0\frac{1 - c_z\rho(r)}{1 - c_i\rho(r)} \tag{3.11}$$

with $c_i = 1/\rho(r_i)$, $c_z = 1/\rho(r_z)$, where r_i is the singular point and r_z is the zero point of $Z(r)$. The coefficients c_i and c_z satisfy the relation

$$c_i - c_z = \alpha Z_1/Z_0, \tag{3.12}$$

so that only one can be exact. In all the examples presented in Fig. 3 to Fig. 6 we have chosen the coefficient c_i to be exact; the other one is calculated from Eq. (3.12). In this way, the function $Z(r)$ given by Eq. (3.11) is singular for $r = r_i$ (as the exact function $Z(r)$), equal to zero for $r = r_z$ (where r_z is close to the zero point of the exact function $Z(r)$), and its first derivative is infinite for $r = r_c$ (as the first derivative of the exact function $Z(r)$).

Alternatively, we may choose the coefficient c_z to be exact, and calculate the other one from Eq. (3.12). The choice depends on what is considered to be the Green function in view of Eq. (2.8): the Fourier transform of $Z(r)$ or of $Y(r) = 1/Z(r)$. Moreover, we may choose both c_i and c_z to be exact, and calculate from Eq. (3.12) the coefficient Z_1. In this case, the approximation of $Z(r)$ in the neighborhood of r_c is a bit worse but for $r = r_c$ its main features remain unchanged: $Z = Z_0$ and the first derivative of Z is infinite.
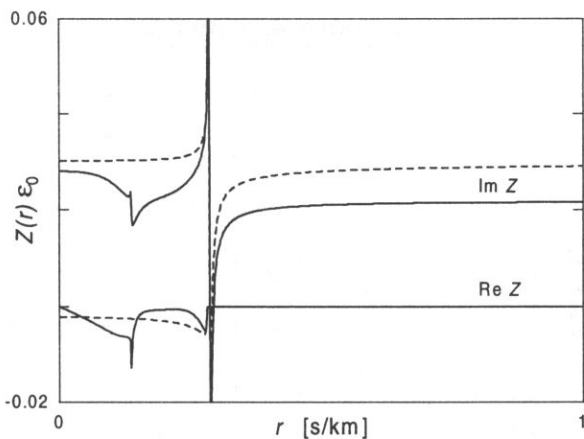
Fig. 3. The function $Z(r)$ (exact: *solid curve*, approximated: *dashed curve*) for lithium niobate (Euler angles: $0°$, $90°$, $90°$).

Fig. 4. The function $Z(r)$ (exact: *solid curve*, approximated: *dashed curve*) for quartz (Euler angles: $0°$, $90°$, $0°$).

Fig. 5. The function $Z(r)$ (exact: *solid curve*, approximated: *dashed curve*) for bismuth germanium oxide (Euler angles: $0°$, $0°$, $45°$). The vertical line marks r_c.

[175]

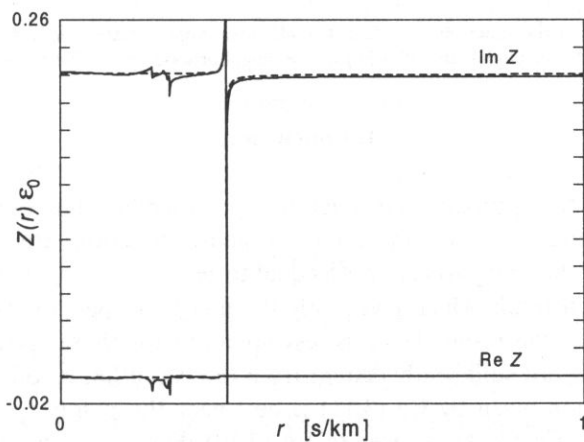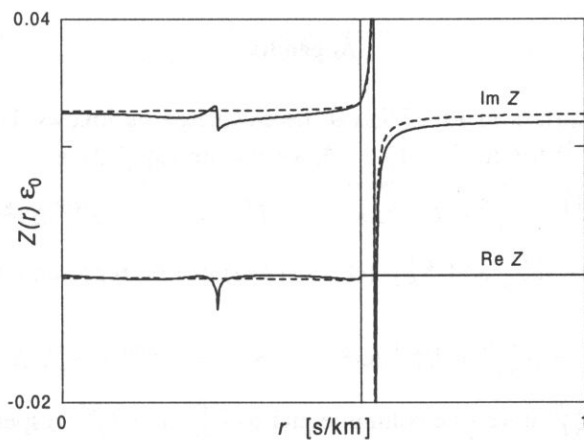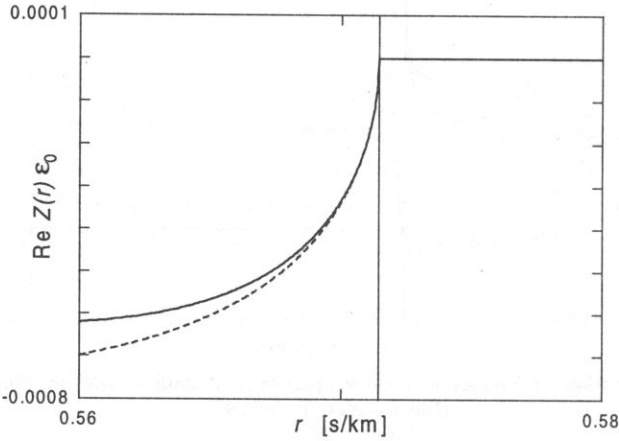Fig. 6. The real part of the function $Z(r)$ (exact: *solid curve*, approximated: *dashed curve*) for bismuth germanium oxide (Euler angles: $0°, 0°, 45°$) in the neighborhood of r_c. The vertical line marks r_c.

4. Conclusion

The behavior of the approximated function $Z(r)$ resembles that of the exact function $Z(r)$ in the whole range of r, and the values of the two functions are quite close to each other. In particular, the real parts are both equal to zero for $r > r_c$ (this feature is absent in the Ingebrigtsen formula which gives only the imaginary part of $Z(r)$). It should be added, however, that the resemblance is less apparent for those crystal cuts for which the cutoff point r_c is not sufficiently distant from the two other cutoff points.

The approximation given by Eq. (3.11) is best near the points r_c, r_i, and r_z. In the neighborhood of r_c, Eq. (3.11) reduces to Eq. (3.10). For $r = r_c$ both the real and the imaginary part of the first derivative of $Z(r)$ have a square-root singularity.

Appendix

The constant matrices in Eq. (3.9) can be calculated as follows. Using the notation $(\widetilde{F}_J^{(\pm)}) = (\widetilde{U}_K^{(\pm)}, \widetilde{T}_L^{(\pm)})$ for $K, L = 1, \ldots, 4$, we rewrite Eq. (3.2) as

$$\widetilde{U}_K^{(\pm)} = \widetilde{U}_K^{(0)} + \widetilde{U}_K^{\bullet(0)}\Delta s^{\pm}, \qquad \widetilde{T}_L^{(\pm)} = \widetilde{T}_L^{(0)} + \widetilde{T}_L^{\bullet(0)}\Delta s^{\pm}. \tag{A.1}$$

Each of the matrices $R_{KL}^{\pm}$ and $S_{KL}^{\pm}$ (cf. Eq. (2.4)) can be represented as a sum of two matrices. We have

$$R_{KL}^{\pm} = R_{KL}^{\pm(0)} + R_{KL}^{\pm(1)}\Delta s^{\pm}, \qquad S_{KL}^{\pm} = S_{KL}^{\pm(0)} + S_{KL}^{\pm(1)}\Delta s^{\pm}, \tag{A.2}$$

where $R_{KL}^{\pm(0)}$ and $S_{KL}^{\pm(0)}$ have one column equal to $\widetilde{U}_K^{(0)}$ and $\widetilde{T}_L^{(0)}$, respectively, and $R_{KL}^{\pm(1)}$ and $S_{KL}^{\pm(1)}$ have all elements equal to zero except in one column which is equal to $\widetilde{U}_K^{\bullet(0)}$ and $\widetilde{T}_L^{\bullet(0)}$, respectively.

The matrix $L_{KL}^{\pm}$ is the inverse of the matrix $S_{KL}^{\pm}$. If we put

$$L_{KL}^{\pm} = L_{KL}^{\pm(0)} + L_{KL}^{\pm(1)}\Delta s^{\pm} \tag{A.3}$$

where $L_{KL}^{\pm(0)}$ is the inverse of $S_{KL}^{\pm(0)}$, then

$$S_{KI}^{\pm}L_{IL}^{\pm} = I_{KL} + (S_{KI}^{\pm(0)}L_{IL}^{\pm(1)} + S_{KI}^{\pm(1)}L_{IL}^{\pm(0)})\Delta s^{\pm}, \tag{A.4}$$

(the higher order terms are neglected), and hence,

$$L_{KL}^{\pm(1)} = -L_{KI}^{\pm(0)}S_{IJ}^{\pm(1)}L_{JL}^{\pm(0)} \tag{A.5}$$

for $I, J = 1, \ldots, 4$. Inserting $R_{KL}^{\pm}$ and $L_{KL}^{\pm}$ into Eq. (2.7), and neglecting the higher order terms, we get Eq. (3.9) with

$$Z_{KL}^{\pm(0)} = R_{KI}^{\pm(0)}L_{IL}^{\pm(0)}, \qquad Z_{KL}^{\pm(1)} = R_{KI}^{\pm(0)}L_{IL}^{\pm(1)} + R_{KI}^{\pm(1)}L_{IL}^{\pm(0)}. \tag{A.6}$$

Acknowledgement

References

[1] K.A. INGEBRIGTSEN, *Surface waves in piezoelectrics*, J. Appl. Phys., **40**, 2681–2686 (1969).

[2] K. BLØTEKJAER, K.A. INGEBRIGTSEN and H. SKEIE, *A method for analyzing waves in structures consisting of metal strips on dispersive media*, IEEE Trans. Electron Devices, ED-20, 1133–1138 (1973).

[3] E. DANICKI, *New theory of SSBW devices*, [in:] 1980 IEEE Ultrasonics Symposium Proceedings, B.R. MCAVOY [Ed.] (IEEE, New York, 1980), pp. 235–239.

[4] E.L. ADLER, *SAW and pseudo-SAW properties using matrix methods*, IEEE Trans. UFFC, **41**, 699–705 (1994).

[5] E. DANICKI and W. LAPRUS, *Piezoelectric interfacial waves in langasite and dilithium tetraborate*, [in:] 1995 IEEE Ultrasonics Symposium Proceedings, M. LEVY, S.C. SCHNEIDER and B.R. MCAVOY [Eds.] (IEEE, New York, 1995), pp. 1011–1014.

[6] E. DANICKI and W. LAPRUS, *Piezoelectric interfacial waves in langasite and dilithium tetraborate*, Arch. Acoust., **21**, 99–107 (1996).

[7] W. LAPRUS and E. DANICKI, *Piezoelectric interfacial waves in lithium niobate and other crystals*, J. Appl. Phys., **81**, 855–861 (1997).

MEASUREMENT OF ULTRASONIC VELOCITY IN METHANOL
BY CAVITY RESONANCE METHOD

J. KRÓLIKOWSKI, R. PŁOWIEC

Institute of Fundamental Technological Research
Polish Academy of Sciences
(00-049 Warszawa, Świętokrzyska 21)

J. SINGH, T. K. SAKSENA

Ultrasonic Section, National Physical Laboratory
(Dr. K. S. Krishnan Road, New Delhi 110012, India)

The study of cavity resonance of the piezoelectric tubular transducer immersed in liquid has been exploited to evaluate the velocity of ultrasonic wave in methanol. Strong correlation has been proved between cavity resonance frequency and velocity of ultrasonic waves. The results are reported in the temperature range $10 - 50°C$. The presented method is simple and permit the measurements of ultrasonic velocity of liquids at low frequencies.

1. Introduction

It is well known that the ultrasonic methods are particularly convenient for the study of physical parameters of liquids [1–5]. Specifically a large number of methods exist for measuring ultrasonic velocity in liquids. These methods include for instance ultrasonic interferometer, pulse technique (including superposition and echo overlap technique), sing around and phase comparison method etc. All these methods are limited to high frequencies. The ultrasonic velocity measurements have scarcely been made at elevated temperatures as well as under higher hydrostatic pressures and practically non existent at lower frequencies.

Most of the piezoelectric transducers used for the ultrasonic velocity measurements work in the frequency range about 1 MHz to several hundred MHz. Thus it is rather difficult to measure the velocity in lower frequency ranges i.e. 10 kHz.

It has been known since some time that radial motion of the cylinder walls can excite symmetrical cavity modes in the enclosed liquid column. This cavity resonance frequency is a function of the velocity of ultrasonic waves in liquid.

In the present study it has been shown that the cavity resonance method may be used to evaluate the ultrasonic velocity in liquid.

As the ultrasonic velocity data at various temperatures and pressures for methanol are available in the literature to appreciate the cavity resonance method, the study of cavity resonance frequency in methanol has been carried out versus temperature.

2. Theoretical

An open ended thin walled piezoelectric cylindrical tube vibrating in air shows a dominant radial mode of resonance. When the same tubular transducer is immersed in liquid besides the radial fundamental resonance, the appears a cavity resonance of the enclosed liquid medium. The angular frequencies of the cavity modes are given by [6]:

$$\omega_c^m = [(2m - 1)\pi c_0]/(h + 2\beta a), \qquad m = 1, 2, 3, \ldots, \tag{1}$$

where h stands for the length of the tubular transducer, β is end correction, a is the inner radius of tubular transducer element and c_0 is the effective velocity of sound in liquid medium due to finite stiffness of the walls of the tubular transducer. The effective velocity c_0 depends on the ultrasonic velocity in open liquid c according to the following relation:

$$c_0 = c(1 + Ba/E_{11}t)^{-1/2}, \tag{2}$$

where E_{11} is the transverse Young's modulus, t is the width of the wall of tubular transducer and B is the bulk modulus of liquid.

$$B = \varrho c^2, \tag{3}$$

where ϱ is the density of liquid. The end correction can be approximated by the expression:

$$\beta = 0.633 - 0.106\omega_c a/c_0. \tag{4}$$

Combining the equations (1)–(4), for $m = 1$, we arrive at the following expression:

$$\frac{1}{c^2} = \frac{1}{f^2} \left(\frac{h/2a + 0.633 - \sqrt{(h/2a + 0.633)^2 - 0.212\pi}}{0.424\pi a} \right)^2 - \frac{2a\varrho}{E_{11}t}. \tag{5}$$

As it is clearly seen this expression represents a linear relation between c^{-2} and f^{-2}. The proportionality coefficient depends only on geometrical parameters of the transducer. Therefore by measuring resonance frequency one can readily evaluate velocity of the ultrasonic waves. Because the mechanical resonance affects the electrical resonance of the piezoelectric transducer [3] the resonance frequency may be evaluated by means of measurement of electrical parameters of the transducer like conductance G or impedance Z.

3. Experimental

The piezoelectric tubular transducer element – outer diameter 25.4 mm, inner diameter 18.85 mm and tube length 25.4 mm — fabricated from piezoelectric material NPLZT–5H (being equivalent to PZT–5H) has been used in our study. The fundamental resonance frequencies of this element in air, have been determined by plotting the variation of impedance (Z) and conductance (G) as a function of frequency. Similar plots were obtained after immersing the tubular transducer element first in deionised water and later in methanol.

These plots were used to determine cavity resonance frequencies as well as fundamental resonance frequencies.

We used methanol in our studies for two reasons. Firstly, it is well known medium studied by many research group. Hence there is a great deal of experimental data (gained at varying pressure and temperature) available in the literature [1]. Secondly, methanol is a non-conductive liquid so the piezoelectric tubular transducer can be safely immersed in it.
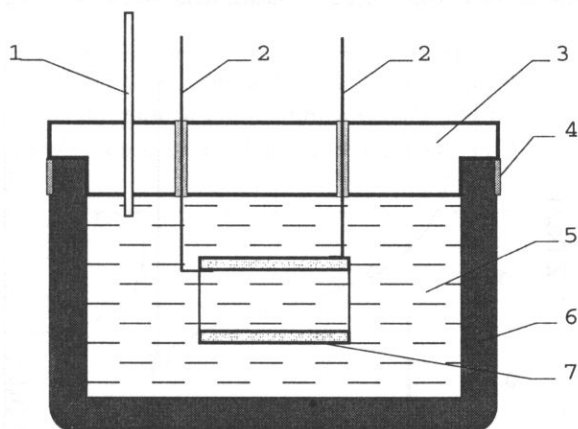

Fig. 1. Experimental setup. 1 – pipe; 2 – electric wires; 3 – aluminium cover; 4 – bandage; 5 – tested liquid; 6 – rubber container; 7 – tubular piezoelectric transducer.

Our measurements of cavity resonance have been carried out using special neoprene rubber container as depicted in Fig. 1. The top of the container is fitted with the aluminium alloy cover by clamp. Two isolated electric wire connection (2) were used for the measurement of required electrical parameters. The Hewlett Packard impedance analyzer 4192A LF was used for the measurements of impedances and conductances. The comparison between plots of impedance (Z) vs. frequency of the piezoelectric tubular transducer element in air (Fig. 2) and deionised water (Fig. 3) clearly indicate the cavity resonance at ~ 20 kHz. Resonant maximum of the same frequency appears at the plot of conductance (G) vs. frequency (Fig. 4).

Similar observations with the different other liquids such as paraffin oil and methanol show the cavity resonances below 20 kHz. The ultrasonic velocities derived using Eq. (5)
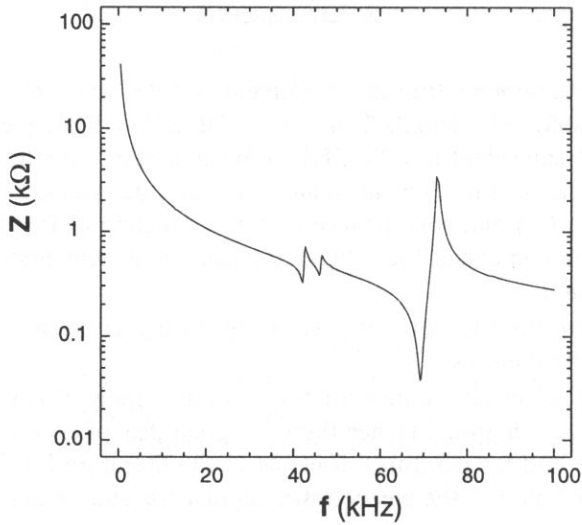
Fig. 2. Dependence of impedance Z of tubular transducer vs. frequency f in air.
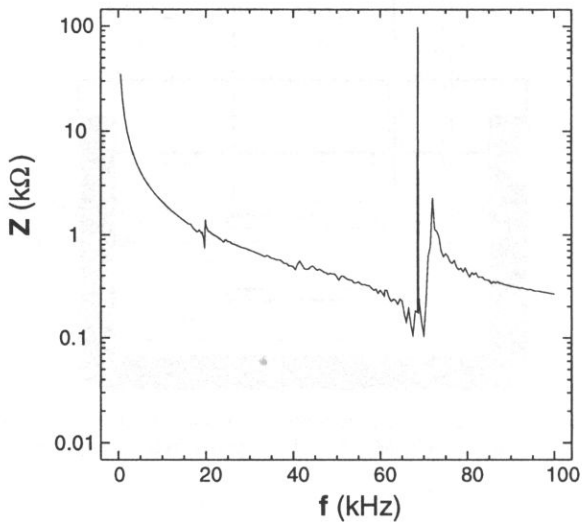
Fig. 3. Dependence of impedance Z of tubular transducer vs. frequency f in deionized water.

from measured cavity resonances are in quite good agreement with those reported earlier in the literature.

Further the cavity resonance in the liquid has been confirmed with direct measurement of transmitted acoustical wave by using hydrophone and test tank. The acoustical output power as a function of frequency has shown significant maximum value at the same cavity resonant frequency as measured by means of impedance/conductance vs. frequency plot.

The very sharp resonance (Fig. 5) is observed for radial mode vibration in air. After immersing the tubular transducer element in methanol one gets rather a complicated plot
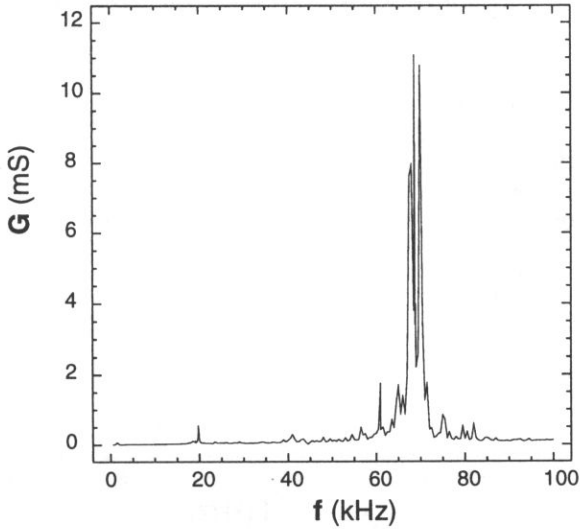
Fig. 4. Dependence of conductance G of tubular transducer vs. frequency f in deionized water.

(Fig. 6). It may be seen that there is an additional resonance frequency at about 14 kHz which was not present in the plot of conductance versus frequency in air. It reflects the cavity resonance of piezoelectric tube which is being used for evaluating the ultrasonic velocity in methanol.
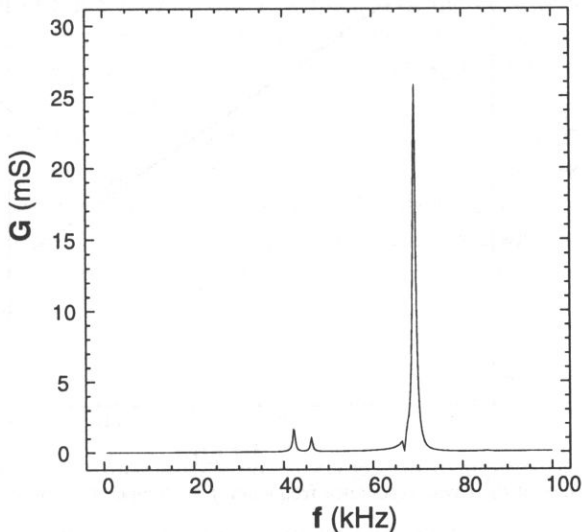
Fig. 5. Dependence of conductance G of tubular transducer vs. frequency f in air.

The measurement of the cavity resonance frequency of tubular transducer immersed in methanol have been carried out at constant normal pressure. The cavity resonance frequency measurements at different temperature indicate that the cavity resonance and sub-
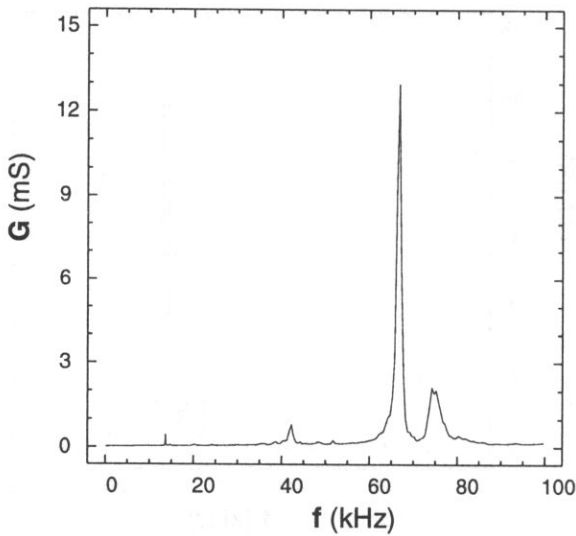
Fig. 6. Dependence of conductance G of tubular transducer vs. frequency f in methanol.

sequently the ultrasonic velocity (Eq. (5)) decreases with increase of temperature (Fig. 7). This result completely agrees with already published data [1].
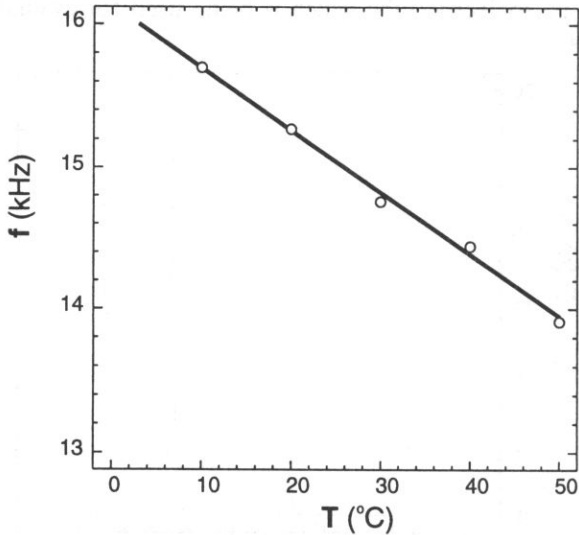
Fig. 7. Dependence of the cavity resonance frequency f vs. temperature of the methanol T.

Further the correlation between cavity resonance and ultrasonic velocity has also been checked theoretically and experimentally by plotting (Fig. 8) the inverse square of velocity $(1/c^2)$ versus the inverse square of cavity resonance frequency $(1/f^2)$. The values of velocity of ultrasonic waves taken from the measurements by WILSON and BRADLEY [1] and the plot $1/c^2$ versus $1/f^2$ a solid line was obtained by means of the least square fit.
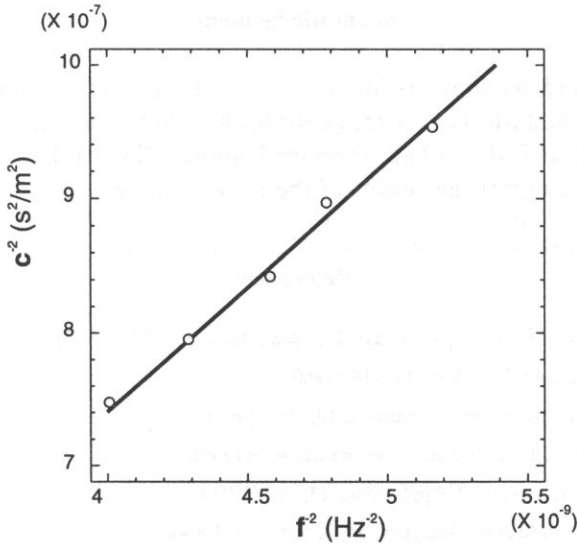
Fig. 8. Invert square of ultrasonic wave velocity in methanol against invert square of cavity resonance frequency.

Correlation coefficient for the both presented parameters is 0.997. The slope of the line obtained in experiment equals to 187.22. The theoretical value of the slope, evaluated by the equation (5) is 196.5 and is close to the experimental value. The slight discrepancies from linearity seen in Fig. 8 may be due to influence of the wave reflected from the walls of neoprene rubber container as the distance between transducer element and walls of the container was comparable with ultrasonic wavelength. Reflected wave affects the mechanical loading of the transducer.

The present studies indicate that the cavity resonance method which is simple technique may successfully be used for the measurement of ultrasonic velocity in the liquids. This method may serve as a very useful tool for the measurement of ultrasonic velocities in liquids particularly at fairly low frequency range which are rather difficult to access by other commonly used methods. We expect that this method can be also used with high pressure experiments.

4. Conclusions

In this work we performed ultrasonic investigation of liquids using cavity resonance method.

The main conclusion one can drawn from experimental results is that cavity resonance method may be successfully applied for ultrasonic investigation of liquids.

Our results indicate that it is is very useful technique, particularly, in the very low frequency regime.

We expect that this method can be also extended to investigate effects of higher hydrostatic pressure.

Acknowledgements

References

[1] W. WILSON and D. BRADLEY, J. Acoust. Soc. Am., 36, 2, 333–337 (1964).

[2] R.T. BEYER, J. Acoust. Soc. Am., 32, 719 (1960).

[3] H. EDEN and E. RICHARDSON, Acoustica, 10, 309 (1960).

[4] S. PARTHASARATHY, Proc. Indian Acad. Sci., 2, 497 (1935).

[5] T. LYONS and T. LITOVITZ, J. Appl. Phys., 27, 197 (1956).

[6] G.W. McMAHON, J. Acoust. Soc. Am., 36, 3, 528–533 (1964).

[7] T.V. CHALIKIAN, A.P. SARVAZYYAN, T. FUNCK, V.N. BELONENKO and F. DUNN, J. Acoust. Soc. Am., 91, 1, 52 (1992).

[8] J.F. HASKINS and J.L. WALSH, J. Acoust. Soc. Am., 29, 6, 729–734 (1957).

[9] D. CHURCH and D. PINCOCK, IEEE Transactions on Sonics and Ultrasonics, SU–32, 1, 61–64, (1985). Phys., 81, 855–861 (1997).

THE INFLUENCE OF TEMPERATURE ON THE SENSITIVITY OF A SAW GAS SENSOR WITH A THIN LAYER OF LEAD PHTHALOCYANINE

M. URBAŃCZYK

Institute of Physics
Silesian Technical University
(44-100 Gliwice, ul. Krzywoustego 2)

The paper deals with experimental investigations concerning the influence of temperature on the sensitivity of a SAW sensor with a thin layer of lead phthalocyanine (PbPc) to NO_2 molecules in the air. Measurements have been carried out with a dual delay line system providing simultaneously a survey of the differential frequency, Δf, and the measuring frequency, f. In all cases the measured frequency, f, was increased, whereas the changes in the difference of frequency, Δf, were negative as a result of the interaction with NO_2 molecules. All the experiments have been made at the same conditions, i.e., with the same PbPc layer of a 310 nm thickness, at 40 ppm NO_2 in air and at a constant gas flow rate of 100 ml/min. In the range $30 - 60°$ C, the sensitivity increased almost linearly with temperature a constant rate of $0.13 - 0.15$ kHz/° C.

1. Introduction

Systems with Rayleigh's acoustic surface waves have been applied in the construction of detectors of toxic gases for a long time [1–4, 9, 10]. The basic system of SAW gas sensors is a generator in which an acoustic delay line works in the positive feedback loop of the amplifier. The acoustic delay line assures the phase condition for generation whilst the amplifier assures the amplitude condition. The amplifier gain should be higher than the delay line insertion losses. For this purpose, two identical circuits are formed on a piezoelectric substrate (e.g. $LiNbO_3$) to facilitate the propagation of a surface wave excited by means of interdigital transducers. Next, a thin layer of an organic semiconductor of metalophthlocyanine type (MPc) is formed in one of the paths by sublimation in vacuum, the thickness of the layer not exceeding 1% of the length of the propagating surface wave. The free path of a crystal serves as a reference. As a result of the interaction of the thin metalophthlocyanine layer with gas, the SAW velocity undergoes a change. This change can be observed and measured as a frequency of the single acoustic delay line or as a difference frequency of the dual acoustic delay lines, i.e. between the delay line with an active thin layer and the reference one.

An essential feature of a surface wave is the concentration of the whole energy just near the surface within a layer of thickness not exceeding two wavelengths (2λ), so that

it becomes possible for the wave to affect easily and effectively the medium placed on the crystal surface. In this way the propagation of waves along the path in which the layer has been placed is slightly disturbed (depending on the thickness of the layer, h, its density, ϱ, and the electric conductivity, σ). Physically this disturbance consists in a reduction of the velocity and an increase of the attenuation of the propagating wave.

The reduction of the velocity of propagation is mainly caused by two phenomena [5, 6]:

a) the mass load on the crystal surface and

b) the electric "load" resulting from the effect of interaction of the electric potential associated with the surface wave with mobile charge carriers in the layer.

The interaction of the thin phthalocyanine layer with active gas molecules can be shown in the form of a diagram [7, 8].

Diagram of the interaction: gas – chemical active layer – SAW – electronic system

Interaction of the thin MPc layer with gas particles
Adsorption resulting from the formation of ionised states at the layer surface due to the exchange of electrical charges Criterion: – electron affinity of the gas – the kind of metal in the MPc particle – **temperature of the reaction**

↓

Change of the surface mass of the layer as well as changes in the electrical conductivity (generation of additional charge carriers)

↓

Interaction of the disturbed layer with the propagating SAW: – mass effect – conductivity effect

↓

Changes of the velocity of the wave propagation, and hence an additional change in the frequency of generation, f, (wavelength is constant; determined by the geometry of the transducer) Changes of the amplitude due to changes in the wave attenuation

↓

Detection of the frequency difference $\Delta f = f - f_0$

This article is aimed mainly at the study of the influence of the temperature on the aforesaid interaction.

2. Experimental and results

The measurements have been carried out with a dual delay line system providing simultaneously a survey of the differential frequency, Δf, and the measuring frequency, f. The temperature was stabilized inside the measuring chamber on the balance principle by means of a power transistor (Fig. 1). The stabilization was within the range $\pm 0.1°$ C.

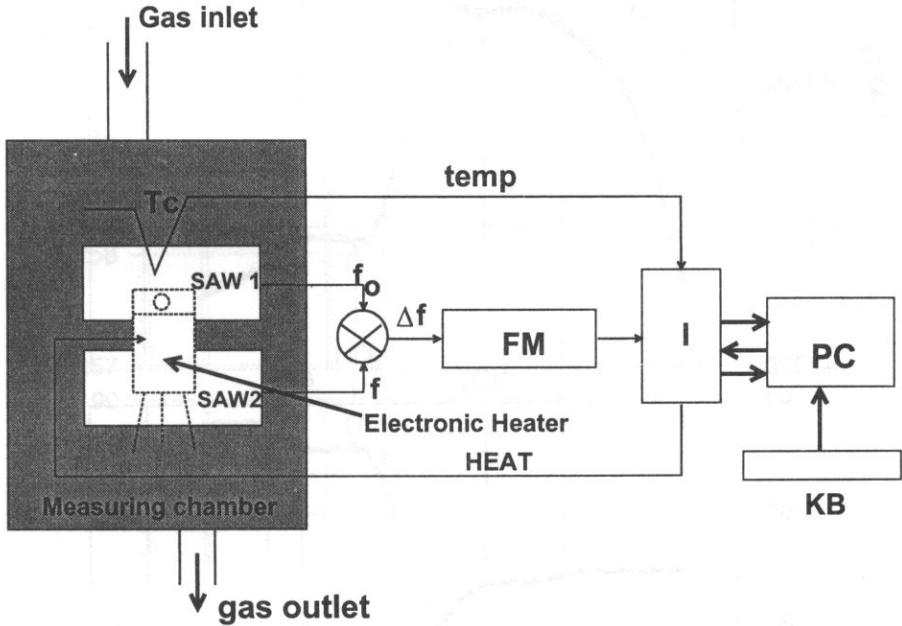Fig. 1. Schematic representation of the experimental set-up. The measuring frequency, f, was measured directly by means of a probe. Symbols: I – interface, PC – personal computer, KB – keyboard, FM – frequency meter., Tc – thermocouple (Cu – const), SAW 1, 2 – surface acoustic wave lines.

Each measurement was carried out after the stabilization of temperature. The long time frequency drift was compensated in the dual delay line system as can be seen in Figs. 2–5. These diagrams show the interaction of a thin PbPc layer with NO_2 molecules in air. Basing on these results, a final diagram was drawn showing the difference and measuring frequency versus temperature of interaction (Fig. 6).

3. Conclusions

In all cases the change of the measuring frequency, f, was positive, whereas the change in the difference frequency, Δf, was negative as a result of the interaction with NO_2 molecules. This is connected with the configuration of the frequency modes f and f_0; since in the normal configuration $f < f_0$, the increase of the measuring frequency f causes a decrease in the difference frequency Δf. The main conclusion is that the sensitivity is increased (a larger change in the frequency) with the increase of the interaction

Fig. 2. Interaction of a 310 nm PbPc layer with NO_2 molecules of concentration of 40 ppm in air at 30° C and at a constant gas flow rate of 100 ml/min.
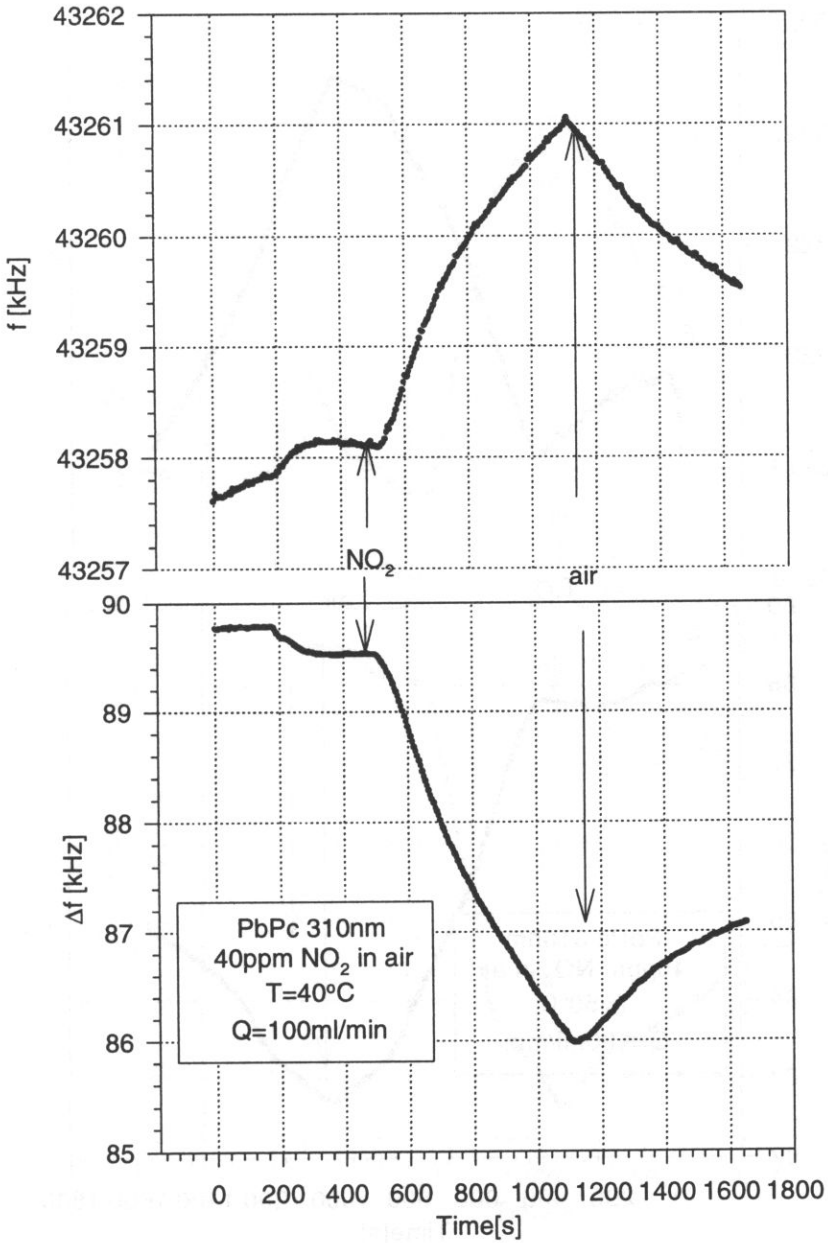
Fig. 3. Interaction of a 310 nm PbPc layer with NO_2 molecules of concentration of 40 ppm in air at 40° C and at a constant gas flow rate of 100 ml/min.
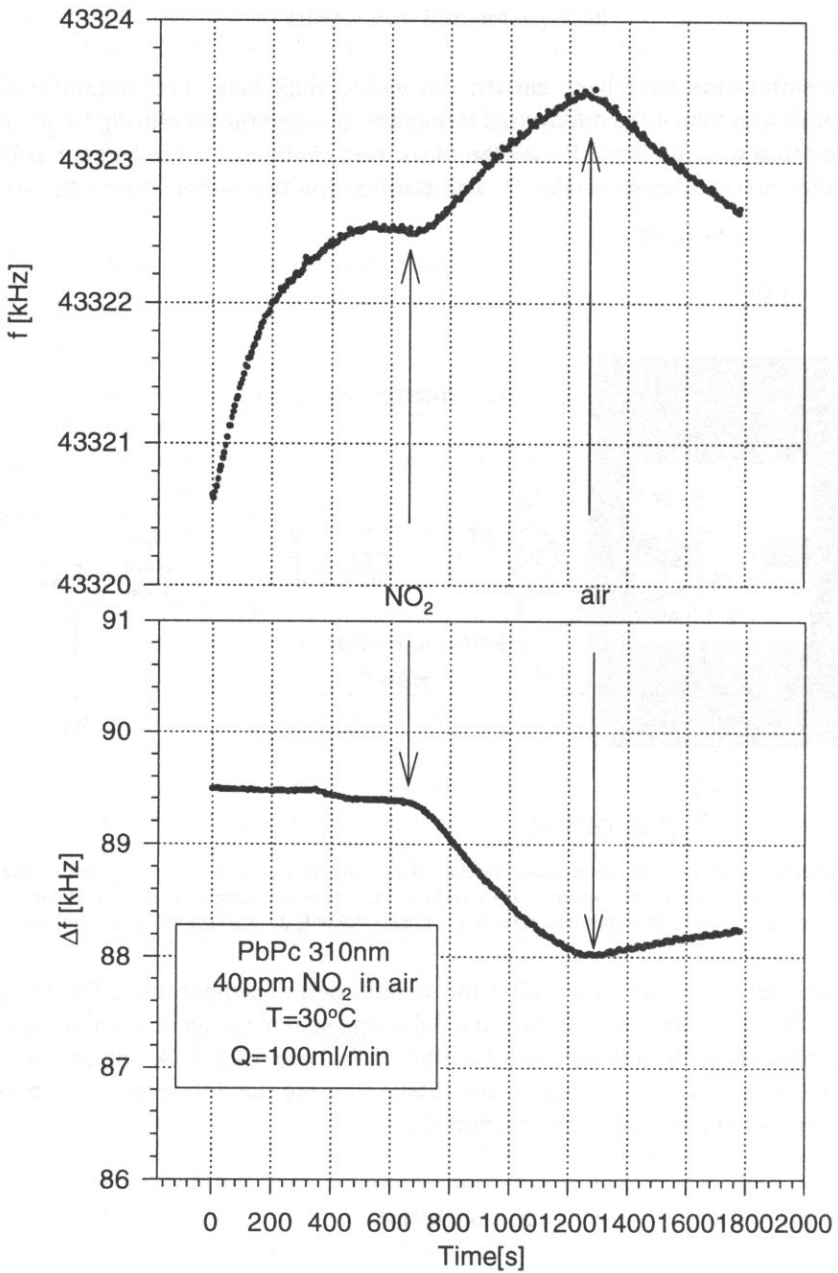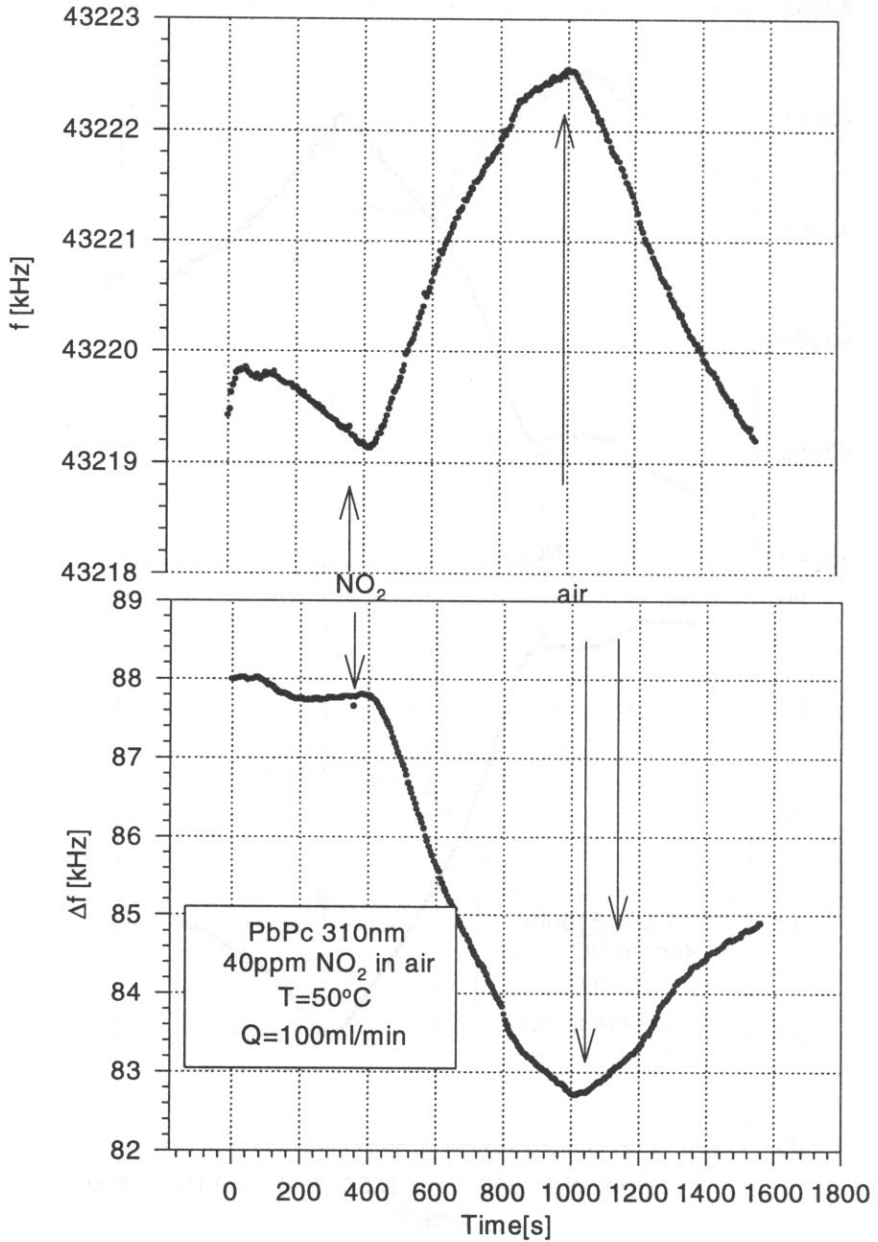
Fig. 4. Interaction of a 310 nm PbPc layer with NO_2 molecules of concentration of 40 ppm in air at 50° C and at a constant gas flow rate of 100 ml/min.
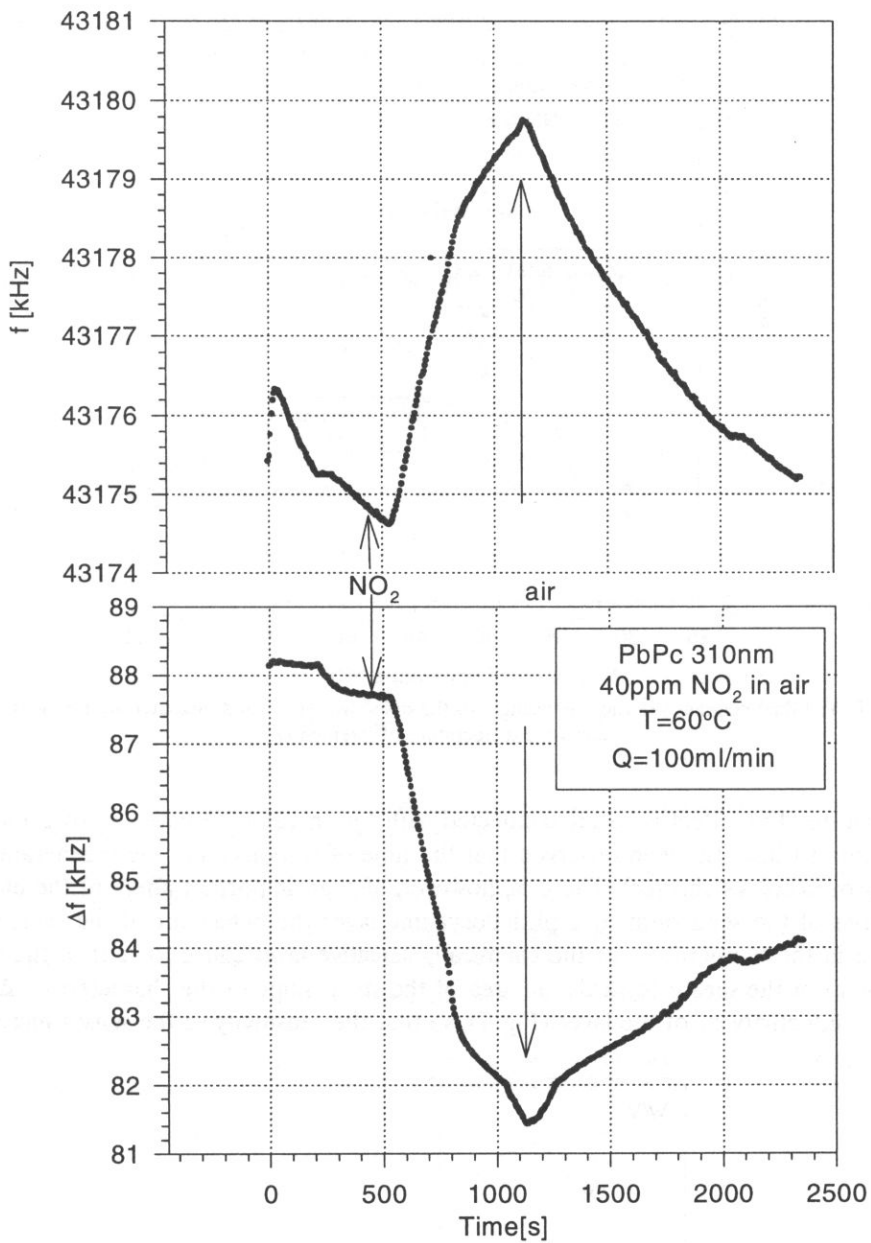
Fig. 5. Interaction of a 310 nm PbPc layer with NO_2 molecules of concentration of 40 ppm in air at 60° C and at a constant gas flow rate of 100 ml/min.
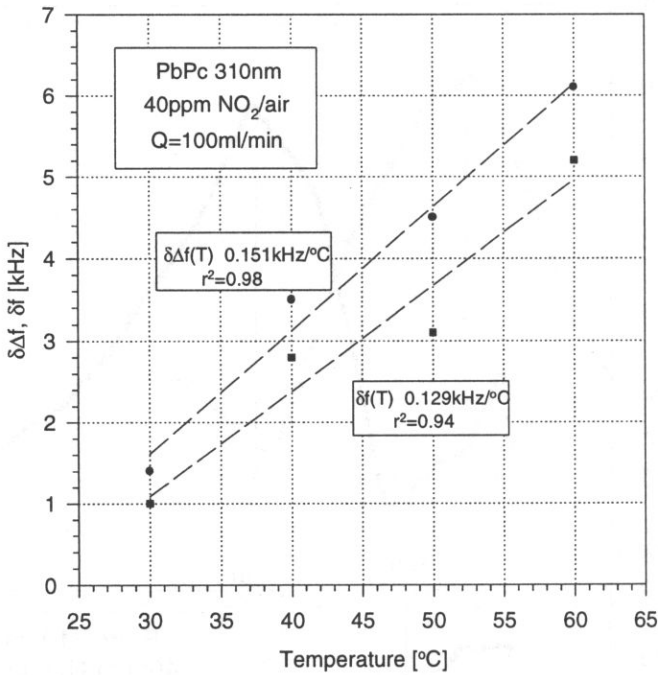
Fig. 6. The final diagram showing the changes of the difference $\delta(\Delta f)$ and measured δf frequencies versus the temperature of interaction.

temperature. This effect is surely connected with the increased kinetics of sorption and desorption (it has also been observed that the time of response and the regeneration of the sensor becomes shorter). There is, however, also an important affect of the electric properties of the semiconductive phthalocyanine layer the behaviour of the sensor. An increase in the temperature of the chemically sensitive layer causes a shift of the operating point of the sensor towards the area of the steep slope of the characteristic $\Delta v/v_0$ versus conductivity σ_s of the layer (Fig. 7), so that the sensitivity of the sensor increases.
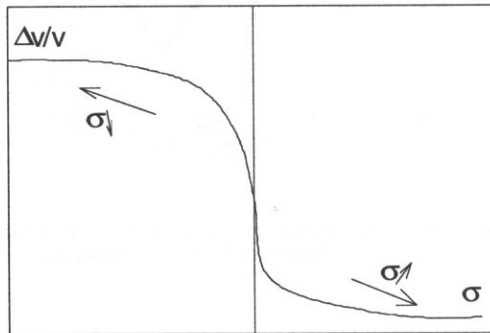
Fig. 7. Velocity of the SAW wave propagation versus electrical conductivity of the sensor layer.

It results also from the diagrams that there is some difference between the change in the frequency difference Δf and that in the measuring frequency f. This can be due to the dipole interaction of polar molecules with the electric field associated with the SAW in the reference acoustic path. This will be the subject of feature research.

Acknowledgement

References

[1] M. VON SCHICFUS, R. STANCEL, T. KAMMERECK, D. WEISKAT, W. DITTRICH and H. FUCHS, *Improving the SAW gas sensor: device, electronic and sensor layer*, Sensors and Actuators B, **18–19**, 443–447 (1994).

[2] M.S. NIEUWENHUIZEN and J.L.N. HARTEVELD, *An automated SAW gas sensor testing system*, Sensors and Actuators A, **44**, 219–229 (1994).

[3] V.I. ANISIMKIN and I.M. KOTELYASKI, *Operating characteristic of SAW gas detectors*, Sov. Phys. Tech. Phys., **37**, 2 (1992).

[4] A. VENEMA, E. NIEUWKOOP, M. VELLEKOOP, W. GHIJSEN, A. BARENDSZ and M. NIEUWENHUIZEN, *NO$_2$ gas-concentration measurement with a SAW-chemosensor*, IEEE Trans. on Ultrasonics, Ferroelectr. Freq. Control, UFFC-34, **2**, 148–155 (1987).

[5] B.A. AULD, *Acoustic Fields and Waves in Solids*, Vol. 2, Wiley, New York 1973.

[6] A.J. RICCO, S.J. MARTIN and T.E. ZIPPERIAN, *Surface acoustic wave gas sensor based on film conductivity changes*, Sensors and Actuators, **8**, 319–333, 1985.

[7] R. VAN EWYK, A. CHADWICK and J. WRIGHT, *Electron donor–acceptor interactions and surface semiconductivity in molecular crystals as a function of ambient gas*, J.C.S. Faraday I, **76**, 2194–2205 (1980).

[8] B. BOTT and T.A. JONES, *A highly sensitive NO$_2$ sensor based on electrical conductivity changes in phthalocyanine films*, Sensors and Actuators, **5**, 43–53 (1984).

[9] M. URBAŃCZYK and W. JAKUBIK, *Optimal conditions for the generation system of a SAW gas sensor*, Arch. Acoust., **21**, 85–88 (1996).

[10] M. URBAŃCZYK, W. JAKUBIK and S. KOCHOWSKI, *Investigation of sensor properties of copper phthalocyanine with the use of surface acoustic waves*, Sensors and Actuators B, **22**, 133–137 (1994).

DEVICES FOR MEASUREMENT OF THE NO₂ CONCENTRATION IN THE AIR BY MEANS OF SURFACE ACOUSTIC WAVES

M. URBAŃCZYK, W. JAKUBIK

Institute of Physics,
Silesian Technical University,
(44-100, Gliwice, ul. Krzywoustego 2)

E. ADAMCZYK

Institute of Fundamental Technological Research
Polish Academy of Sciences
(00-049 Warszawa, Świętokrzyska 21)

J. RZESZOTARSKA

Faculty of Chemistry, Warsaw University

The development of techniques concerning macromolecular compounds have made it possible to get thin layers which change their physico-chemical properties in result of their interaction with the ambient atmosphere. Changes of the physical properties of specially prepared chemically sensitive layers influence the conditions of the propagation of an acoustic surface wave arranged in the layered system piezoelectric waveguide – layer of the compound. Particularly, if the mass and electric conductivity of the chemically sensitive layer is changed, the velocity of the propagation of the acoustic wave changes too.

The presented paper include a short review of the SAW gas sensor field and some experimental results for detection a low concentration of NO₂ in air.

1. Introduction

The constantly growing pollution of the natural environment, particularly of the atmosphere, require a continuous monitoring of these contaminations. In recent years an intensive development of new method of diagnosing the state of our natural environment are to be observed. Among them acoustic methods deserve special attention; these are based on the propagation of surface acoustic wave (SAW) in layered structure, in which the chemical active layer is a macromolecular compound.

Literature [1] quotes the following types of sensors with a chemically sensitive layer:

a) chemiresistors, in which use is made of changes in the resistant layer due to the adsorption of gaseous particles from the environment,

b) piezoelectric quartz gauges with an acoustic bulk wave,

c) systems with surface acoustic waves.

Conducting macromolecular complexes are characterized by much more complex mechanism of conductivity than inorganic semiconductors; therefore acoustic methods may provide new information concerning the mechanism of conductivity, which is essential also from the viewpoint of the application of these compounds in indicators of gases.

Of much interest is the application of acoustic surface wave propagated in the layered system "piezoelectric waveguide – thin chemically sensitive layer" in the designing of indicators of gases. This results from the fact that a surface wave is extremely "sensitive" to all changes of the properties of the surface of the medium in which it is propagated. In the case of a piezoelectric medium changes in the velocity of the acoustic wave are to be observed which are caused by changes in the mass loaded with the chemically sensitive layer (due to the adsorption of gaseous particles), or by changes of the electric conductivity of this layer [2, 3]. The theoretical sensitivity of an oscillator with an acoustic surface wave at a frequency of about 100 MHz amounts according to [1] to about 17 Hz/ng/cm^2; for an active surface of the sensor amounting to 0.17 cm^2 this means a rather low level of detection of the changes of mass, i.e. 0.2 ng. At a frequency of about 3 GHz the sensitivity of the system amounts theoretically to about 3×10^{-15} g.

Analysers of gases applied so far, making use of electrochemical and photoacoustic phenomena, as well as gas chromatography do not warrant a satisfying accuracy, or they are only labour-consuming laboratory methods. The photoacoustic analysers advertised by BRUELL and KJAER [4] are very expensive. Therefore, various research centres all over the world try to design new kinds of gas sensors. Similar investigations have also been started at IFTR in Warsaw on the design of an apparatus for the SAW method [17] which is applied in the Institute of Physics at the Technical University of Silesia.

2. Layers applied for covering the SAW sensors

Compounds of metalphthalocyanines [2], known since the beginning of our century, have only recently attracted attention as thin active layers permitting a selective detection of vapours and gases. A modification of the interior structure of the macromolecule, consisting in the replacement of the metal ion and substituents in the aromatic rings, makes it possible to obtain metalphthalocyanines with various properties. At presence there are more than 70 varieties of them [1]. Phthalocyanines belong to the group of low-dimension organic semiconductors [2, 5]. Roentgenographic investigations of phthalocyanines have proved the existence of three polymorphic forms, viz. α, β and x [5]. The crystalline structure increases by sublimation at a temperature of $400 - 500°$ C in the presence of nitrogen (7Tr). Depending on the technological conditions of sublimation, phthalocyanine crystallises in the monoclinic or triclinic system. The metal atom included into the structure of the macromolecule affects essentially the physicochemical properties of phthalocyanine. Literature indicates that the most frequently investigated macromolecular

complexes of metalphthalocyanines are copper CuPc, lead PbPc and ferrous phthalocyanine FePc, as well without metal – H_2Pc.

CHANG et al. [6] have investigated monolayers of phosphateidylcholine obtained by means of Langmuir–Blodgett's method. O'DONNEL et al. [7] quote the results of investigations on the adsorption of NO_x by a layer of phthalocyanine. The achieved level of gas detection amounted to $5 - 200$ ppm. Copper phthalocyanine CuPc was investigated, among others, as an active layer in a NO_2 – sensor by NIEUWENHUIZEN and his team [8]. The achieved sensitivity was within the range from $0.3 - 70$ Hz/ppm, the time response/regeneration amounting from 1/6 to 107/156 minutes. At the same time a rather high sensitivity of such a type of layers to effects of NH_3, but no effect of CO_2, CO, CH_4, SO_2 could be detected, and neither of toluene vapours and water vapour.

A comprehensive publication dealing with investigations concerning the layers of the phthalocyanines H_2Pc, MgPc, FePc, CoPc, NiPc, CuPc and PbPc is [9], in which it has been attempted to evaluate the usability of these compounds for the purpose of detecting CO, CO_2, CH_4, NH_3, SO_2, water vapour and toluene vapours. Among others, the authors stress the fact that phthalocyanines, being semiconductive organic compounds of the type p, strongly interact with electronegative gases. This interaction involves a change in the conductivity of the macromolecular layer. It has been found that the tested layers do not interact so strongly with water vapour and oxygen.

Many papers inform about the application of the phthalocyanine H_2Pc, metalphthalocyanine as well as other complexes containing electronic systems of the type for the purpose of detecting the presence of NO_2 and chlorine.

The results of investigations on copper and iron phthalocyanines have been published in [10]. Among others, the influence of O_2 and strongly electronegative gases (NO_2, NO, Cl_2, Br_2 and I_2) on the properties of thin layers could be determined. These investigations confirmed that the sensitivity of these phthalocyanines to the aforesaid gases differs. The response time of the system amounted to $1-70$ minutes. The sensitivity of the active layer depends on the carrier gas (air or nitrogen) forming the background of the investigated gas.

Attempts have also been made to construct a prototype of a microprocessor system of monitoring nitrogen dioxide. This was affected at the University of Kent (in the United Kingdom) in 1991, sponsored by British Gas [11]. The principle of detection was based on utilization of changes in the electric conductivity of thin layer of lead phthalocyanine exposed to the influence of electronegative NO_2. In this way a very high sensitivity of detection was achieved on the level of single ppb's as well as a comparatively short response time (about 30 s). With such parameters the sensor excels all the conventional commercial sensors.

Most publications on this subject matter come from the end of the 80's and the 90's of this century; they mainly deal with investigations concerning the sensory properties of these complexes. These publications prove that this problem is highly actual. The connection of the sensory properties of macromolecular compounds with investigations on the structure of thin chemically sensitive layers exposed to the interaction of gases has been deal with in these papers only incompletely or not taken into account at all. Extremely important is the correlation of such sensory parameters as sensitivity, the

dynamics of the sensor, the response time and the regeneration of the active layer, as well as the processes of ageing, including structural investigations of selected layers and taking into account the effect of the technological conditions of the process of sublimation on their structure and properties. In order to utilize the properties of phthalocyanine complexes fully it seems to be expedient to undertake the widest possible investigations on their electric properties (dependence of conductivity and energy of activation on the gaseous environment) and changes of their acoustic properties (absorption, dispersion).

As we know from literature, sensors of the type SAW may be divided into two categories, viz. sensors measuring physical quantities and sensors used to measure chemical quantities. The physical properties which can be measured by means of such sensors have been gathered in Table 1.

Table 1. Physical SAW sensor, after [18].

Measured quantity	Sensitivity/detecability
Temperature	0.0001 °C
Pressure	0.1 ppm/atm
Force – acceleration	18 Hz/g
Electric field	15 − 30 ppm/kV/mm
Displacement	300 Hz/μm
Flow rate	11 Hz/sccm

If SAW is applied as a chemical sensor, a thin layer reacting with the analysed agent must be put on the surface of the piezoelectric substrate. The interaction of this agent must lead to changes of the properties of this layer, e.g. its density, viscosity, modulus of elasticity, dielectric constant or conductivity. In this way parameter of the propagation of the surface wave is changed. The sensitivity and selectivity of SAW sensors depends on the physicochemical properties of the covering layer. Most often two retarding lines are applied (discussed further on in this paper), forming two oscillating systems. One of these lines is covered with a layer reacting with the investigated medium, the other one remaining uncovered. The difference of frequencies between the generations of oscillators, resulting from physicochemical changes of the active layer amounts to several score of Hz up to several kHz, applying resonance frequencies of the oscillators within the range from several score to several hundred MHz.

Exemplary coverings of the retarding lines have been presented in Table 2.

The change of frequency oscillation in the generator system may result from two effects: the effect of conductivity, when in result of changes in the electric conductivity of the chemically sensitive covering due to the interaction of the ambient medium the conditions of propagation of the acoustic wave in piezoelectric waveguide are changed, and the mass effect, when due to changes in the mass of this layer the velocity of propagation of the acoustic wave is changed [3]. The operation of SAW sensors is based on the utilization of changes of the mass or electric conductivity of the chemically sensitive layer.

There are also other constructions of sensors which utilize Love's shear waves. Such sensors enable us to measure the properties of polymers and to determine their glassy

Table 2. Coverings applied in chemical SAW sensors.

Determined gas/vapour	Covering	Sensitivity/detecability
H$_2$	CuPc + Pd (doping)	50 ppm
NH$_3$	ZnO + In	1 – 10 ppm
NO$_x$	PbPc, CuPc, H$_2$Pc	2 ppb – 500 ppm
H$_2$S	WO$_3$, SnO$_2$ + Pt	0.01 – 60 ppm
SO$_2$	Heteropolysiloxane, Triethanolamine, CeO$_2$	1 – 100 ppm
H$_2$O	Polyimide no film	1.1 kHz/% Rh dipole interactions

temperature, their melting point, the coefficient of expansion and the energy of thermal activation.

For several years now in the Institute of Physics at the Technical University of Silesia researches have been carried out in co-operation with the IFTR Polish Academy of Sciences on the application of thin layers of macromolecular complexes for the purpose of detecting the presence of gases. This year our researches concern mainly nitrogen dioxide.

3. Applied apparatus

For measurements of the NO$_2$ concentration the prototype of a device has been constructed, the block diagram of which is to be seen in Fig. 1. It consists of a cylindrical test chamber with the sensor plate inside – a system of the double line SAW on lithium niobate with a chemically sensitive layer in one path. The plate was fastened on a base with 14 feet, the dimensions of which were 20×17.3 mm. This base was mounted on a typical support as applied for the assembly of integrated circuits. The plate of laminated foil supports the other elements of the device – electronical elements and the numerical read – out. The acoustic waveguides have been denoted as $L1$ and $L2$. On one of the waveguides was padded with a thin chemically sensitive layer of lead phthalocyanine, serving as the sensory element. The other waveguide serves as a reference system. Each acoustic line operates in the feed-back loop of the wide-band amplifiers $A1$ and $A2$ as oscillators. The voltages of oscillation from the amplifiers of both lines are conveyed to the input of the mixing system M, at the output of which the signal of the beat frequency is given. The change of the beat frequency is a measure of the concentration of the monitored gas. In the monostable element F-FM1 the beat frequency is transformed into rectangular impulses with a constant width. The beat frequency is measured by summing up these impulses in some given time. The quartz-crystal oscillator at the output of the frequency dividers D1 and D2 generates one – second impulses, which at the gate G1 determine the summing – up time of the impulses of the differential signal in the counter COUNT. The four-decade read-out of the counter is decoded in the four-position LCD

display. The control system of the counter is set to zero, by the impulse R (reset) from the monostable element F-FM2, and next triggered from the divider D3 through the gate G2 by means of the impulses CLC (clock).
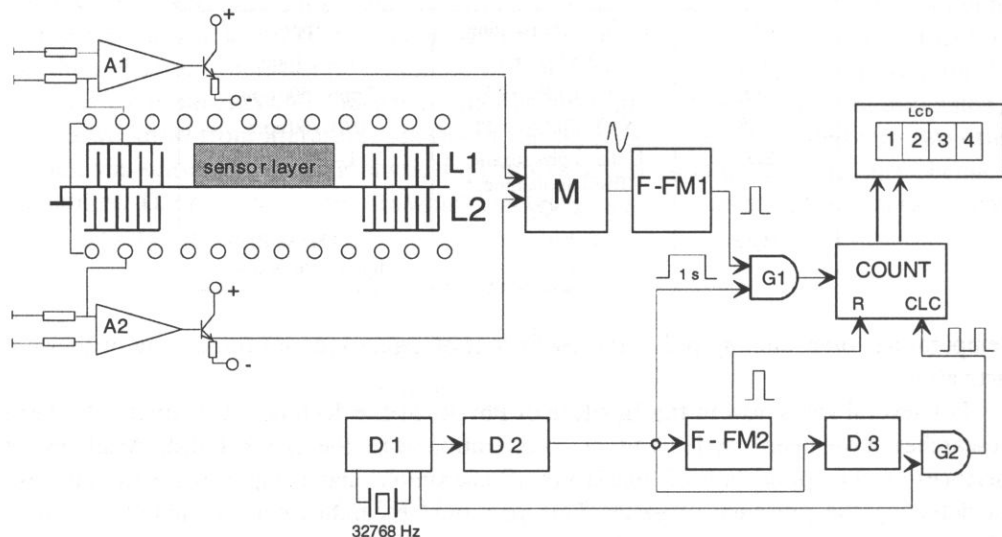

Fig. 1. Block diagram of the measuring instrument.

The deviders, the counter and the control system have been produced by means of the CMOS technique, the digital read-outs are liquid crystals. Such a system makes it possible to miniature the overall dimensions of the measuring instrument (to about 150×80 mm) and to save energy by applying batteries. Thus this device may be applied also as a portable one. It has been assumed that the measuring instrument will be used to detect and to measure the concentration of nitrogen dioxide in the air. The concentration of nitrogen dioxide admissible for a longer time amounts to $30 - 50$ mg/m^3, the maximum one for 30 minutes being $150 - 500$ μg/m^3.

4. The procedure of measurements

In order to get thin layers of the applied phthalocyanines their sublimation in a vacuum was applied. The initial material was powdered PbPc, FePc, CuPc, NiPc and H$_2$Pc produced by the firm SIGMA. Chemically sensitive layer were sublimed in a vacuum by a system of the type NA501P. As a source of vapours a quartz crucible was used, placed inside a tungsten spiral. Before its sublimation the initial material was degassed for 15 minutes in a vacuum 10^{-4} Tr at a temperature of 150° C to 200° C. Particularly intensive gassing was to observed in the case of iron phthalocyanine, the weakest when pure phthalocyanine was applied. The temperature of the source of vapours was controlled by means of a Cu – Konstantan thermocouple with the reference point placed in a container with melting ice. In the course of one cycle of sublimation the layers were placed on a

substrate consisting of lithium niobate with previously prepared (photholithographically) interdigital transducers, and on a glass substrate of the type Corning 7059 used to investigate the structure and to measure the thickness by means of the interferential method. The distance between the source of vapours and the substrate amounted to 25 cm. During the process of sublimation the thickness of the layer was controlled by means of a quartz thickness meter of the type MGS 100, and after evaporation had been completed, the thickness was measured optically. The thickness of the obtained layers to $0.08 - 0.35\,\mu$m and $1.3 - 1.4\,\mu$m.

Fig. 2. The dependence of the differential frequency of an SAW sensor on the concentration of nitrogen dioxide in the air at a temperature of 27° C. The piezoelectric material was LINbO$_3$, the nitrogen dioxide was absorbed by a layer of lead phthalocyanine (PbPc), 83 nm thick.

The most essential part of the sensor is the differential system of two acoustic oscillators (active and compensating oscillator) eliminating the effect of the unsteadiness of temperature on the signal of the sensor. Each oscillator consists of two transducers of the surface wave (20 pairs of electrodes with a width of $12.5\,\mu$m and an aperture of 4 mm), produced photholithographically, and an exterior broadband amplifier. The mid-band frequency of the transducer amounted to about 43 MHz. The distance between the transducers amounted in the surface line to about 14 mm. Together with the acoustic retardation line and the transducers of the surface wave forms a closed electroacoustic loop. The system oscillates if the amplitude conditions for amplification of the signal in the loop is greater than 1, and the phasal condition (full phase shift in the loop equals a multiple of 2π) are satisfied. The measuring signal is a change of the differential frequency of the oscillators at the output of the mixer.
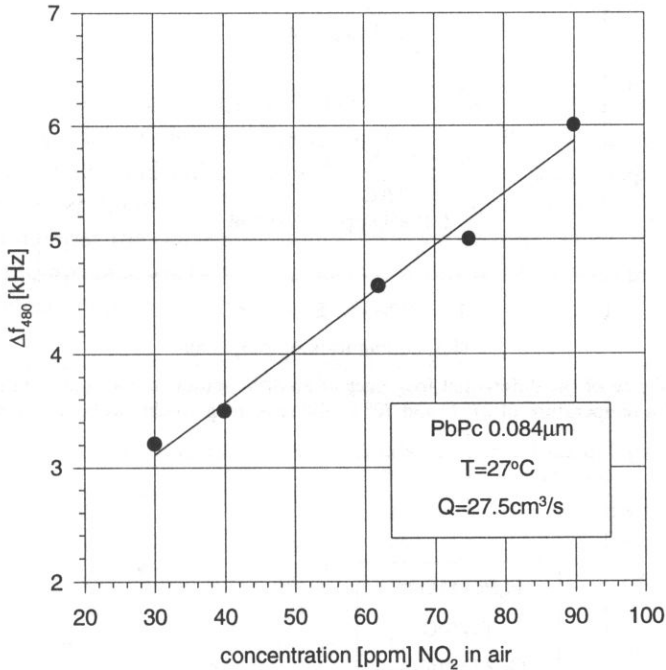
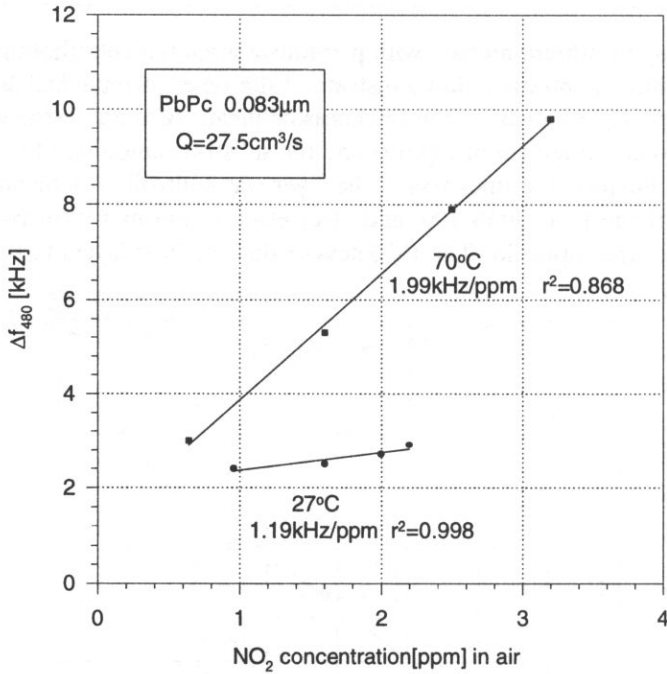Fig. 3. The dependence of the differential frequency of an SAW sensor on the concentration of nitrogen dioxide in the air at a temperature of 27° C and 70° C, the remaining conditions being the same as in Fig. 2.
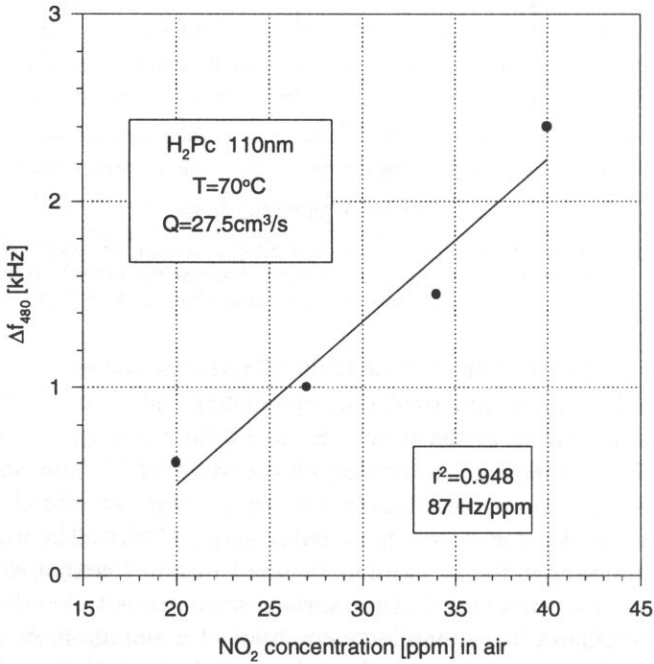

Fig. 4. The dependence of the differential frequency of an SAW sensor with an adsorbing layer of phthalocyanine (H₂Pc), 110 nm thick, on the concentration of nitrogen dioxide in the air at a temperature of 70° C.

The prolonged drift (30 minutes) of the temperature of the sensor amounted to about 50 Hz.

The time of filling, until a steady concentration of gas has been reached, amounts in the applied test chamber with a total volume of about 55 ccm at a flow rate of the gas equal to 55 ccm/s and 27.5 ccm/s to 7 and 14 seconds, respectively, being considerably shorter that the assumed time of exposure (480 s) of the investigated layer to the interaction of the given gas.

5. Results

The test results have been gathered in Table 3. The presented date indicate that most sensitive to the presence of nitrogen dioxide in the air are PbPc layers, followed by layers of CuPc, whereas FePc and NiPc practically do not adsorb NO_2. The influence of CO and CH_4 on the determination of NO_2 have been investigated too. The presence of these gases does not hamper the determination of nitrogen dioxide; FePc, on the other hand, is sensitive to the presence of methane and will in future be applied in the design of an SAW sensor determining the presence of methane.

Table 3. The influence of kind of phthalocyanine, its thickness and temperature on the sensitivity of an SAW sensor designed to determine the content of nitrogen dioxide in the air.

Layer type	Layer thickness [nm]	Temperature [°C]	Sensitivity to NO_2 [Hz/ppm]
PbPc	83	70	2000
PbPc	83	30	1200
CuPc	270	30	130
CuPc	720	30	18
H₂Pc	110	70	87
FePc	30	70	0
NiPc	230	70	0

References

[1] A.R. KATRITZKY and R.J. OFFERMAN, *The development of new microsensor coatings and a short survey of microsensor technology*, Analytical Chemistry, **21**, 2 (1989).

[2] A. GRAJA, *Lowdimensions organic conductors* [in Polish], Fizyka dla Przemysłu, WNT, Warszawa 1989.

[3] B.A. AULD, *Acoustic Fields and Waves*, vol. 1, John Willey and Sons, New York (1973).

[4] A Firm catalogue, Bruel & Kjaer 1991.

[5] J. SIMON and J.J. ANDRE, *Molecular Semiconductors*, Springer-Verlag (1985).

[6] S.M. CHANG et al., *Development of chemical vapour sensor using SAW resonator oscillator incorporating odorant receptive L-B films*, Biosensors & Bioelectronics, **6**, 4 (1991).

[7] J. O'DONNEL et al., *Acousto-electronic and surface plasmon resonant responses from NOx – dopped L-B films of monocycles*, J. Phys. Cond. Matter, Nov, **3**, (1991).

[8] M.S. NIEUWENHUIZEN *et al.*, *A SAW gas sensor for NO₂*, Anal. Chem., 330, 123 (1988).

[9] M.S. NIEUWENHUIZEN *et al.*, *Metallophtalocyanines as chemical interfaces on SAW gas sensor for nitrogen dioxide*, Anal. Chem., **60**, 3 (1988).

[10] M.S. NIEUWENHUIZEN *et al.*, *SAW gas sensor...*, Anal. Chem., **60**, 3 (1988).

[11] A. WILSON, J.D. WRIGHT and A.V. CHADWICK, *A microprocessor-controlled nitrogen dioxide sensing system*, Sensors and Actuators, B. 4, 499 (1991).

[12] M. URBAŃCZYK and W. JAKUBIK, *An influence of vapours of some organic compounds and water on acoustic properties of selected polymers layers*, Arch. Acoust., **18**, 1, 157 (1993).

[13] A. OPILSKI, M. URBAŃCZYK and W. JAKUBIK, *The effect of the vapours of some organic compounds and water on the acoustic properties of some selected polymer layers* [in Polish], Materiały konferencyjne COE'92 Zegrze k. Warszawy, 25-28 maja 1992 r E.2.2. (221–225).

[14] W. JAKUBIK, S. KOCHOWSKI and M. URBAŃCZYK, *Sensor properties investigation of copper phthalocyanine with the use of surface acoustic wave (SAW)*, Sensors and Actuators, B. Chemical, **22**, 2, 133–137 (1994).

[15] W. JAKUBIK, S. KOCHOWSKI, A. OPILSKI and M. URBAŃCZYK, *Sensor properties investigations of the copper phthalocyanine in a layerd structer of the SAW type* [in Polish], Akustyka Molekularna i Kwantowa (1993).

[16] H. WOHLTJEN, *Mechanism of operation and design considerations for surface acoustic wave device vapour sensors*, Sensors and Actuators, **5**, 307 (1984).

[17] J. RANACHOWSKI, E. ADAMCZYK and J. RZESZOTARSKA, *Surface acoustic wave using in the chemical analysis of the gases* [in Polish], Akustyka Molekularna i Kwantowa, **12**, 131 (1991).

[18] D.S. BALANTINE and H. WOHLTEIN, *Surface acoustic wave devices for chemical analysis*, Anal. Chem., **61**, 11, 704A, 1472 (1989).

C   H   R   O   N   I   C   L   E

102nd AES Convention, Munich
22–25 March 1997

Year after year, the consecutive AES Spring Conventions, those held in Europe and designated with even numbers, attract an increasingly higher number of participants. This time in Munich the number, iuncluding exhibitors, was about nine thousand. About 350 companies from all over the World presented their products. Further several tens of press agencies and associations co-worked. The exhibition of the latest technical achievements in the audio field was the biggest ever to have been organized by the AES in Europe, at least in terms of stand space. The newly modernized and enlarged Convention Centre secured a comfortable work area for all activities connected with the Convention programme.

The scientific part of the Convention was also impressive. 112 contributed papers were presented by ca.225 authors and co-authors, during fifteen Papers sessions, devoted to particular problems of the Audio Engineering domain. Discussions followed after presentation of every paper. Particular attention of the German Organizing Committee was paid to the Workshop Sessions. Thirteen Workshop Sessions were held and thanks to their actual themes and well-prepared programmes they awoke the vivid interest of the participants.

As AES Vice-President for Central Europe region, where 17 Sections are active (Austrian, Czech, North German, South German, Hungarian, Israel, Lithuanian, Polish, Russian-Moscow, Russian-St. Petersburg, Slovakian, Swiss, Ukrainian, and three Student Sections: in Moscow, St. Petersburg, and Gdańsk – ca. 1500 members altogether) I had the opportunity to observe their activities during the Board of Governors' meetings in Munich, where all their organizational needs were to be dealt with and many problems solved.

Although I was very busy due to my numerous tasks and participation in various organizational meetings, I was, as during the previous Convention, paying particular attention to the Polish AES members participation and achievements. As to the number of papers Polish authors were ahead of those of many other countries. They were in third position, after the UK and Germany, their contribution being more than 11% of the total number of Convention papers. This result is better than that of the previous European AES Convention (10% at the 100th AES Copenhagen, in 1996).

For the first time since the introduction of workshops into the Convention programmes the Polish acoustician, professor A. Czyżewski, from the Sound Engineering Department of Gdańsk University of Technology organized and moderated, as Chairman, the workshop session entitled Audio technology for the Hearing-Impaired. Three panelists, prof. L. Moser, from Würzburg University, prof. S. Peeters, from Antwerp University and dr T. Fidecki from Warsaw Academy of Music, assisted him at presentations and demonstrations, answered questions and explained problems raised by numerous interested participants.

New forms included in the Convention programme were the Education Fair and Education Forum. The first was aimed at providing all interested visitors with information concerning schools, colleges and institutes and their courses in audio-engineering, as well as apropriate literature. The second one, hosted by the AES Education Committee, afforded the opportunity for discussions among educators and students on academic activities useful for further development of the audio-domain in cooperation with industry.

The attendance of Polish AES members in Munich was numerous as in previous Conventions. A group of students, mostly from the Gdańsk University of Technology, participated in workshop sessions and took advantage of the free access to the most modern equipment demonstrated at exhibition stands. Moreover, they had an opportunity for sightseeing excursions to Munich and their neighbouring countryside as well as to visits to interesting cultural and technical sites of the City.

Traditionally, the Convention site is friendly place for informal meeting and professional contacts between all those interested in the audio domain, coming from various countries of Europe and the rest of the World. Let the Polish share in future Conventions remain as active and fruitful as it has been so far. I address this wish to future organizers of education process in the field of Acoustics and Sound Engineering.

Marianna Sankiewicz

Post Scriptum: As usual, all papers contributed were edited in principle in the form of Convention Preprints prior to the debates. Those Preprints may be available now either from their authors or the AES Editorial Office. Thus, information concerning titles of papers contributed by Polish authors may be useful for Archives of Acoustics readers. This information is as follows:

K. BAŚCIUK, S. BRACHMAŃSKI, *The automation of the subjective measurements of logatom intelligibility*, (Session: Measuring and modelling – Paper A-5) Preprint 4407.

B.W. KULESZA, W. RYSZKOWSKI, *The sound reinforcement system of large halls*, (Sound reinforcement – B-1) No Preprint available.

K. KROSCHEL, A. CZYŻEWSKI, M. IHLE, M. KUROPATWIŃSKI, *Adaptive noise cancellation of speech signal in a noise reduction system based on a microphone array*, (Array Acoustics – H-1) Preprint 4450.

M.J. KIN, A.B. DOBRUCKI, *Roughness effect as a result of amplitude or frequency modulation of single components in harmonic complex* (Psychoacoustics – L-2) Preprint 4481.

A. Czyżewski, R. Królikowski, *New methods of intelligent filtration and coding of audio*, (Psychoacoustics – L-7) Preprint 4486.

A. Czyżewski, A. Lorens, W. Wojnarowska, *Multimedia catalogue of hearing impairments*, (Psychoacoustics – L-8) Preprint 4487.

W. Majewski, Cz. Basztura, *Methods of tape recording authentication*, (Recording and Reproduction Systems-M-6) Preprint 4493.

B. Kostek, A. Wieczorkowska, *A system for musical database creation and analysis*, Sound Archiving-Musical Acoustic – N-3) Preprint 4498.

S.K. Zieliński, G. Szwoch, *Application of Chebychev polynomials to calculation of the nonlinear characteristics of the digital waveguide model of the organ pipe*, (Musical Acoustics – N-4) Preprtint 4499.

G. Budzyński, M. Sankiewicz, M. Szczerba, *A new swinging-bell system applicable to carillon bells or change-ringing peals*, (Musical Acoustics – N-6) Preprint 4501.

B. Kostek, M. Szczerba, *Applications of algorithms dealing with time domain uncertainty for the automatic recognition musical phrases*, (Musical Acoustics – N-7) Preprint 4502.

K. Szlifirski, T. Łętowski, A. Miśkiewicz, *Timbre solfège: teaching tools for developing technical listening skills*, (Musical Acoustics – NB-8) NoPreprint available.

M.S.

1997 IEEE International Ultrasonic Symposium

October 5 – 8, 1997
Toronto Marriot Eaton Centre
Toronto, Ontario, Canada
Sponsored by the Ultrasonics, Ferroelectrics & Frequency Control Society

General Chair:
Stuart Foster
University of Toronto
416-480-5716 (480-5714 fax)
stuart@src1.sunnybrook.utoronto.ca

7-th Spring School on Acousto-Optics and Applications

18 – 22 May, 1998 Gdańsk

The School is organized by
University of Gdańsk
Institute of Experimental Physics
in co-operation with the
Quantum Molecular Acoustics and Sonochemistry
section of the **Polish Acoustical Society** and the **Committee of Acoustics of the Polish Academy of Sciences**, sponsored by **Ministry of Education, Polish Council for Scientific Research** and by SPIE – **the International Society of Optical Engineering** in association with the **Polish Chapter of SPIE.**

Organizing Committee

President:	Prof. dr hab. A. Śliwiński
Vice President:	Prof. dr hab. P. Kwiek
Secretary:	Dr B. Linde
Members:	Dr M. Borysewicz
	Mgr G. Gondek
	Dr M. Kosmol
	Dr A. Markiewicz
	Dr A. Sikorska
	Dr J. Szurkowski
Technical Responsability Staff:	B. Dalek
	Mgr I. Głębocka
	Mgr inż. A. Katkowski
	Mgr inż J. Paczkowski

Scientific Programme

According to the wishes of the participants of the last Spring School on Acousto-optics in 1995 we have pleasure to announce the Seventh Spring School as a continuation of these every third year meetings.

As before, the aim of the School is to cover all physical topics concerning light and sound (mainly in the ultra-and hypersonic range) interaction in liquids and solids. Applications of acousto-optic devices such as deflectors, modulators, filters and other proces-

sors of integrated optics, visualization of ultrasound and holographic imaging etc. will be included in the programme. The School activities will be devided into:

- invited lectures (45 minutes),
- original papers (20 minutes),
- poster session,
- round table discussions,
- equipment exhibition.

The proceedings of the School will be published by the SPIE. The technical requirements for typing the papers will be send in the second circular.

Since the number of original papers is limited the selection will be done by the Organizing Committee.

The official language of the School will be English.

The number of participants is limited to 80.

The exhibition of acoustical and optical equipment is predicted during the meeting. The potential exhibiters are invited to contact the organizers for details.

The organizeres are opened to accept a sponsorship upon the School of a prominent firm which could be interested in the opportunity to promote their goods among acousto-opticians.

All correspondence should be directed to:
Dr Bogumił LINDE
Institute of Experimental Physics
Organizing Committee
of the 7-th School on Acousto-optics
University of Gdańsk, ul. Wita Stwosza 57
80-952 Gdańsk, Poland
Phone: (+48) (58) 52-92-48 or (58) 521-92-13 or (58) 41-31-75
E-mail: fizas@univ.gda.pl; fizbl@univ.gda.pl
Fax +(+48) (058) 41-31-75

Joint Meeting of the 16-th International Congress on Acoustics and the Acoustical Society of America

Seattle, Washington, USA
20–28 June 1998

The 16th International Congress on Acoustics (ICA) and the 135-th meeting of the Acoustical Society of America (ASA) will convene in Seattle, Washington in June 1998. Seattle, a major city in the northwestern United States, is located between the Cascade Mountains and Puget Sound and is served by an international airport.

Joint Meeting As a joint meeting of the ICA and ASA, the Congress will bring together experts from all fields of acoustics and will provide an international forum for the open exchange of scientific information. The meting is organized by the Acoustical Society of America under the aegis of IUPAP and its Commision on Acoustics.

Technical Presentations The meeting will consist of plenary lectures, invited and contributed papers, poster sessions, and exhibits. The plenary lectures will be presented by renowned acousticians and will cover a wide variety of interesting topics in acoustics.

The working languages for the Congress will be English, French, and German. Papers will be presented in the language of the author's choice. A complete set of proceedings will be available at the Congress.

Social Activities Technical visits and excursions of general interest will be arranged: technical tours to local companies will include Boeing, Microsoft, and the Applied Physics Laboratory, University of Washington, as well as a trip to Mt. Rainier and a salmon dinner on Blake Island.

For more information about the Joint Meeting of ASA/ICA'98

16-th ICA Secretariat
Applied Physics Laboratory
University of Washington
1013 NE 40th Street
Seattle, WA 98105-6698, USA